LBL-25698 c.2
Preprint

Lawrence Berkeley Laboratory
UNIVERSITY OF CALIFORNIA

Physics Division

RECEIVED
LAWRENCE
BERKELEY LABORATORY

DEC 2 1988

LIBRARY AND
DOCUMENTS SECTION

Mathematics Department

To be submitted for publication

A Boundary Integral Approach to Unstable Solidification

J. Strain

July 1988

TWO-WEEK LOAN COPY

This is a Library Circulating Copy which may be borrowed for two weeks.

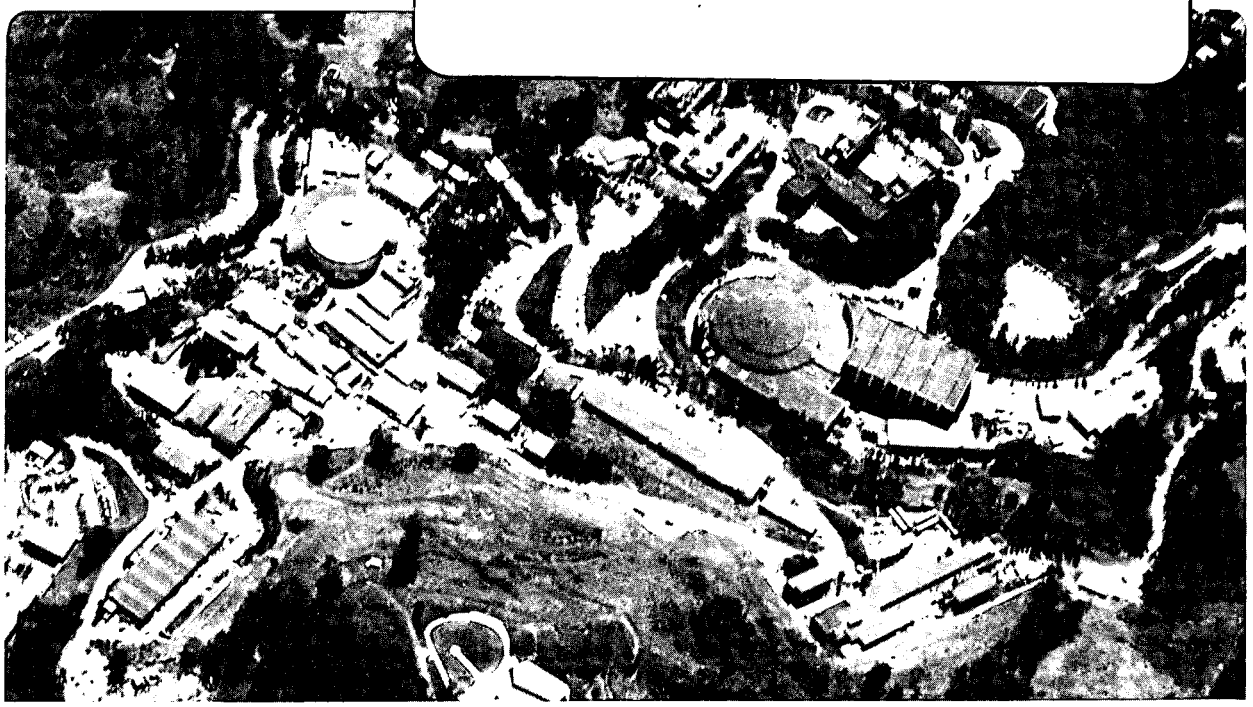

Prepared for the U.S. Department of Energy under Contract Number DE-AC03-76SF00098.

LBL-25698 c.2

DISCLAIMER

This document was prepared as an account of work sponsored by the United States Government. While this document is believed to contain correct information, neither the United States Government nor any agency thereof, nor the Regents of the University of California, nor any of their employees, makes any warranty, express or implied, or assumes any legal responsibility for the accuracy, completeness, or usefulness of any information, apparatus, product, or process disclosed, or represents that its use would not infringe privately owned rights. Reference herein to any specific commercial product, process, or service by its trade name, trademark, manufacturer, or otherwise, does not necessarily constitute or imply its endorsement, recommendation, or favoring by the United States Government or any agency thereof, or the Regents of the University of California. The views and opinions of authors expressed herein do not necessarily state or reflect those of the United States Government or any agency thereof or the Regents of the University of California.

LBL-25698

A BOUNDARY INTEGRAL APPROACH TO UNSTABLE SOLIDIFICATION[1]

John Strain

Department of Mathematics
and
Lawrence Berkeley Laboratory
University of California
Berkeley, CA 94720

July 1988

[1]This work was supported by an IBM Predoctoral Fellowship, an NSF Graduate Fellowship, and the Applied Mathematical Sciences subprogram of the Office of Energy Research, U.S. Department of Energy under contract DE-AC03-76SF00098.

Abstract

We consider the supercooled Stefan problem with a general anisotropic curvature- and velocity-dependent boundary condition on the moving interface. This is a well-known model for pattern formation in unstable solidification.

We reformulate the problem in terms of a quasilinear history-dependent singular integral equation for the velocity of the boundary. Using this equation, we carry out a new linear stability analysis of a planar solidification front with a general boundary condition. This analysis disagrees with the classical linear stability theory, because our approach includes transient effects due to initial conditions and linearizes the boundary conditions more accurately. Our analysis exhibits the smoothing role of velocity-dependence and the destabilizing effect of anisotropy.

We then present numerical methods, also based on the integral equation formulation. These methods are able to follow the evolution of a periodic solidification front far into the nonlinear regime, with $O(\Delta t)$ accuracy, where Δt is the time step. Previous work has been limited to short times and achieved slightly less than $O(\Delta t^{1/2})$ accuracy. Our methods also include a new algorithm for moving curves with curvature-dependent velocity.

We present numerical results obtained with these new methods. After demonstrating first-order convergence for short time spans, we compare accurate numerical results with the predictions of the new and classical linear stability theories. Our results agree very well with the new theory, and disagree with the classical theory by as much as 25%. Then we study the long-time evolution of a dendritic front. We confirm the smoothing effect of velocity-dependence numerically. Our computations exhibit the beginnings of a sidebranching instability, followed by formation of a periodic cellular front, with an anisotropic boundary condition. Tip-splitting occurs instead, in the isotropic case.

Table of Contents

Introduction 1

1. Some Previous Work
- 1. Physics 3
- 2. Existence theory 5
- 3. Numerical methods 7
- 4. Classical linear stability theory 8

2. The Integral Equation and Linear Stability Theory
- 1. Introduction 12
- 2. The integral equation formulation 12
- 3. Linear stability theory 16

3. Numerical Methods for Periodic Graphs
- 1. Introduction 23
- 2. The periodic graph equation of motion 23
- 3. Curve discretization 25
- 4. Curvature discretization and linear stability 27
- 5. Time discretization 30
- 6. Numerical results 33

4. Numerical Methods for General Periodic Fronts
- 1. Introduction 37
- 2. The ϕ equation 37
- 3. Keeping track of arclength 39
- 4. The numerical method 41
- 5. Numerical results 44

Discussion and Conclusions 47

References 50

Tables 56

Figures 63

A Boundary Integral Approach to Unstable Solidification*

John Strain

Department of Mathematics
and
Lawrence Berkeley Laboratory
University of California
Berkeley, California 94720

Introduction

Recently, there has been much interest in the supercooled Stefan problem with a curvature-dependent boundary condition on the phase interface, as a model for the spontaneous pattern formation believed to occur in dendritic solidification of a pure substance from an undercooled melt. This model was introduced in the metallurgical and physical literature [52, 53, 65, 64, 66, 69, 82] and has now become a topic of applied mathematics as well [15, 21, 46, 94, 99, 105, 108].

Most of the physical literature (e. g. [4, 7, 67]) has studied the problem via asymptotic analysis, and applies numerical methods only to solve various approximate equations, as in [66]. Numerical methods have been successfully applied to steady-state equations [72, 91] and to equations for smoothed interfaces [13, 34]. Only a few methods have been proposed to solve the full time-dependent problem [21, 94, 99], and it seems that none have been capable of computing the interface accurately far into the nonlinear regime, where interesting phenomena like side-branching [53], tip-splitting [85], and formation of cellular fronts [66] are presumed to occur.

In this paper, we present a numerical method for solving the supercooled Stefan problem in two space dimensions, with a very general anisotropic curvature- and velocity-dependent temperature boundary condition on the phase interface. Our method is based on eliminating the temperature field and computing only the moving boundary. There are two difficulties in this approach; first, computing the velocity requires solution of a nonlinear history-dependent singular integral equation on the moving boundary, second, moving a curve with curvature-dependent velocity is difficult even if the velocity is a simple function of curvature [86, 93]. The first difficulty is easiest to understand in the simple case when the interface is the graph of a function, so we resolve it there. The second requires a reformulation of the general problem of curve motion.

Our method computes the interface to first order accuracy; this compares favorably with previous approaches, which achieve less than half order accuracy, even for the simpler

*This work was supported by an IBM Predoctoral Fellowship, a NSF Graduate Fellowship, and by the Applied Mathematical Sciences subprogram of the Office of Energy Research, U.S. Department of Energy, under Contract DE-AC03-76SF00098.

curvature-independent classical Stefan problem without supercooling. We present several long-time computations in which physically interesting phenomena occur.

In Chapter 1, we review previous theoretical and numerical work on this and related problems, and describe derivations from nonequilibrium thermodynamics. We also review the classical linear stability theory [82] of the (approximately generic) planar constant-speed solution, and point out its incompleteness; its predictions of instability are reliable, but not of stability.

We begin Chapter 2 with a reformulation of the moving boundary problem as a nonlinear history-dependent singular integral equation for the normal velocity of the interface. We use the integral equation immediately, to carry out a linear stability analysis of the planar constant-speed solution, with a general boundary condition. This analysis produces results quite different from those of the classical theory; the time-dependence of a perturbation amplitude is exponential only in the — questionably relevant — long-time limit. For short times, transient effects due to the initial temperature field control the growth of perturbations. Hence the classical theory predicts the wrong amplitudes, though it gets the right exponents in the long-time limit.

In Chapter 3, we describe a numerical method for computing the moving boundary while it remains the graph $\{ x = s,\ y = y(t,s) \mid -\infty < s < \infty \}$ of a 2π-periodic function $y(t,s)$. We deal with this simple case first because it allows us to learn how to solve the integral equation for the velocity, without worrying about how to move the curve. Of course, the boundary does not remain a graph, so this method is good only for moderate time spans and relatively small deformations of a flat interface. However, moderate time spans suffice for a comparison with linear stability theory which conclusively upholds our new theory and disagrees with the classical theory. We also study the convergence rate of the numerical method experimentally, and show the method to be first order accurate for time spans short enough that the interface remains the graph of a smooth function.

In Chapter 4, we present a numerical method for computing a general boundary, no longer restricted to graphs. This requires some study of the general problem of moving curves. We reformulate this problem, following Duchon and Robert [27], as an evolution equation for the normal angle ϕ. Using this equation to move the boundary and computing the velocity V from the integral equation gives a complicated but reliable numerical method, which is first-order accurate and stable. An additional ordinary differential equation keeps track of arclength, and we introduce an algorithm which keeps points equally spaced on the curve without redistribution.

Our numerical results suggest several conclusions; these form the content of Chapter 5. Numerically, we have shown that the principle of computing only the moving boundary leads to an effective and accurate numerical method. Physically, we have confirmed the linear stability theory based on the integral equation formulation. It is also interesting that we see the beginnings of a sidebranching instability only with an anisotropic Gibbs-Thomson relation, as predicted by Langer [67]; we see a fairly well-developed tip-splitting instability instead, in the isotropic case.

This paper is based on the author's doctoral dissertation, "Numerical Study of Dendritic Solidification," for the Department of Mathematics, University of California at Berkeley.

1. Some previous work

1.1. Physics

Consider, for the sake of comparison with our problem, the melting of ice in water. This is a smooth, stable phenomenon, modeled by the classical two-phase Stefan problem: The temperature field u satisfies the heat equation

$$\partial_t u = \Delta u \qquad (\Delta = \partial_x^2 + \partial_y^2)$$

in each phase (water or ice) separately, the normal velocity is the jump in the normal component of heat flux,

$$V = -\left[\frac{\partial u}{\partial \nu}\right],$$

across the interface (ν is the unit outward normal to the solid phase), and the temperature on the interface is the equilibrium melting temperature; by a shift of origin in the temperature scale, $u = 0$ on the interface. With appropriate initial and boundary conditions for u, this is a fairly well-understood and mathematically well-posed problem, for which many results of existence, uniqueness and regularity have been proven. Many of the more recent results [11, 12, 61] rely on the weak formulation introduced by Duvaut [29] and the theory of variational inequalities [62], but earlier work was done with integral equations, maximum principles, and other tools from the classical theory of partial differential equations; see [35, 36] and [89].

In the physical situations with which we will be concerned, on the other hand, it often happens that the liquid phase is supercooled; $u < 0$ in the liquid phase. In practice, water can be cooled substantially below 0° Centigrade without freezing, if there is no "seed" to start the freezing process. A small disturbance can then begin a rapid and unstable change of phase, *dendritic solidification*. The large-scale shape of the resulting solid — for example the diameter of a snowflake — is typically a reproducible function of a few physical parameters such as the undercooling, but the detailed small-scale structure has a complex but organized appearance. Currently many workers [5, 6, 24, 67, 66, 58, 59, 60, 85, 7, 91] are interested in this problem of *pattern formation*.

Supercooling of the liquid phase requires a re-examination of the assumptions and formulation of the classical Stefan problem. Classically, the water is the set where $u > 0$, the ice the set where $u < 0$, and the interface the set where $u = 0$. When supercooling is present, however, a snapshot of the temperature field at any given time does not determine the interface, because u can be negative in either phase. Thus the only way we can keep track of the interface is by following it continuously in time. This requires that the interface itself *move* smoothly in time. Physically, this means that liquid can solidify only adjacent to preexisting solid.

Unfortunately, both linear stability analysis [98, 64, 82, 87, 88] and rigorous theory [8] show that the interface does not remain smooth when the liquid is supercooled. Linear stability theory gives a growth exponent $y(k) = V\,|k|$, where V is the velocity of the unperturbed planar solution and k is the wavenumber of the perturbation; disturbances to a planar interface grow like $e^{ty(k)}$, with small wavelengths growing faster, so the interfacial structure becomes very complicated. Since a real snowflake, for example, exhibits a complicated structure only down to a

certain length scale, below which the interface is microscopically smooth, this indicates that supercooled solidification is not well modelled by the classical Stefan problem. Furthermore, an analysis of the classical Stefan problem by di Benedetto and Friedman shows that finite-time blowup occurs when the water is supercooled; solutions fail to exist after a certain time. See [8]. Hence some modification of the classical Stefan problem is necessary, if we are to model supercooling of the liquid phase.

The various modified models proposed usually differ from the classical Stefan problem only in the boundary condition $u = 0$ on the moving boundary; exceptions, however, are models proposed by Visintin [105], who constructs a weak formulation of superheating and supercooling, and Wollkind and Notestine [108], who suggest modification of the jump condition $V = -\left[\frac{\partial u}{\partial \nu}\right]$ as well. The most classical models use surface tension arguments to assign the interface an energy proportional to its area, and result in a curvature-dependent "Gibbs-Thomson relation" [41]

$$u = -\varepsilon_C C \tag{1}$$

on the interface. Here ε_C is a small constant and C is the curvature of the interface, taken to be positive where the center of the osculating circle lies in the solid phase. More recently, several authors [47, 83, 15] have proposed anisotropic curvature- and velocity-dependent boundary conditions of the form

$$u = -\varepsilon_C(\phi)C - \varepsilon_V(\phi)V, \tag{2}$$

where ϕ is the angle between the normal to the interface and a fixed axis and V is the normal velocity. Typically

$$\varepsilon_C(\phi) = \varepsilon_C(1 - A\cos k_A\phi)$$

$$\varepsilon_V(\phi) = \varepsilon_V(1 - A\cos k_A\phi)$$

where $A \in [0,1)$ is the coefficient of anisotropy and k_A is a small integer connected with the crystalline anisotropy of the solidifying substance. These relations involve the non-equilibrium concept of velocity, and therefore cannot follow from equilibrium thermodynamics, unlike the curvature-dependent (but velocity-independent and isotropic) Gibbs-Thomson relation (1).

There are now two theoretical frameworks within which the general boundary condition (2) can be derived; the phase field model of phase transitions and thermodynamics with interfacial energy and entropy.

The phase field model assumes a van der Waals-Cahn-Hilliard free energy functional [16, 81], quadratic in the gradient of a phase field ψ and linear in the temperature field u:

$$F[\psi] = \int \frac{1}{2}|\nabla\psi|^2 + g(\psi) + u\psi$$

where g is a double well potential like $(1-\psi^2)^2$ and the integration is over both phases. The phase field ψ is close to 1 in the liquid phase, close to -1 in the solid phase, and makes a smooth transition from 1 to -1 near the boundary. In this model the boundary is smeared out into the region $-\xi < \psi < \xi$, where ξ is a measure of the interfacial thickness. The evolution equation for

ψ is the Model A equation of Landau-Ginzburg theory [50];

$$\tau\partial_t \psi = \frac{\delta F}{\delta \psi}$$

where $\frac{\delta F}{\delta \psi}$ is the functional derivative of F with respect to ψ and τ is a relaxation time. One couples this to a modified heat equation for u to obtain a parabolic system. The system can be solved numerically [13, 34] or studied by singular perturbation theory as in [15]. In the limit when the interfacial thickness vanishes (ψ becomes a step function), asymptotic analysis produces several modified Stefan problems including boundary conditions like (1) and (2); see [15] and references therein for the details. Some equilibrium existence results are also known for these phase field models; see [81, 14, 63].

A related approach [83] considers the same free energy functional, with $u = 0$ and ψ now a concentration rather than a phase field, but replaces the Model A equation with

$$\tau\partial_t \psi = \Delta \frac{\delta F}{\delta \psi}$$

where Δ is the Laplacian. This equation, unlike the Model A equation, has the free energy F as a Lyapunov functional, and is therefore a reasonable way to approach equilibrium. Again, a singular perturbation analysis [84] produces a modified Stefan problem, this time for ψ. This approach models supersaturated rather than supercooled solidification, but results in a similar moving boundary problem.

The approach via thermodynamics with interfacial energy and entropy produces a simpler derivation at the expense of a theoretical structure farther removed from microscopic physics. Gurtin [46, 44, 47, 45] derives (2) from fairly general and reasonable assumptions about the structure of the constitutive relations of a thermodynamics in which zero-thickness interfaces are assigned energy and entropy, typically proportional to their surface area.

1.2. Existence theory

No rigorous existence and uniqueness results are known for the supercooled Stefan problem with the curvature-dependent boundary conditions (1.1.1) or (1.1.2). In this section, we describe a local existence and uniqueness result for a simpler model problem, because it suggests the curve movement algorithm of our numerical method and because it seems likely that similar techniques could provide a local existence result for our problem. This result is due to Duchon & Robert [27].

Consider the modified Stefan problem with an isotropic velocity-independent Gibbs-Thomson relation with $\varepsilon_C = 1$, with the heat equation replaced by its steady-state counterpart $\Delta u = 0$, and with temperature variation in the solid phase neglected. The problem can then be stated in one sentence: *A curve moves with velocity equal to the normal derivative of the harmonic function with boundary values equal to the curvature of the curve.*

Thus we seek a curve $\Gamma(t)$ moving with normal velocity

$$V = \frac{\partial U}{\partial \nu},$$

where $\Delta U = 0$ above $\Gamma(t)$ and

$$U = C \qquad \text{on } \Gamma(t).$$

Here C is the curvature and ν the normal of $\Gamma(t)$. Consider the special situation in which $\Gamma(t)$ is the graph $\{x = s,\ y = y(s) \mid -\infty < s < \infty\}$ of a Lipschitz function y. Parametrize $\Gamma(t)$ by arclength, identify functions on $\Gamma(t)$ with functions on the real line $\mathbb{R}$ by the arclength s, and let ϕ be the angle between ν and the y-axis. Let $\Lambda = \Lambda_\Gamma$ denote the Dirichlet-Neumann operator for $\Gamma = \Gamma(t)$, defined for $f \in L^2(\Gamma) \cong L^2(\mathbb{R})$ by

$$\Lambda f = \frac{\partial U}{\partial \nu}$$

where

$$\Delta U = 0 \quad \text{above } \Gamma$$
$$U = f \qquad \text{on } \Gamma;$$

thus the normal velocity is given as a functional of curvature by $V = \Lambda C$. One can then derive the following evolution equation for ϕ (see [27] or Chapter 4 for details);

$$\partial_t \phi - D\Lambda C = C \int_0^s C\Lambda C\, ds', \qquad C = D\phi, \tag{1}$$

with initial condition $\phi(0,s) = \phi_0(s)$. This is a nonlinear third-order pseudodifferential evolution equation, since Λ is a first-order pseudodifferential operator [92, 28, 22, 101] acting on the spatial variable s. Let $H^2 = H^2(\mathbb{R})$ be the usual Sobolev space, consisting of square integrable functions on $\mathbb{R}$ with square integrable first and second distributional derivatives [1, 100] and let $|\phi|_\infty = \max_{\mathbb{R}} |\phi|$ be the max-norm. Then the following result holds:

Theorem (Duchon & Robert [27]) *Let ϕ_0 belong to H^2, and $|\phi_0|_\infty < \frac{\pi}{2}$. (Thus $\Gamma(0)$ is a Lipschitz graph.) Then there is $T > 0$ and ϕ continuous from the interval $[0,T]$ into H^2 satisfying (1) and having $\phi(0,s) = \phi_0(s)$. Furthermore, there is a ball in $L^\infty(0,T;H^2)$ in which the solution of (1) is unique.*

The proof is computational, relying mainly on estimates for Λ and especially on their dependence on the Lipschitz constant of Γ. Hence we merely summarize it.

To begin the proof, subtract the operator Λ_0 corresponding to a flat interface,

$$\Lambda_0 = HD$$

where H is the Hilbert transform [96], from both sides of (1) to get

$$(\partial_t + \Lambda_0^3)\phi = C \int_0^s C\Lambda C ds' + D(\Lambda - \Lambda_0)C = F(\phi) \tag{2}$$

where $C = D\phi$ is the curvature. Solve (2) for ϕ in terms of $F(\phi)$ by the Fourier transform [97] and apply the contraction mapping principle [42] to the resulting fixed point equation. The estimates needed to apply the principle are consequences either of classical potential theory [37, 57] or of more recent work on singular integrals [22, 23]. They rest on the compactness of the

operator $\Lambda - \Lambda_0$ as an operator on L^2; the necessary preliminaries are summarized in [28]. Thus the key step of the proof is subtraction of the constant-coefficient operator Λ_0, which already contains the singularity of Λ.

Extension of this theorem to our supercooled Stefan problem would require two steps. The first — inclusion of temperature variation in the solid phase — seems to present no additional difficulties, but the second — solution of the heat equation on a time-dependent domain — is much more difficult than the solution of the Laplace equation, which does not involve the previous history of the interface. Even the solution of the equation corresponding to (2) for ϕ in terms of $F(\phi)$ becomes a nontrivial undertaking, because Λ acts on the time variable.

However, this general viewpoint — in which the temperature field is treated as an intermediate step between the curvature and the normal velocity, rather than as an independent unknown — pervades the work of this paper. Both our analysis and our numerical methods are based on equations which involve only the moving boundary.

1.3. Numerical methods

We briefly describe some of the many existing numerical methods for the curvature-independent classical Stefan problem without supercooling, to provide a background for our work on the curvature-dependent and supercooled case.

Methods for the classical Stefan problem in more than one space dimension (the one-dimensional case is of little interest to us here) tend to fall into two general classes; front-tracking methods which follow the boundary explicitly, either as a curve or as the boundary of a region, and enthalpy methods which use a weak formulation to avoid tracking the boundary explicitly.

In front tracking methods, the usual procedure is to solve the heat equation in each phase with zero Dirichlet data on $\Gamma(t)$ by finite element or finite difference methods, compute an approximate normal velocity by numerical differentiation of the temperature field and an approximate normal by some method depending on the representation of the moving boundary, and move the boundary in some fashion with the computed velocity. Variations on this procedure include solving with Neumann data and adjusting the boundary to be where $u = 0$, or using an implicit time discretization and iterating on the temperature and the boundary until the boundary location and velocity agree with those obtained from the temperature field. Front tracking methods have been applied to the Stefan problem by Meyer [74, 75, 76, 77] and to several similar problems (*e.g.* Rayleigh-Taylor instability) by Glimm *et al.* [43]. A general review of numerical methods for moving interfaces can be found in Hyman [54].

In enthalpy methods, the Stefan problem is transformed to a single nonlinear heat equation of the form $\partial_t u = \Delta f(u)$, with f a step function, to hold weakly on the entire domain occupied by the two phases. After computing u, the boundary may be found, if desired, as the set $\{ u = 0 \}$. Various methods have been proposed to solve $\partial_t u = \Delta f(u)$; Majda [70] analyzes the convergence of the simplest finite difference method, and Chorin [21] reports numerical experiments with the method. Berger *et al.* [10, 9] derive similar finite difference methods in a very general framework; their methods are very simple to use but have rather large temperature field error estimates of the form $O((\Delta t \log(1 + T/\Delta t))^{1/2})$ where Δt is the timestep and T is the time at

which the error is bounded. Their numerical results show these estimates to be sharp. Alexander *et al.* [2] have applied Miller's moving finite elements [78] to the enthalpy formulation. Review articles on the subject are [33] , [25] and [76]; these articles also describe many methods which we have omitted. Other weak solution methods are presented by Visintin & Verdi [103, 104], with similar error estimates.

Numerical methods for the curvature-dependent supercooled Stefan problem, however, are much scarcer. Smith [94] and Chorin [21] have constructed methods based on the enthalpy formulation, but incorporating some type of front tracking to evaluate the curvature. Smith's method suffered from *grid effects;* the shape of a computed unstable interface is strongly and unphysically dependent on the orientation of the numerical grid used to solve the problem. This effect prevents the numerical results from being even qualitatively accurate in the presence of morphological instability and in particular prevents agreement with linear stability theory. Chorin [21] introduced a partial volume representation [54] of the interface and an accurate curvature evaluation algorithm for curves given by partial volumes, but this did not remove the grid effects. In addition, these methods are based on the enthalpy formulation and therefore are limited to the $O((\Delta t \log(1+T/\Delta t))^{1/2})$ error estimate which we saw. Chorin's numerical results indicate this estimate to be of the right order of magnitude. Recently, Sullivan *et al.* [99] have solved the problem using finite element methods on a moving mesh, but their results so far are limited to the case when the interface is the graph of a function, and therefore cannot follow the interface into the nonlinear regime.

Thus it seems fair to say that there are no completely satisfactory methods for solving the supercooled Stefan problem with a general anisotropic curvature- and velocity-dependent boundary condition. This paper will therefore present a first-order accurate method which can follow the interface far into the nonlinear regime. Our approach is essentially a boundary integral method [71, 73, 79, 31] which eliminates grid effects by eliminating the spatial grid; indeed, we eliminate the temperature field altogether. We must then solve a singular integral equation [17, 96] for the velocity of the moving boundary, but it turns out that this can be done quite accurately. Given the velocity, it is still not altogether trivial to move the curve, because the velocity is curvature-dependent. Sethian [93] has exhibited some of the difficulties in moving curves with curvature-dependent speed. However, we use an evolution equation for the normal and an algorithm which automatically keeps points on the curve equidistant in arclength, to avoid the instability observed by Sethian.

1.4. Classical linear stability theory

In this section, we review the classical linear stability theory, due to Mullins & Sekerka [82], of the isotropic velocity-independent Gibbs-Thomson relation

$$u = -\varepsilon C.$$

Another approach to this analysis is presented by Pinus & Taylor [87, 88]. The predictions of this analysis will be compared with numerical results in Chapter 3.

Consider the planar interface in $\mathbb{R}^2$ parametrized by

$$\Gamma(t) : (y = Vt, x = s) \qquad s \in \mathbb{R} \tag{1}$$

with temperature field

$$u(x,y,t)=\begin{cases} e^{-V(y-Vt)}-1 & y>Vt \\ 0 & y<Vt \end{cases} \tag{2}$$

independent of x. The interface moves into the liquid phase with positive velocity V, and the temperature field propagates without change of structure.

Perturb this solution by adding temperature fields δu_S and δu_L in the solid and liquid phases respectively, and let $y = Vt + \delta y(t,x) + O(\delta^2)$ be the resulting perturbed interface. Thus u_S, u_L, and y satisfy

$$\partial_t u_S = \Delta u_S \qquad y < Vt + \delta y(t,x)$$

$$\partial_t u_L = \Delta u_L \qquad y > Vt + \delta y(t,x)$$

$$\delta u_S = e^{-V\delta y} - 1 + \delta u_L = \frac{\varepsilon\delta\partial_x^2 y}{(1+\delta^2(\partial_x y)^2)^{3/2}} \qquad y = Vt + \delta y(t,x)$$

$$-Ve^{-V\delta y} + \delta(\partial_y u_L - \partial_y u_S) = -V - \frac{\delta\partial_t y}{(1+\delta^2(\partial_x y)^2)^{1/2}} \qquad y = Vt + \delta y(t,x).$$

Linearize these equations by extending u_L and u_S up to the unperturbed boundary as solutions of the heat equation, and using Taylor expansion to construct an effective boundary condition there. Drop terms of order δ^2 to get

$$\partial_t u_S = \Delta u_S \qquad y < Vt \tag{3}$$

$$\partial_t u_L = \Delta u_L \qquad y > Vt \tag{4}$$

and the effective boundary conditions

$$u_S = -Vy + u_L = \varepsilon\partial_x^2 y \qquad y = Vt \tag{5}$$

$$\partial_y u_L - \partial_y u_S = -\partial_t y - V^2 y \qquad y = Vt \tag{6}$$

Note that the conditions (5) do not preclude continuity of the real temperature field across the *perturbed* interface. The apparent discontinuity arises because extending a solution of the heat equation to a larger domain can be an unstable process, as the exact solution (2) shows: it grows exponentially past $y = Vt$.

These are linear equations with constant coefficients on a rectangular domain, so we can find exponential solutions of the form

$$\begin{aligned} u_S &= u_0 e^{ikx} e^{y_1 t} e^{q(y-Vt)} \\ u_L &= u_0' e^{ikx} e^{y_1 t} e^{-q'(y-Vt)} \\ y &= y_0 e^{ikx} e^{y_1 t}. \end{aligned} \tag{7}$$

Furthermore, an arbitrary smooth perturbation of the initial temperature field and interface can be decomposed into such solutions by means of a Laplace transform in y and a Fourier transform in x resp. s [95]. Thus one might expect to analyze stability by computing the linear stability exponent y_1 for all positive q and q' and real k, as in the conventional linear stability

analyses carried out in Chandrasekhar [20].

Unfortunately, the dispersion relations

$$u_0(y_1 - Vq - q^2 + k^2) = 0 \tag{8}$$

$$u_0'(y_1 + Vq' - q'^2 + k^2) = 0 \tag{9}$$

$$u_0 = -Vy_0 + u_0' = -\varepsilon k^2 y_0 \tag{10}$$

$$q'u_0' + qu_0 = (y_1 + V^2)y_0, \tag{11}$$

which must be satisfied by solutions of the form (7), fix q and q' in terms of k. To see this, eliminate the amplitudes from (10) and (11) to get three equations

$$y_1 - Vq - q^2 + k^2 = 0 \tag{12}$$

$$y_1 + Vq' - q'^2 + k^2 = 0 \tag{13}$$

$$y_1 + V^2 + \varepsilon k^2(q + q') - Vq' = 0 \tag{14}$$

in the four unknowns y_1, q, q', and k^2. These can be solved for y_1, q and q' in terms of k. But to represent an arbitrary perturbation of the initial temperature field and interface requires *three* independent parameters, q, q' and k. Thus we have too few degrees of freedom to carry out a complete stability analysis. Since the solution is stable if no modes grow, but unstable if any modes grow, we can reliably predict instability by this analysis, but not stability.

Despite this difficulty, we proceed with the classical calculation. First consider the case $\varepsilon = 0$. Then (8) becomes vacuous since $u_0 = 0$ by (10), and a minute or two of algebra gives

$$y_1 = \begin{cases} \pm V|k| & |k| < V \\ V|k| & |k| > V. \end{cases} \tag{15}$$

The choice of sign is forced by the positivity of q' for $|k| > V$, while q is left undetermined. Thus the classical theory predicts instability of all modes, for $\varepsilon = 0$.

Now suppose $\varepsilon > 0$. Eliminate q and q' between (12) and (13) and between (13) and (14) to get

$$q' = q + V \tag{16}$$

$$q = -\varepsilon k^2 + |k|\sqrt{1 - V\varepsilon + \varepsilon^2 k^2}. \tag{17}$$

Observe that Req can be positive for all k only if $V\varepsilon < 1$. Thus the classical theory *exists* only for $V\varepsilon < 1$. The growth factor is given, from (12), by

$$y_1 = q(q + V) - k^2 \tag{18}$$

$$= 2\varepsilon k^2(\varepsilon k^2 - V) + (V - 2\varepsilon k^2)|k|\sqrt{1 - V\varepsilon + \varepsilon^2 k^2}. \tag{19}$$

Asymptotically,

$$y_1 \sim \begin{cases} \sqrt{1 - V\varepsilon}\, V|k| & \text{as } k \to 0 \\ -k^2 & \text{as } k \to \infty. \end{cases} \tag{20}$$

Thus the classical theory predicts the stabilization of short waves by curvature-dependence. Of course this prediction applies, strictly speaking, only to those perturbations of the form (7) with q, q', and k related by (12-14). Nevertheless, its qualitative features will reappear in the exact theory of Section 2.3, suitably modified to handle transient effects due to the initial temperature gradients q and q' and extended to include anisotropy and velocity-dependence.

2. The integral equation and linear stability theory

2.1. Introduction

Chapter 2 contains analysis preliminary to the numerical methods developed in Chapters 3 and 4. After recalling the moving boundary problem, we use heat potential theory to convert it to a singular integral equation for the interface alone. The integral equation is then used to carry out a linear stability analysis of the planar constant-speed solution. This analysis shows that the curvature-dependence of the Gibbs-Thomson relation removes the high-wavenumber instability of the classical supercooled Stefan problem and leaves only a finite band of low-wavenumber unstable modes. Velocity-dependence has a further smoothing effect. These conclusions can be expected to apply more generally, because a planar constant-speed front is the first term in a Taylor expansion of a general front, and is therefore generic (as a first approximation). The analysis also allows us to calculate consistent initial temperature fields for small perturbations of a flat initial interface; these are used in the numerical experiments of Chapters 3 and 4.

2.2. The integral equation formulation

We are working with the moving boundary problem

$$\begin{aligned}
\partial_t u &= \Delta u && \text{on } \Omega(t) \\
\partial_t u &= \Delta u && \text{on } \tilde{\Omega}(t) \\
\left[\frac{\partial u}{\partial \nu}\right] &= -V && \text{on } \Gamma(t) \\
-u &= \varepsilon_C C + \varepsilon_V V && \text{on } \Gamma(t) \\
u &\to u_\infty && \text{at } \infty \text{ in each phase} \\
u &= u_0 && \text{at } t = 0.
\end{aligned} \tag{1}$$

The notation is as follows:

Δ	is the Laplacian $\partial_x^2 + \partial_y^2$,
$\Omega(t)$	is the solid phase at time t,
$\tilde{\Omega}(t)$	is its complement, the liquid phase,
u_∞	is the temperature at ∞ in each phase,
$\nu = (\cos\phi, \sin\phi)$	is the outward unit normal to $\Omega(t)$,
$[\ ]$	denotes the difference between liquid and solid phase values,
$\Gamma(t)$	is the boundary between $\Omega(t)$ and $\tilde{\Omega}(t)$,
V	is its normal velocity, positive if liquid is freezing,

C is its curvature, positive where the solid is convex, and

ϕ is the angle between ν and the y-axis.

In the Gibbs-Thomson relation, we take anisotropic material parameters

$$\varepsilon_C(\phi) = \varepsilon_C(1 - A\cos k_A\phi)$$
$$\varepsilon_V(\phi) = \varepsilon_V(1 - A\cos k_A\phi)$$

where ε_C and ε_V are positive constants much less than unity, A is a constant between 0 and 1, and k_A is a small integer describing the crystalline anisotropy of the substance under consideration.

In this section, we transform the moving boundary problem (1) to a singular integral equation (2) involving only $\Gamma(t)$ and the initial temperature field u_0. Supercooling is present in (2) only through the consistency requirement that $u_0 \to u_\infty$ at infinity. The procedure is straightforward. We use the free-space heat kernel

$$K(\underline{x},t) = \frac{e^{-\|\underline{x}\|^2/4t}}{(4\pi t)^{n/2}} \qquad x \in \mathbb{R}^2, t > 0,$$

to express u in each phase as the sum of single, double and initial layer heat potentials with densities $\frac{\partial u}{\partial \nu}$, u and u_0 respectively. We use a jump formula for the double layer potential to evaluate each expression on $\Gamma(t)$ and add the results. This procedure produces the integral equation

$$\varepsilon_C C + \varepsilon_V V + U(\underline{x},T) + \int_0^T \int_{\Gamma(t)} K(\underline{x}-\underline{x}',T-t)V(\underline{x}',t)dx'dt = 0 \tag{2}$$

to hold for $\underline{x}$ on $\Gamma(T)$. Here U is the free solution of the heat equation with initial data u_0;

$$U(\underline{x},T) = K * u_0(\underline{x},T) = \int_{\mathbb{R}^2} K(\underline{x}-\underline{x}',T)u_0(\underline{x}')dx',$$

$*$ denotes convolution, and dx' denotes the element of integration on $\Gamma(t)$. This equation possesses nearly every possible complication: it is nonlinear (though quasilinear), history-dependent (through the dependence of SV on the previous history of the interface), and includes derivatives as well as integration over the curve. The Gibbs-Thomson relation produces a term resembling a nonlinear heat equation (for a parametrization of $\Gamma(t)$), while the release of latent heat generates the singular integro-differential term SV, which is nonlinear and history-dependent as well. The initial temperature field term U is merely a nonlinear forcing term, which adds little complexity by comparison.

Here are the details: Let $T > 0$ be fixed, and let $\underline{x}$ lie in $\Omega(T)$. Fix $\delta > 0$ and put

$$f(\underline{x}',t) = K(\underline{x}-\underline{x}',T-t+\delta).$$

Let Ω_T be the product set

$$\Omega_T = \prod_0^T \Omega(t).$$

Then the Green identity [56] implies that

$$\int_{\Omega_T} u\Delta f - f\Delta u = \int_0^T \int_{\Gamma(t)} u\frac{\partial f}{\partial \nu} - f\frac{\partial u}{\partial \nu}$$

and the divergence theorem on Ω_T reads

$$\int_{\Omega_T} \partial_t(fu) = \int_{\partial\Omega_T} fun_t.$$

Here n_t is the time component of the outward unit normal to Ω_T, considered as a subset of $\mathbb{R}^2\times\mathbb{R}^+$;

$$n_t = \begin{cases} 1 & t=T & \underline{x}\in\Omega(T) \\ -1 & t=0 & \underline{x}\in\Omega(0) \\ \dfrac{-V}{\sqrt{1+V^2}} & 0<t<T & \underline{x}\in\Gamma(t) \end{cases}$$

Add these two formulas, use the backward heat equation satisfied by f, and take the limit $\delta\to 0$ to get

$$u(\underline{x},T) = \int_{\Omega(0)} f\,u_0 - \int_0^T\int_{\Gamma(t)} f\,u\,n_t - f\frac{\partial u}{\partial \nu} + u\frac{\partial f}{\partial \nu} \tag{3}$$

for $\underline{x}$ in $\Omega(T)$. Repeat the calculation for the liquid phase; only the sign of the double integral changes;

$$u(\underline{x},T) = \int_{\tilde{\Omega}(0)} f\,u_0 + \int_0^T\int_{\Gamma(t)} f\,u\,n_t - f\frac{\partial u}{\partial \nu} + u\frac{\partial f}{\partial \nu} \tag{4}$$

for $\underline{x}$ in $\tilde{\Omega}(T)$. Now we need a jump formula for the double layer heat potential D defined by

$$Dg(\underline{x},T) = \int_0^T\int_{\Gamma(t)} g(\underline{x}',t)\frac{\partial K}{\partial \nu}(\underline{x}-\underline{x}',T-t)dx'dt;$$

Dg is discontinuous across $\Gamma(T)$. For $\Gamma(t)$ smooth, it is shown formally in [98] that

$$[Dg](\underline{x},T) = g(\underline{x},T)$$

for $\underline{x}$ on $\Gamma(T)$. A detailed proof for $\Gamma(T)$ independent of T appears in Fabes & Riviere [32]; they use a Fourier transform in the time variable to reduce it to potential theory for the Laplace equation [37] in which the jump condition is well-known. This case is easier than ours because there is no motion of the boundary: The Fourier transform approach fails at the first step when the boundary moves with time. A proof for $\Gamma(T)$ time-dependent is found in Gevrey [40] for $n = 1$. Apparently no proof of the jump formula with $\Gamma(t)$ time-dependent has been published for $n > 1$, so we will simply assume it as plausible here, on the basis of the formal argument presented in [98].

Thus apply the jump formula to evaluate the expressions (3) and (4) for u on $\Gamma(t)$ and add the results to get

$$u(\underline{x},T) = \int_{\mathbb{R}^2} K(\underline{x}-\underline{x}',T-t)u_0(\underline{x}') - \int_0^T\int_{\Gamma(t)} K(\underline{x}-\underline{x}',T-t)\left[\frac{\partial u}{\partial \nu}\right]dx'dt$$

for $\underline{x}$ on $\Gamma(T)$. The boundary conditions now imply (2):

$$\varepsilon_C C + \varepsilon_V V + U(\underline{x},T) + \int_0^T \int_{\Gamma(t)} K(\underline{x}-\underline{x}',T-t)V(\underline{x}',t)dx'dt = 0, \tag{5}$$

for $\underline{x}$ on $\Gamma(T)$.

Remarks: 1. Although K has a $\frac{1}{T-t}$ singularity at $t=T$, the actual singularity of the integrand in the time integral is mollified to a square root by integration over the curve. To see this, we compute the asymptotic behavior of the curve integral as $t \to T$. Parametrize $\Gamma(t)$ by $\underline{x}(t,s)$, and let $\underline{x} = \underline{x}(S,T) \in \Gamma(T)$. Then $dx' = \sqrt{x_s^2 + y_s^2}ds$ and

$$\int_{\Gamma(t)} K(\underline{x}-\underline{x}',T-t)V(\underline{x}',t)dx' = \int_{-\infty}^{\infty} K(\underline{x}-\underline{x}',T-t)V(s,t)\sqrt{x_s^2+y_s^2}ds.$$

It is easy to see that only a neighborhood of the singularity contributes, because K decays exponentially in the spatial variables. But in a small enough neighborhood of the singularity, the Taylor expansion

$$\|\underline{x}(S,T)-\underline{x}(s,t)\|^2 = (S-s)^2(x_s^2+y_s^2) + \|\underline{x}(S,T)-\underline{x}(S,t)\|^2 + \cdots$$

holds with a negligible error. The second term, exponentiated, gives a s-independent factor in the integrand, the first a Gaussian integral. The result is therefore

$$\int_{\Gamma(t)} K(\underline{x}-\underline{x}',T-t)V(\underline{x}',t)dx' \sim K(\|\underline{x}(S,T)-\underline{x}(S,t)\|,T-t)V(S,t) \quad \text{as} \quad t' \to t, \tag{6}$$

where on the right-hand side K denotes the one-space-dimensional heat kernel.

2. To simplify the notation, introduce the single layer potential

$$SV(\underline{x},T) = \int_0^T \int_{\Gamma(t)} K(\underline{x}-\underline{x}',T-t)V(\underline{x}',t)dx'dt \tag{7}$$

and write the integral equation as

$$\varepsilon_C C + U(\underline{x},T) + (\varepsilon_V + S)V = 0. \tag{8}$$

As an integral equation for V, this is of the second kind when $\varepsilon_V \neq 0$. Since first-kind equations with compact operators (as is S) are notoriously hard to solve, we expect velocity-dependence to make the solution of the integral equation easier. Taking $\varepsilon_V \neq 0$ can even be thought of as a physically motivated *regularization* of the $\varepsilon_V = 0$ problem. The velocity is therefore given in terms of $\Gamma(t)$ by

$$V = -(\varepsilon_V + S)^{-1}(\varepsilon_C C + U),$$

if $\varepsilon_V + S$ is invertible in an appropriate function space. Fabes & Riviere [31] show, for $\Gamma(t)$ independent of t, that S is smoothing of order 1 in space and order 1/2 in time: If g is in L^p on the set

$$\Gamma_T = \prod_0^T \Gamma(t),$$

then Sg has one space derivative in $L^p(\Gamma_T)$ and — in a sense we shan't make precise — half a time derivative in $L^p(\Gamma_T)$. They also show that $\varepsilon_V + S$ is invertible on $L^p(\Gamma_T)$ if and only if $\varepsilon_V \neq 0$. If ε_V vanishes, therefore, V loses one derivative's worth of spatial regularity. Hence non-trivial velocity-dependence in the Gibbs-Thomson relation exerts a substantial smoothing effect on the interfacial velocity.

2.3. Linear stability theory

The integral equation (2.2.5) has an exact solution for which the interface is a straight line moving in the positive y-direction with velocity V. Thus $\Gamma(t)$ is parametrized by

$$x(t,s) = s \qquad (1)$$
$$y(t,s) = Vt$$

as s runs over the real line. The corresponding temperature field has the similarity form

$$u(x,y,t) = u_0(y - Vt) \qquad (2)$$

with

$$u_0(y) = \begin{cases} e^{-Vy} - 1 - \varepsilon_V V & y > 0 \\ -\varepsilon_V V & y \leq 0. \end{cases} \qquad (3)$$

Here ε_V is evaluated at its minimum, $\phi = 0$.

We compute the evolution of a small perturbation to the initial interface, subject to a small perturbation of the initial temperature field, within the framework of linear stability theory. Thus we ignore terms above first order in the perturbation amplitude δ.

Thus begin with an initial interface parametrized by

$$x(0,s) = s$$
$$y(0,s) = \delta y_1(0,s).$$

(We don't need to perturb $x(0,s)$, because imposing the arclength constraint $x_s^2 + y_s^2 = 1$ to first order would eliminate the x-perturbation anyway.) Make a perturbation $\delta u_1(x,y)$ of the initial temperature field $u_0(y)$, and let the resulting interface be parametrized by

$$x(t,s) = s + O(\delta^2)$$
$$y(t,s) = Vt + \delta y_1(t,s) + O(\delta^2).$$

We assume here that $\Gamma(t)$ remains the graph of a function $y(t,x)$. Since linear stability theory is a short-time paradigm, and the initial interface is a graph, this is a reasonable assumption. To first order in δ, the curvature and normal velocity are

$$C = -\partial_s^2 \delta y_1 \qquad (4)$$
$$V(t,s) = V + \partial_t \delta y_1(t,s)$$

and the perturbed forcing term U in the integral equation is

$$U(s, Vt + \delta y_1, t) = U_0(Vt,t) + \delta y_1 \partial_y U_0(Vt,t) + \delta U_1(s, Vt, t) \qquad (5)$$

Here U_0 is the unperturbed free temperature field

$$U_0(y,t) = \frac{1}{2}e^{-y^2/4t}\left[\operatorname{erfce}\left[\frac{2Vt-y}{\sqrt{4t}}\right] - \operatorname{erfce}\left[\frac{-y}{\sqrt{4t}}\right]\right] - \varepsilon_V V, \tag{6}$$

where erfce is the exponentially scaled complementary error function

$$\operatorname{erfce}(z) = \frac{2}{\sqrt{\pi}}e^{z^2}\int_z^\infty e^{-y^2}dy,$$

and

$$U_1(s,y,t) = K * u_1(s,y,t) \tag{7}$$

is the free temperature field due to u_1. Substitute (4) and (5) into the integral equation, drop terms above first order in δ, and use the unperturbed equation to cancel zero order terms. The result is the linear stability equation

$$\begin{aligned}(\varepsilon_V\partial_t - \varepsilon_C\partial_s^2)y_1(t,s) + y_1\partial_s U_0(s,t) + U_1(s,Vt,t) + \\ + V\int_0^t\int(y_1-y_1')K(s-s',t-t')\partial_y K(V(t-t'),t-t')ds'dt' + \\ + \int_0^t\int K(s-s',t-t')K(V(t-t'),t-t')\partial_t y_1' ds'dt' = 0.\end{aligned} \tag{8}$$

Here ε_C and ε_V are evaluated at $\phi = 0$, or equivalently contain a factor $1-A$.

Exponentials are eigenfunctions of the heat kernel, so (by a Fourier transform) it is enough to consider initial temperature field perturbations of the form

$$u_1(x,y) = f(y)e^{ikx}$$

and resulting interfacial perturbations of the form

$$y_1(t,s) = g(t)e^{iks}.$$

Then g satisfies the reduced equation

$$(2\varepsilon_V\partial_t + 2\varepsilon_C k^2 - V)g(t) + \int_0^t \frac{e^{-(k^2+V^2/4)(t-s)}}{\sqrt{\pi(t-s)}}(\partial_s + \frac{V^2}{2})g(s)ds = e^{-(k^2+V^2/4)t}F(t), \tag{9}$$

where

$$F(t) = -2e^{V^2t/4}K * f(Vt,t). \tag{10}$$

The change of unknown function

$$G(t) = e^{(k^2+V^2/4)t}g(t) \tag{11}$$

produces a fractional differential equation

$$[cD + b + D^{-1/2}(D-a)]G(t) = F(t), \tag{12}$$

with constant coefficients

$$a = k^2 - V^2/4$$

$$b = 2\varepsilon_c k^2 - V - 2\varepsilon_v k^2 - \varepsilon_v \frac{V^2}{2} \tag{13}$$

$$c = 2\varepsilon_v$$

Here $D = \partial_t$ and $D^{-1/2}$ is the Riemann-Liouville fractional integral [48, 68] defined by

$$D^{-1/2}G(t) = \int_0^t \frac{g(s)}{\sqrt{\pi(t-s)}} ds. \tag{14}$$

It has the following useful properties, for smooth G;

$$D^{-1/2}D^{-1/2}G(t) = D^{-1}G(t) = \int_0^t G(s)ds \tag{15a}$$

$$DD^{-1/2}G(t) = D^{1/2}G(t) = \frac{G(0)}{\sqrt{\pi t}} + D^{-1/2}DG(t) \tag{15b}$$

$$D^{-1/2}(f * g) = (D^{-1/2}f) * g = f * (D^{-1/2}g), \tag{15c}$$

where $*$ denotes the finite convolution

$$f * g(t) = \int_0^t f(t-s)g(s)ds.$$

The fractional differential equation (12) can be solved explicitly if we take f of the form

$$f(y) = \begin{cases} u_0' e^{-q'y} & y > 0 \\ u_0 e^{-qy} & y < 0 \end{cases} \tag{16}$$

with q and q' positive. By a Laplace transform, this implies the solution for the general case. F then becomes

$$F(t) = -u_0' \mathrm{erfce}(p'\sqrt{t}) - u_0 \mathrm{erfce}(p\sqrt{t}) \tag{17}$$

with $p = q + V/2, p' = q' - V/2$. If $G(p,t)$ is the solution corresponding to $u_0 = -1$, $u_0' = 0$, then G is given by

$$G(t) = -u_0 G(p,t) - u_0' G(p',t)$$

Thus it suffices to consider

$$F(t) = \mathrm{erfce}(p\sqrt{t}) = (1 - pD^{-1/2})e^{p^2 t}. \tag{18}$$

The second equality, derived by a change of variable, will greatly simplify the calculation.

We describe the solution of (12) before plunging into the details: We solve the $c = 0$ (no velocity dependence) case explicitly by "squaring" the operator in (12) to remove fractional derivatives. The result is an ordinary differential equation whose solution is asymptotically a linear combination of exponentials

$$g(t) \sim \sum_{i=1}^{2} g_i(k) e^{ty_i}.$$

Thus stability theory is reduced to the study of the exponents y_i and amplitudes $g_i(k)$. It turns out that y_1 is briefly positive for small k and then decays like $-k^2$ for large k. Unfortunately, $y_2 \sim k^4$ as $k \to \infty$, so it looks at first as though the interface is catastrophically unstable. However, a slight additional calculation reveals that $g_2(k)$ vanishes identically for k above a cutoff k_c. Thus the high-k instability is indeed stabilized by the introduction of curvature dependence in the Gibbs-Thomson relation, just as predicted by the classical theory. The same picture appears in the case $c > 0$ of nontrivial velocity dependence, except that y_i are now roots of a cubic rather than a quadratic. The algebra involved in exhibiting the cutoff directly becomes too formidable, but we present a calculation which effectively bounds the cutoff from above. This calculation exhibits the stabilizing effect of velocity-dependence: the cutoff k_c is lowered even further. The effects of anisotropy, on the other hand, are much easier to include in the analysis.

Here are the details: For $c = 0$, the linear stability equation (12) becomes

$$L^+G(t) = [b + D^{-1/2}(D-a)]G(t) = F(t), \tag{19}$$

and evaluation at $t = 0$ implies $bG(0) = F(0)$ if G is C^1. Apply the operator

$$L^- = b - D^{-1/2}(D-a),$$

the properties (15a) and (15b) of $D^{-1/2}$, and the second form (18) of F. The result is the *ordinary* differential equation

$$[b^2D - (D-a)^2]D^{-1}G(t) = a(G(0) + \frac{1}{p}) - \frac{1}{p}(a - bp - p^2)F(t), \tag{20}$$

with initial conditions

$$D^{-1}G(0) = 0 \qquad G(0) = \frac{1}{b}, \tag{21}$$

for the new unknown $D^{-1}G(t) = \int_0^t G(s)ds$. The solution is, by (15c),

$$G(t) = (\frac{D-a}{b} - \frac{a}{p})S(t) + \frac{1}{p}(a - bp - p^2)(1 - pD^{-1/2})T(t) \tag{22}$$

where

$$S(t) = \frac{e^{tx_1}}{x_1 - x_2} + (x_1 \leftarrow x_2)$$

$$T(t) = DS * e^{p^2t} = \frac{x_1}{x_1 - x_2}\frac{e^{p^2t} - e^{tx_1}}{p^2 - x_1} + (x_1 \leftarrow x_2)$$

Here $(x_1 \leftarrow x_2)$ stands for the previous term with x_1 and x_2 interchanged, and x_i are the roots of the quadratic

$$x^2 - (b^2 - 2a)x + a^2 = 0. \tag{23}$$

They are real, positive and distinct for $k^2 > V^2/4$.

As $t \to \infty$, integration by parts shows that

$$(1 - pD^{-1/2})e^{p^2t} \to 0 \tag{24}$$

$$(1-pD^{-1/2})e^{tx} \to 0 \qquad x < 0$$
$$(1-pD^{-1/2})e^{tx} \sim (1-\frac{p}{\sqrt{x}})e^{tx} \quad x > 0$$

Thus as $t \to \infty$,

$$g(t) = e^{-(k^2+V^2/4)t}G(t) \sim \sum_{i=1}^{2} \frac{(-1)^{i+1}}{x_1-x_2} G_i(k)e^{ty_i} \tag{25}$$

where $y_i = x_i - k^2 - V^2/4$ and

$$G_i(k) = \frac{x_i-a}{b} - \frac{a}{p} - \frac{1}{p}(a-bp-p^2)\frac{x_i-p\sqrt{x_i}}{p^2-x_i} = \frac{a-bp-p^2}{b(x_i-p^2)}(x_i-b\sqrt{x_i}-a).$$

Solve the quadratic to get

$$y_1 = \frac{1}{2}(b^2-V^2) - \frac{1}{2}|b|\sqrt{b^2+4a} \sim -k^2 \tag{26}$$
$$y_2 = \frac{1}{2}(b^2-V^2) + \frac{1}{2}|b|\sqrt{b^2+4a} \sim 4\varepsilon_c^2 k^4$$

as $k \to \infty$. Thus y_2 produces a catastrophic instability in which high-k modes grow fastest. However, the last factor in $G_2(k)$ is

$$x_2 - b\sqrt{x_2} - a = \frac{1}{2}(|b|-b)(\sqrt{b^2+4a}-b) = 0$$

for $b \geq 0$ or $2\varepsilon_c k^2 \geq V$. Thus the threatened instability is cut off by the vanishing of the coefficient of e^{ty_2} as soon as

$$k^2 \geq k_c^2 = \frac{V}{2\varepsilon_c}, \tag{27}$$

leaving only a finite band of low-k unstable modes for which y_1 is positive. Figure 1 displays typical dispersion relations $y_i(k)$, with the cut-off exponent y_2 dashed.

Now consider the case $c > 0$ of nontrivial velocity dependence. The linear stability equation is then

$$[cD + b + D^{-1/2}(D-a)]G(t) = F(t), \tag{28}$$

and evaluation at $t = 0$ requires

$$cDG(0) + bG(0) = F(0).$$

This can be solved by squaring, as in the case $c = 0$, but the algebra becomes highly tedious; x_i satisfy a cubic instead of a quadratic, and explicit expressions for the roots are too cumbersome to allow evaluation of the cutoff. Thus we present the following calculation, which gives a simple upper bound for the cutoff, with the right qualitative behavior. The $c = 0$ case and experiments with squaring suggest the *ansatz*

$$G(t) = \sum_{i=1}^{3} A_i e^{tx_i} + B_i(1-pD^{-1/2})\frac{e^{p^2t}-e^{tx_i}}{p^2-x_i}, \tag{29}$$

where x_i, A_i and B_i are determined by substituting (29) into (28), equating coefficients of e^{tx_i}, $D^{-1/2}e^{tx_i}$, and $(1-pD^{-1/2})e^{p^2t}$, and requiring $G(t)=G_0$ at $t=0$. (Note that the specification $F(0)=1$ implicit in (18) determines $G(0)$, as in the case $c=0$.) This procedure results in a set of ten equations in the ten unknowns A_i, B_i, x_i and $G(0)$, linear in all the variables except x_i. For our purposes, we need only the equations obtained by equating the coefficients of e^{tx_i} and $D^{-1/2}e^{tx_i}$. These are

$$(cx_i+b)A_i-\frac{cx_i+b-p(x_i-a)/x_i}{p^2-x_i}B_i=0 \tag{30}$$

$$(x_i-a)A_i+\frac{p(cx_i+b)-(x_i-a)}{p^2-x_i}B_i=0, \tag{31}$$

for $i=1,2$, and 3. Consistency of (30) and (31) requires that for each i we have

$$\begin{aligned}(cx_i+b)A_i &= \frac{1}{p^2-x_i}(cx_i+b-\frac{p}{x_i}(x_i-a))B_i \\ &= -\frac{cx_i+b}{x_i-a}\,\frac{p(cx_i+b)-(x_i-a)}{p^2-x_i}B_i.\end{aligned} \tag{32}$$

This implies that x_i are the roots of the cubic

$$(cx+b)^2x-(x-a)^2=0; \tag{33}$$

they have positive real parts since

$$\operatorname{Re} x=\operatorname{Re}\left[\frac{x-a}{cx+b}\right]^2>0.$$

Using this in the second equation in (32) gives

$$\frac{A_i}{B_i}=\frac{1}{p^2-x_i}[1-p\frac{cx_i+b}{x_i-a}] = \frac{-\sigma}{\sqrt{x_i}(p+\sigma\sqrt{x_i})} \tag{34}$$

where $\sigma=\operatorname{sgn}(\frac{cx_i+b}{x_i-a})$. This is all we need to analyze linear stability in the limit $t\to\infty$. Indeed, (29) implies that

$$g(t)\sim\sum_{i=1}^{3}G_i(k)e^{ty_i} \tag{35}$$

as $t\to\infty$. Here $y_i=x_i-k^2-V^2/4$ and

$$G_i=B_i(\frac{A_i}{B_i}-\frac{1-p/\sqrt{x_i}}{p^2-x_i}). \tag{36}$$

But (34) shows that G_i is proportional to

$$\frac{-\sigma}{\sqrt{x_i}(p+\sigma x_i)}+\frac{1}{\sqrt{x_i}(p+\sqrt{x_i})}$$

which vanishes whenever $\sigma > 0$. Instability of g requires $y_i > 0$, so $x_i - a > V^2/2 > 0$ and

$$\sigma = \mathrm{sign}(cx_i + b).$$

Hence any instability is cut off by the vanishing of its coefficient whenever k exceeds the critical value k_c given by $cx_i(k_c) + b(k_c) = 0$. We can bound k_c from above by omitting the positive term $cx_i(k_c)$ to get

$$k_c^2 \leq \frac{V(1-\varepsilon_V V/2)}{2(\varepsilon_C + \varepsilon_V)}. \tag{37}$$

This agrees with the $\varepsilon_V = 0$ result

$$k_c^2 = \frac{V}{2\varepsilon_C}, \tag{38}$$

as it should.

To summarize, linear stability analysis of the (approximately generic) planar constant-speed solution shows that the curvature-dependent Gibbs-Thomson relation replaces the catastrophic small-scale instability of the classical Stefan problem for supercooled water by a finite band of small-k unstable modes. Velocity dependence further narrows this band. Anisotropy tends to destabilize the situation, replacing ε_C and ε_V by $(1-A)\varepsilon_C$ and $(1-A)\varepsilon_V$.

Note also that the integral equation approach gives results which agree with the classical theory *only* in the long-time limit. The relevance of this limit is not clear *a priori* , because linear stability theory is a small-amplitude paradigm, and both calculations indicate that some modes are almost always growing. Thus the theory may well break down long before the long-time limit is approached; if this happens, the classical theory would be invalidated, but the new theory would not.

3. Numerical Methods for Periodic Graphs

3.1. Introduction

This chapter contains a numerical method for computing the moving boundary $\Gamma(t)$ when it is representable as the graph $\{x = s, y = y(t,s) \mid -\infty < s < \infty\}$ of a 2π-periodic function $y(t,x)$ of x. Thus we compute an infinite periodic array of dendritic structures. After specializing the integral equation formulation to such a periodic graph, we discretize the curve, replacing it by a set of points. This produces a consistency condition on the time and space step sizes Δt and Δs. Then we present a heuristic analysis which exhibits the importance of the high-wavenumber behavior of the curvature approximation. The interface can be destabilized by a local curvature discretization if Δs is too large; we use the finite Fourier transform to construct a discretization of curvature which avoids this difficulty.

We discretize the problem in time next, working first with the planar case, when the interface is a straight line, for simplicity of analysis. After using the insights gained from the planar case to discretize the full periodic equation of motion, we present numerical results which demonstrate first-order accuracy of the method and agree with the linear stability theory presented in Section 2.3. Our results disagree with the classical theory, because of transient effects due to the initial temperature field.

Working first with periodic graphs allows us to learn how to compute the velocity without worrying about the complications of moving a general curve; the latter are reserved for Chapter 4. In general, we study each part of our method in a simple situation where analysis is easy.

3.2. The periodic graph equation of motion

In Chapter 2, we derived the integral (actually nonlinear history-dependent partial integro-differential) equation (2.2.5)

$$\varepsilon_C C + \varepsilon_V V + U(\underline{x},t) + \int_0^t \int_{\Gamma(t')} K(\underline{x}-\underline{x}', t-t') V(\underline{x}', t') dx' dt' = 0 \tag{1}$$

for a parametrization $\underline{x} = \underline{x}(t,s)$ of $\Gamma(t)$. Primes denote evaluation at primed variables, and dx' is the element of integration on $\Gamma(t')$. While $\Gamma(t)$ remains a periodic graph, we can work with the special parametrization

$$x = s$$

$$y = y(t,s)$$

where y is 2π-periodic in s. Then the curvature, normal velocity, and element of arclength are given by [18, 106]

$$C = -\partial_s \frac{y_s}{\sqrt{1+y_s^2}}, \tag{2}$$

$$V = \frac{\partial_t y}{\sqrt{1+y_s^2}}, \tag{3}$$

and

$$dx' = \sqrt{1+y_s^2}\,ds'.$$

Periodicity makes numerical methods simpler by restricting the variable s to a finite interval. Indeed, if y is 2π-periodic then

$$\int_{-\infty}^{\infty} K(s-s',y-y',t-t')\partial_t y'ds' = \sum_{-\infty}^{\infty}\int_{-\pi}^{\pi} K(s-(2n\pi+s'),y-y',t-t')\partial_t y'ds'$$

$$= \int_{-\pi}^{\pi} \Theta(s-s',t-t')K(y-y',t-t')\partial_t y'ds',$$

where Θ is the Jacobi theta function [30, 107] or periodic heat kernel [95, 56] defined by

$$\Theta(s,t) = \sum_{-\infty}^{\infty} K(s+2n\pi,t) \tag{4}$$

and K is now the one-dimensional Gauss kernel. Thus the integral equation becomes

$$\varepsilon_C C + \varepsilon_V V + U(\underline{x},t) + \int_0^t \int_{-\pi}^{\pi} \Theta(s-s',t-t')K(y-y',t-t')\partial_t y'ds'dt' = 0, \tag{5}$$

to hold for $-\pi \le s \le \pi$, with periodic boundary conditions.

The elementary properties of the theta function which we shall need all flow from the Poisson summation formula [30]. As an example, we derive an efficient algorithm for evaluating Θ numerically. The sum (4) converges very fast for small t, since then

$$K(x,t) = \frac{e^{-x^2/4t}}{\sqrt{4\pi t}} \tag{6}$$

decays very fast as $x \to \infty$. For t large, however, convergence is extremely slow. Thus we use the Poisson summation formula

$$\sum_{-\infty}^{\infty} f(k) = \sum_{-\infty}^{\infty} \hat{f}(k)$$

to transform the sum (4) defining Θ. Here $\hat{f}$ denotes the Fourier transform

$$\hat{f}(k) = \int_{-\infty}^{\infty} e^{2\pi ikx} f(x)dx,$$

so that for each fixed t, evaluation of a Gaussian integral gives

$$\hat{K}(k,t) = \frac{1}{2\pi} e^{-tk^2}.$$

Hence Θ is also given by

$$\Theta(s,t) = \frac{1}{2\pi}\sum_{-\infty}^{\infty} e^{iks} e^{-k^2 t}, \tag{7}$$

which is its Fourier series representation. The error in truncating the series (7) after terms with

$|k| = N-1$

can be bounded by a geometric series; we have

$$\left|\frac{1}{2\pi}\sum_{|k|\geq N} e^{-k^2t}e^{iks}\right| \leq \frac{1}{\pi}\sum_{N}^{\infty} e^{-Nkt} = \frac{1}{\pi}\frac{e^{-N^2t}}{1-e^{-Nt}}.$$

Similarly, for $|s| \leq 2\pi$ and $|n| \geq N+1$, we have $(s+2n\pi)^2 \geq 4\pi^2 N(|n|-1)$: Hence the error in truncating (4) after terms with $|n| = N$ is bounded by

$$\frac{1}{\sqrt{4\pi t}}\sum_{|n|\geq N+1} e^{-(s+2n\pi)^2/4t} \leq \frac{1}{\sqrt{\pi t}}\sum_{n=N+1}^{\infty} e^{-\pi^2 N(n-1)/t}$$

$$= \frac{1}{\sqrt{\pi t}}\frac{e^{-\pi^2N^2/t}}{1-e^{-\pi^2N/t}}.$$

The two error bounds are equal when $t = \pi$, which suggests the following

Algorithm: (8)

if $t \leq \pi$ then

$$\Theta(s,t) \cong \frac{1}{\sqrt{4\pi t}}\sum_{-N}^{N} e^{-(s-2\pi k)^2/4t}$$

else if $t > \pi$ then

$$\Theta(s,t) \cong \frac{1}{2\pi}(1 + 2\sum_{1}^{N}\cos(ks)e^{-k^2t}).$$

Its absolute error is bounded by

$$\frac{1}{\sqrt{\pi}}\frac{e^{-\pi N^2}}{1-e^{-\pi N}}\frac{1}{\sqrt{\min(t,\pi)}},$$

which is less than $3\cdot 10^{-11}$ for $t > 10^{-4}$ and $N = 3$. Thus Θ can be evaluated at the cost of half a dozen exponentials or trigonometric functions, with enough accuracy for our purposes. This is important, because the major cost of our numerical method will be evaluation of the single layer potential, which requires many evaluations of Θ.

3.3. Curve discretization

In this section, we discretize the periodic integral equation (3.2.5) in the spatial variable s to produce a semidiscrete equation of motion. Let $s_j = j\Delta s = j\pi/J$ with $-J \leq j \leq J$, and let $y_j(t)$ approximate $y(t,s_j)$. Replace C and V by

$$C_j = -D\frac{Dy_j}{\sqrt{1+Dy_j^2}} \tag{1}$$

$$V_j = \frac{\partial_t y_j}{\sqrt{1+Dy_j^2}} \tag{2}$$

where D is a discrete approximation of ∂_s, left unspecified for the moment.

Next, replace the s'-integral by a numerical integration rule. Because of periodicity, the trapezoidal rule is attractive. But $\Theta(s,t)$ becomes a point mass $\delta(s)$ as $t \to 0$, so we cannot use a trapezoidal sum all the way up to $t' = t$. Hence we study the error in the trapezoidal rule approximation to the convolution $\Theta * g$;

$$\frac{\pi}{J}\sum_{-J}^{J}{}' \Theta(s-s_j,t)g(s_j) \cong \Theta * g(s,t) = \int_{-\pi}^{\pi} \Theta(s-s',t)g(s')ds'. \tag{3}$$

Here J is a positive integer, $s_j = j\Delta s = j\pi/J$, and the prime on the sum means that the first and last terms of the sum are halved.

By a Fourier series expansion, it is enough to analyze the error for exponentials $g(s) = e^{iks}$ with integer wavenumber k. Then by the geometric series formula

$$\frac{\pi}{J}\sum_{-J}^{J}{}' e^{iks_j} = \begin{cases} 2\pi & k \equiv 0 (\mathrm{mod}\ 2J) \\ 0 & \text{otherwise,} \end{cases}$$

the trapezoidal approximation (3) becomes

$$\frac{\pi}{J}\sum_{-J}^{J}{}' \Theta(s-s_j,t)e^{iks_j} = \frac{1}{2\pi}\sum_{-\infty}^{\infty} e^{-n^2t}e^{ins}\,\frac{\pi}{J}\sum_{-J}^{J}{}' e^{i(k-n)s_j} \tag{4}$$

$$= e^{iks}(e^{-k^2t} + \sum_{n\neq 0} e^{-(k+2Jn)^2t}). \tag{5}$$

Rearranging the exponents shows that (5) is equal to

$$e^{-k^2t}e^{iks}2\pi\,\Theta(2J(s+ikt),4J^2t) = \Theta * g(s,t) + O(e^{-4J^2t}) \qquad \text{as } J^2t \to \infty, \tag{6}$$

$$= O\left(\frac{1}{\sqrt{J^2t}}\right) \qquad \text{as } J^2t \to 0. \tag{7}$$

Thus the trapezoidal sum approximates $\Theta * g$ with an error which decays exponentially as $J^2t \to \infty$, but blows up like $\frac{1}{\sqrt{J^2t}}$ as $J^2t \to 0$. Hence we can use the trapezoidal rule up to a time cutoff Δt away from $t' = t$, if we arrange to have $J^2\Delta t \to \infty$ as the mesh size and cutoff are refined.

Now we return to our real interest, the integral

$$\int_{-\pi}^{\pi} K(y-y',t-t')\Theta(s-s',t-t')\partial_t y(s',t')ds'. \tag{8}$$

The previous analysis suggests the following procedure: Approximate (8) by the trapezoidal rule for $t' < t-\Delta t$, for some cutoff Δt. For $t' \geq t-\Delta t$, replace (8) by its asymptotic value (2.2.6);

$$\int_{-\pi}^{\pi} K(y-y',t-t')\Theta(s-s',t-t')\partial_t y(s',t')ds' \sim K(y(t,s)-y(t',s),t-t')\partial_t y(t',s)$$

as $t' \to t$.

Finally, substitute the discrete curvature and velocity (1) and (2) and this approximation of the s'-integral (8) into the periodic graph equation of motion (3.2.5) to get the semidiscrete

equation of motion

$$\varepsilon_c C_j + \varepsilon_v V_j + U(s_j, y_j, t) + \tag{9}$$
$$+ \int_0^{t-\Delta t} \Delta s \sum_{-J}^{J}{}' \Theta(s_j - s_k, t-t') K(y_j - y_k', t-t') \partial_t y_k' dt'$$
$$+ \int_{t-\Delta t}^{t} K(y_j - y_j', t-t') \partial_t y_j' dt' = 0$$

Consistency requires that $J^2 \Delta t \to \infty$ as $J \to \infty$, $\Delta t \to 0$. We usually satisfy this condition by setting $J \Delta t = 1$.

3.4. Curvature discretization and linear stability

In this section, we analyze the effect of curvature discretization on the linear stability of the interface, and thereby construct an appropriate curvature approximation.

Let $\varepsilon_v = 0$ for ease of calculation, so the semidiscrete equation is

$$\varepsilon_c C_j + U(s_j, y_j, t) + \tag{1}$$
$$+ \int_0^{t-\Delta t} \Delta s \sum_{-J}^{J}{}' \Theta(s_j - s_k, t-t') K(y_j - y_k', t-t') \partial_t y_k' dt'$$
$$+ \int_{t-\Delta t}^{t} K(y_j - y_j', t-t') \partial_t y_j' dt' = 0.$$

The exact planar constant-speed solution (Section 2.3) is

$$y(t, s) = Vt \tag{2}$$

with forcing term

$$U(y, t) = \frac{1}{2} e^{-y^2/4t} \left[\operatorname{erfce}\left[\frac{2Vt - y}{\sqrt{4t}} \right] - \operatorname{erfce}\left[\frac{-y}{\sqrt{4t}} \right] \right]. \tag{3}$$

This solution satisfies the semidiscrete equation (1) up to a residual R satisfying

$$0 < R = \int_0^{t-\Delta t} K(V(t-t'), t-t') V \left[\Delta s \sum_{-J}^{J}{}' \Theta(s_j - s_k, t-t') - 1 \right] dt' \tag{4}$$
$$= 2V \sum_1^{\infty} e^{-4J^2 n^2 \Delta t} \int_0^{\infty} K(Vs, s) ds$$
$$= O(e^{-4J^2 \Delta t})$$

as $J^2 \Delta t \to \infty$. In this section, we ignore errors of exponential order in $J^2 \Delta t$, assuming $J^2 \Delta t$ is fairly large. Because these errors are precisely those due to numerical integration over the curve, this is equivalent to studying the exact periodic graph equation (3.2.4) with curvature C replaced by

$$C_j = -D\frac{Dy_j}{\sqrt{1+Dy_j{}^2}}, \tag{5}$$

and not discretizing the curve itself. As in Section 2.3, consider a perturbation

$$u_0(x,y) = u_0(y) + \delta u_1(x,y)$$
$$y_j(t) = Vt + \delta y_j(t).$$

Let L be the linearized discrete curvature operator;

$$Ly_j = \lim_{\delta\to 0}\frac{C_j(\delta)-C_j(0)}{\delta} = -D^2 y_j, \tag{6}$$

so that

$$C_j = \delta L y_j + O(\delta^2)$$

as $\delta\to 0$. Then the linear stability equation is

$$\begin{aligned}&\varepsilon_c L y_j(t) + y_j(t)\partial_y U_0(Vt,t) + U_1(s_j,Vt,t) + \\ &+ \int_0^{t-\Delta t}\Delta s \sum_{-J}^{J}{}' K(V(t-t'),t-t')\left[\partial_t y_k{}' - \frac{V^2}{2}(y_j - y_k{}')\right]\Theta(s_j-s_k,t-t')dt' + \\ &+ \int_{t-\Delta t}^{t} K(V(t-t'),t-t')\left[\partial_t y_j{}' - \frac{V^2}{2}(y_j - y_j{}')\right]dt' = 0,\end{aligned} \tag{7}$$

where notation is as in Section 2.3. In the previous section, we saw that

$$\Delta s \sum_{-J}^{J}{}' e^{iks_j}\Theta(s_j-s_k,t) = e^{-k^2 t}e^{iks_j}(1 + O(e^{-4J^2 t})). \tag{8}$$

Therefore, if we consistently ignore terms of order $O(e^{-J^2\Delta t})$, we can still produce separated solutions of the form

$$u_1(x,y) = e^{ikx}f(y)$$
$$y_j(t) = e^{iks_j}g(t). \tag{9}$$

The reduced equation for g is then

$$(2\varepsilon_c\hat{L} - V)g(t) + \int_0^t \frac{e^{-(k^2+V^2/4)(t-s)}}{\sqrt{\pi(t-s)}}(\partial_s + \frac{V^2}{2})g(s)ds = F(t), \tag{10}$$

where F is given by (2.3.3) and $\hat{L}$ is the symbol of the linearized curvature operator L;

$$\hat{L} = e^{-iks_j}Le^{iks_j}$$

where L acts on s_j. This is the same as equation (2.3.9) in the exact theory, except that k^2 is replaced by $\hat{L}$ in the first term. Hence we can repeat the calculation of Section 2.3 to get a discrete exponent

$$y_1^- = 2\varepsilon_c\hat{L}(\varepsilon_c\hat{L} - V) + (V - 2\varepsilon_c\hat{L})\sqrt{k^2 + \varepsilon_c\hat{L}(\varepsilon_c\hat{L} - V)}, \tag{11}$$

The exact exponent, by comparison, is given by (2.3.26), restricted to integer k by 2π-periodicity:

$$y_1 = 2\varepsilon_c k^2(\varepsilon_c k^2 - V) + (V - 2\varepsilon_c k^2)\sqrt{k^2 + \varepsilon_c k^2(\varepsilon_c k^2 - V)}. \tag{12}$$

Almost any reasonable curvature approximation will have $\hat{L}(k) \to k^2$ and therefore $\tilde{y_1} \to y_1$, for each k, as $J \to \infty$. But finite difference approximations (even such sophisticated ones as those of [80]) to C typically represent low-k behavior of the exact symbol k^2 much better than high-k behavior. This causes trouble for $|k|$ near J.

Consider, for example, the simplest finite difference approximation to the curvature; let

$$C_j = -\frac{D_+ D_- y_j}{\left[1 + D_+ y_j{}^2\right]^{3/2}} \tag{13}$$

where $D_\pm$ are the usual (periodic) finite difference approximations to the derivative ∂_s. Then $L = -D_+ D_-$ and

$$\hat{L} = 4\frac{J^2}{\pi^2}\sin^2(\pi k/2J). \tag{14}$$

As $J \to \infty$, $\hat{L} \to k^2$ for any fixed k. However, for J fixed and ε_c of any reasonable size, the numerical and exact dispersion relations can have very different behavior for $|k|$ near J; see Figure 2(a). The finite difference approximation (13) can produce a catastrophic small-scale instability, if Δs is not small enough. This can be cured by taking a finer mesh, as in Figure 2(b). Nevertheless, this phenomenon reflects a rather unpleasant sensitivity to discretization of the supercooled Stefan problem, perhaps tending to confirm the misgivings of Chorin [21].

Thus it is essential to have a curvature approximation for which the linearized curvature operator has the right symbol k^2, or at least a symbol which — substituted into $\tilde{y}_1$ — damps those modes which should be damped. The simplest way to do this is to take

$$C_j = -D\frac{Dy_j}{\sqrt{1 + Dy_j{}^2}} \tag{15}$$

where D is designed to have symbol ik. Equivalently, C_j is the exact curvature of a trigonometric polynomial interpolating the points (s_j, y_j). To do this, represent y_j by the trapezoidal discrete Fourier transform [55]

$$y_j = \frac{1}{\sqrt{2J}} \sum_{-J}^{J}{}' e^{ijs_k}\hat{y}_k \tag{16}$$

where

$$\hat{y}_k = \frac{1}{\sqrt{2J}} \sum_{-J}^{J}{}' e^{-iks_j} y_j. \tag{17}$$

Define D^α, for $\alpha = 1$ or 2, by requiring $\widehat{D^\alpha} = (ik)^\alpha$;

$$D^\alpha y_j = \frac{1}{\sqrt{2J}} \sum_{-J}^{J}{}' (ik)^\alpha e^{ijs_k}\hat{y}_k = \sum_{-J}^{J}{}' D^\alpha_{jk} y_k, \tag{18}$$

so that D^{α}_{jk} are the trapezoidal matrix elements of D^{α}. Some tedious algebra involving sums of finite geometric series shows that

$$\begin{aligned} D_{jk} &= \frac{(-1)^{j-k}}{2}\cot\left[\frac{(j-k)\pi}{2J}\right] && j \neq k \\ D_{jk} &= 0 && j = k \\ D^2_{jk} &= \frac{(-1)^{j-k+1}}{2}\csc^2\left[\frac{(j-k)\pi}{2J}\right] && j \neq k \\ D^2_{jk} &= -\frac{1}{6}(1 + 2J^2) && j = k. \end{aligned} \tag{19}$$

Now this method will have the right linearized behavior, if the consistency condition

$$J^2\Delta t \to \infty \qquad \text{as } J \to \infty,\ \Delta t \to 0 \tag{20}$$

is satisfied. To get a reasonable approximation to a given physical situation with a practical J, we will need to capture at least all growing modes. For $V\varepsilon_C \ll 1$,the exponent y_1 changes sign when $k^2 \cong \frac{V}{2\varepsilon_C}$, so we require $J \geq \sqrt{V/2\varepsilon_C}$ to get a reasonable approximation. Typical test parameters (see Chorin [21] or Sullivan *et al.* [99]) like $V = 1$, $\varepsilon_C = .01$ require $J \geq 7$ which is not hard to satisfy. Velocity dependence weakens this requirement, but a nonzero coefficient of anisotropy A makes it more stringent by replacing ε_C with $(1-A)\varepsilon_C$. Thus in general we need roughly

$$J^2 \geq \frac{V(1-(1-A)\varepsilon_V V/2}{2(1-A)(\varepsilon_C+\varepsilon_V)}$$

to capture all growing modes, assuming ε_C and ε_V are much smaller than unity.

3.5. Time discretization

So far we have discretized the spatial variable and found out how to get the right linearized behavior, if the consistency condition (3.4.20) is satisfied. Now we discretize the time variable.

It is helpful to begin with the planar case, i.e. with the periodic graph equation specialized to $y(t,s)$ independent of s;

$$\varepsilon_V \partial_t y(t) + U(y(t),t) + \int_0^t K(y(t)-y(t'),t-t')\partial_t y(t')dt' = 0. \tag{1}$$

(Here ε_V is evaluated at $\phi = 0$.) Since curve discretization effects are not present, this allows us to study time discretization in a simpler environment than the full equation (3.3.9). A time discretization method which fails here can presumably be eliminated, though one which works here may still fail in the general case.

To produce a time discretization, replace y by a continuous piecewise linear approximation; let

$$y(t) \cong y^n + \frac{t-n\Delta t}{\Delta t}(y^{n+1}-y^n) = y^{n+\alpha} \qquad \text{for } n\Delta t < t = (n+\alpha)\Delta t \leq (n+1)\Delta t \tag{2}$$

and require (1) to hold at the mesh points $t = n\Delta t$. The resulting numerical equations are

$$\varepsilon_V \frac{y^n - y^{n-1}}{\Delta t} + U(y^n, n\Delta t) + \sum_{m=0}^{n-1} (y^{m+1} - y^m) \int_0^1 K(y^n - y^{m+\alpha}, (n-m-\alpha)\Delta t)\, d\alpha = 0. \tag{3}$$

We must also choose some method of evaluating the *weights*

$$\int_0^1 K(y^n - y^{m+\alpha}, (n-m-\alpha)\Delta t)\, d\alpha \tag{4}$$

because only the top weight, with $m = n-1$, can be evaluated in closed form. (It is simply

$$\frac{1}{y^n - y^{n-1}} \operatorname{erf}\left[\frac{y^n - y^{n-1}}{\sqrt{4\Delta t}}\right]$$

where

$$\operatorname{erf}(z) = \frac{2}{\sqrt{\pi}} \int_0^z e^{-y^2} dy$$

is the error function.) We choose to evaluate them by Gaussian quadrature [26] for $m \le n-2$. Satisfactory error bounds can be given for evaluating (4) by Gaussian quadrature, because the integrands in (4) with $m \le n-2$ have the square-root singularity of K sufficiently distant from the interval of integration. The importance of accurate weight evaluation is well-known in the theory of numerical solution of integral equations; see van der Houwen and te Riele [51] for discussion and analysis. It is a stroke of extreme good fortune that the top weight, which contains the singularity of the single layer potential, can actually be evaluated in closed form.

We can then solve the equation

$$\varepsilon_V \frac{y^n - y^{n-1}}{\Delta t} + U(y^n, n\Delta t) + \operatorname{erf}\left(\frac{y^n - y^{n-1}}{\sqrt{4\Delta t}}\right) + \tag{5}$$
$$\sum_{m=0}^{n-2} (y^{m+1} - y^m) \int_0^1 K(y^n - y^{m+\alpha}, (n-m-\alpha)\Delta t)\, d\alpha = 0.$$

for y^n, at each time step. Newton's method is suitable for this.

We found this method to be stable and at least first-order accurate, with sufficiently accurate weight evaluation; typically 6-point Gaussian quadrature sufficed for this. Newton's method converges quickly, taking no more than 5 iterations to reduce the residual below 10^{-10} in double precision (14-digit) arithmetic.

It is inappropriate for us to test this method by computing the planar constant-speed solution, because we are approximating the solution by piecewise linear functions and that solution is itself linear. Thus only the error due to numerical integration will appear. Put another way, this method is misleadingly accurate for computing this exact solution.

Thus we measured the error instead on the planar Neumann solution (see [49]) for which $\varepsilon_V = 0$, $y(t) = 2p\sqrt{t}$, and

$$u_0(y) = \begin{cases} u_\infty & y > 0 \\ 0 & y \le 0. \end{cases} \tag{6}$$

Here $p > 0$ is the solution of

$$p\sqrt{\pi}\,\mathrm{erfce}\,(p) = -u_\infty,$$

which exists if and only if the liquid-phase supercooling $-u_\infty$ lies between 0 and 1. This solution is linearly stable because of the smaller supercooling [19, 90], but singular at $t = 0$. For numerical purposes, we avoid the singularity by fixing some small time $t_0 > \Delta t$ and taking the first $t_0/\Delta t$ steps exactly.

Table 1 shows the errors obtained with $p = 0.5$, $t_0 = .05$, and $N =$ 20, 40, 80, 160, and 320 time steps used to compute up to time $t = 1$. We used $I =$ 4,6,8,10, and 12 Gaussian quadrature points. The convergence is clearly better than first order in Δt. (Since our spatial discretization in the periodic case is at most first order accurate and $J\Delta t = 1$, we are satisfied as long as the time discretization errors are no worse.) The last column of Table 1 also shows errors at $t = 4$, with higher undercooling ($p = 0.9$) and larger time steps. Again, the convergence is ultimately better than first order. We conjecture that the error is $O(\Delta t^{3/2})$, because of the square-root singularity in K.

This time discretization method can now be applied to the periodic graph equation of motion. Let

$$y_j(t) = y_j^n + \frac{t - n\Delta t}{\Delta t}(y_j^{n+1} - y_j^n) = y_j^{n+\alpha} \qquad \text{for} \quad n\Delta t < t = (n+\alpha)\Delta t \le (n+1)\Delta t \tag{7}$$

be a continuous piecewise linear approximation of $y_j(t)$. Substitute (7) into (3.3.8) and require the equation to hold at the mesh points $t = n\Delta t$. The result is the discrete equation of motion

$$\varepsilon_c Ci + \varepsilon_v V_i + U(s_i, y_i^n, n\Delta t) + \mathrm{erf}\left[\frac{y_i^n - y_i^{n-1}}{2\sqrt{\Delta t}}\right] + \tag{8}$$

$$+ \sum_{m=0}^{n-2} \Delta s \sum_{-J}^{J}{}' \left[y_j^{m+1} - y_j^m\right] \int_0^1 \Theta(s_i - s_j, (n-m-\alpha)\Delta t) K(y_i^n - y_j^{m+\alpha}, (n-m-\alpha)\Delta t)\, d\alpha = 0.$$

The weights can again be evaluated by Gaussian quadrature, the curvature and velocity are built with the derivative approximation D of the previous section, and consistency requires $J^2\Delta t \to \infty$ as $J \to \infty$, $\Delta t \to 0$.

Attention to several computational details can dramatically improve efficiency. First, note that the Θ-function values are fixed once we fix the time step, the mesh size, and the number of Gaussian quadrature points. Since they are used again and again, and each value is as expensive as half a dozen exponentials or trigonometric functions, a great increase in speed can be had by evaluating them at the beginning of the computation and storing them in an array. Next, it is very inexpensive to use Newton's method for solving the nonlinear system (8) for y_j^n at time step n. This is because once we have the Θ-function values and exponentials necessary to evaluate (8), we can use them simultaneously to evaluate the Jacobian;

$$\partial_y K(y,t) = -\frac{y}{2t} K(y,t),$$

so it costs very little to evaluate $\partial_y K$, given K. The Θ-function values are the same in (8) and in its Jacobian. This general situation — in which it costs very little to evaluate the Jacobian once

the function itself has been evaluated — will recur in Chapter 4, though precomputation of Θ will not be possible then. And finally, it is also important to evaluate the error functions quickly and accurately. For this, we used Gautschi's algorithm [38], which relies on a power series expansion of erfce for small arguments and on Legendre's continued fraction for large arguments. The resulting values were spot-checked against 12-digit tables.

In all our computations, we took symmetric initial conditions and used symmetry of the solution to reduce the computational effort by a factor of 4. Thus we computed only the side of the curve corresponding to $s \geq 0$, effectively cutting J in half. Since the cost of the method is

$$O\,(N^2 J^2 I),$$

this reduces the total cost of the computation by a factor of 4.

3.6. Numerical Results

This section describes two numerical experiments with the method described in Section 5. In the first experiment, we compute the evolution of a cosine perturbation to a flat interface, compare the growth of the perturbation with that predicted by linear stability theory, and demonstrate the first-order convergence rate of the method by analyzing the variation of the solution with mesh size. In the second experiment, we study the evolution of an theta-function bump on a flat interface and again establish first-order convergence. In both cases, the solutions fail to converge after a certain time, when the gradients become too large. We see this as evidence of breakdown of a fundamental assumption of the periodic graph formulation; the interface is no longer a graph.

For the cosine perturbation, we took initial data $y_0(s) = g_0 \cos(ks)$ and initial temperature field

$$u_0(x,y) = u_0(y) + f(y)\cos(kx) \tag{1}$$

where

$$f(y) = \begin{cases} u_0' e^{-q'y} & y > 0 \\ u_0 e^{qy} & y < 0 \end{cases} \tag{2}$$

and $u_0(y)$ is given in (2.3.3). The forcing term is then

$$U(x,y,t) = U_0(y,t) + u_0' e^{-k^2 t}\cos(kx) F(y,t,q') + u_0 e^{-k^2 t}\cos(kx) F(-y,t,q)$$

where U_0 is given by (2.3.6) and

$$F(y,t,q) = \frac{1}{2} e^{-y^2/4t}\,\mathrm{erfce}\left[\frac{2tq - y}{\sqrt{4t}}\right]. \tag{3}$$

A moment's calculation shows that $\partial_y U$ blows up like $1/\sqrt{t}$ as $t \to 0$ unless the initial temperature field is continuous; $u_0 = u_0'$. Consistency of the initial interface and temperature perturbations requires (according to Section 2.3) that

$$u_0 = u_0' = -\frac{1}{2}(2\varepsilon_c k^2 - V) g_0 \tag{4}$$

if $\varepsilon_V = 0$. In this section, we take $\varepsilon_V = 0$ for simplicity.

First, we measured the convergence rate of the numerical method. We fixed the physical parameters

$$q = q' = V = 1, \quad \varepsilon_C = .01, \quad \varepsilon_V = 0, \quad g_0 = .02, \quad k = 4,$$

so that the cosine grows with the maximum exponent $y_1 = 2.43975 = \max_k y_1(k)$, and computed up to $t = 1.5$, with numerical parameters

$$J = 16,32,64,128 \quad N = 24,48,96,192$$

and $I = 4,6,8,10$ Gaussian quadrature points per weight. The initial and final curves are shown in Figure 3, for the solution with $J = 64$; the final amplitude has increased by a factor of 50.

Since we don't know the exact solution, we estimate the error by studying the variation of the solution with successive halvings of the mesh size and time step. Table 2 displays the max-norm differences

$$\max_j \; y_{2j}^{2n}(2J) - y_j^n(J) \tag{5}$$

of the computed solution $y_j^n(J)$, as a function of time t and the number of points J. The halving of the differences as the mesh size is halved indicates first-order convergence;

$$y_j^n(J) = y(n\Delta t, j\Delta s) + \Delta s \cdot e(n\Delta t, j\Delta s) + O(\Delta s^2), \tag{6}$$

where $J\Delta t = 1$, $y(t,s)$ is the exact solution, and e is an unknown smooth function of t and s. The important fact is that e is independent of J; thus halving the mesh size gives

$$y_{2j}^{2n}(2J) = y(n\Delta t, j\Delta s) + \frac{1}{2}\Delta s \cdot e(n\Delta t, j\Delta s) + O(\Delta s^2). \tag{7}$$

Hence we can build a second-order accurate solution by Richardson extrapolation [55]. To do this, multiply (7) by 2, subtract (6) and rearrange to get

$$\tilde{y}_j^n = 2y_{2j}^{2n}(2J) - y_j^n(J) = y(n\Delta t, j\Delta s) + O(\Delta s^2). \tag{8}$$

The last two columns of Table 2 exhibit the maximum differences of the extrapolated solution $\tilde{y}$. There is some improvement in convergence, though the rate never quite reaches $O(\Delta t^2)$. But the final extrapolated solution is accurate to 3 digits all the way up to $t = 1$, as far as we can tell by examining differences.

Next we compare the extrapolated results with the prediction

$$y(t,s) = Vt + g(t)\cos ks + O(g_0^2)$$

of linear stability theory. Here $g(t)$ is the solution of the linear stability equation (2.3.19). Since $g(t)$ is not an exponential, comparison with linear theory is complicated, and requires comparison of the computed and exact functions $g(t)$ for a range of t, not just comparison of the computed and exact linear stability exponents y_1. For simplicity, we took $\varepsilon_V = 0$ ($\varepsilon_V \neq 0$ requires slightly more programming) and calculated the exact $g(t)$ by applying the second-order Runge-Kutta method [39] to the ordinary differential equation (2.3.20). For the computed $g(t)$, we measured the amplitude

$$\tilde{g} = \frac{1}{2}(\max \tilde{y}_k - \min \tilde{y}_k) \tag{9}$$

of the extrapolated solution $\tilde{y}$. Figure 3 shows that an initial cosine wave remains a cosine with considerable fidelity. Clearly no other modes are being excited to any significant extent, despite the nonlinearity of the problem. Thus the crude method (9) of amplitude fitting is reasonable.

Table 3 exhibits the results, for $k = 1, 4$, and 7. Each entry in Table 3 is accurate to within 2 units in the last place, as estimated by measuring differences. For each k, we tabulated the numerical and exact amplitudes $\tilde{g}$ and g, as well as the ratio between g and the prediction $g_0 e^{ty_1}$ of the classical linear stability theory reviewed in Section 1.4. The $k = 1$ column exhibits remarkably close agreement between g and $\tilde{g}$, while the classical prediction is in error by as much as 25%. (Though the classical theory gets the right exponent, the amplitude is strongly affected by short-term transients neglected in the classical theory.) In this slow-growth situation, g behaves quite differently from an exponential.

In the $k = 4$ column, the entries increase much faster; the exponent y_1 here reaches its maximum over k. Thus linear theory cannot be expected to be accurate very long — and in fact it is good even to one digit only up to about $t = 1.25$. Our method breaks down then as well, to some extent; presumably the interface develops excessively large gradients, because it is about to stop being the graph of a single-valued function.

For $k = 7$, both theories agree well with the computed results, perhaps because the perturbation is decaying slowly and smoothly.

In the second experiment, we computed the evolution of an initial Θ-function bump

$$y_0(s) = \frac{g_0}{\Theta(0,\delta)}\Theta(s,\delta) \tag{10}$$

on a flat interface. (The coefficient is chosen to make the maximum amplitude of the initial data equal to g_0.) An approximately consistent initial temperature field perturbation can be constructed via linear stability theory, for small g_0: Decompose Θ into its Fourier components, construct a consistent initial temperature field perturbation for each component by linear stability theory, as in the first experiment, and add up the results to get

$$u_0(x,y) = u_0(y) + e^{-q|y|}(\frac{V}{2} + \varepsilon_c \partial_x^2) y_0(x).$$

Here we assume $q = q'$, $\varepsilon_v = 0$, for simplicity. The forcing term is easily computed, because we chose Θ-function initial data;

$$U(x,y,t) = U_0(y,t) + (F(y,t,q) + F(-y,t,q))\frac{g_0}{\Theta(0,\delta)}(\frac{V}{2} + \varepsilon_c \partial_x^2)\Theta(x,t+\delta).$$

F is given in (3). Figure 4 displays a sample result from a computation with

$$\delta = .05, \quad g_0 = .02, \quad q = q' = V = 1,$$

and an isotropic velocity-independent Gibbs-Thomson relation with $\varepsilon_c = .01$. We computed the solution with

$$J = 16,32,64,128 \text{ points and}$$

$$N = 24,48,96,192 \quad \text{time steps}$$

up to time $t = 1.5$, using $I = 4$, 6, 8, and 10 Gaussian quadrature points. Table 4 exhibits the max-norm differences; again, the convergence was monotone and Richardson extrapolation gave a roughly second-order solution up to time $t = 1$. Differences of the extrapolated solution are shown in the last two columns of Table 4. The full computation required 30 minutes of Cray X-MP CPU time, and we believe the final extrapolated solution to have three digit accuracy until $t = 1.5$.

Physically, there are two interesting features of the solution: First, the accuracy with which the flat ends of the interface move with the unperturbed velocity V. Thus a localized bump propagates slowly. Second, the depressions which form at each side of the central bump. These are not predicted by any physical argument known to us: they indicate that ice is melting immediately adjacent to the bump where water is freezing, a significant effect of curvature dependence.

4. Numerical Methods for General Periodic Fronts

4.1. Introduction

In Chapter 4, we present numerical methods for computing an arclength parametrization of $\Gamma(t)$. These methods do not require $\Gamma(t)$ to be the graph of a function. They take advantage of a natural conserved quantity, the arclength deviation

$$Q = 1-(x_s)^2-(y_s)^2$$

to eliminate x and y in favor of the new unknowns V and ϕ. Our numerical method conserves a natural analogue to Q, the scaled distance between one point and the next, by reconstructing x and y from V and ϕ in a special way. We calculate V from the integral equation and solve an evolution equation for the normal angle ϕ. A slight additional calculation is necessary to keep track of the arclength of one branch of the periodic curve.

The following algorithm may seem more natural: Put a set of marker points on the curve, evaluate the velocity at each point, and move each point along an approximation to the normal. This amounts to solving the equations

$$x_t = V\frac{y_s}{\sqrt{x_s^2+y_s^2}}$$

$$y_t = -V\frac{x_s}{\sqrt{x_s^2+y_s^2}}$$

for a non-arclength parametrization (x,y) of $\Gamma(t)$. However, Sethian [93] has described the difficulties in this approach when the velocity is a simple local function of curvature;

$$V = 1-\varepsilon C.$$

(We cannot expect our much more complicated velocity to behave better.) Briefly, Sethian observes that marker points tend to spread far apart in regions of larger curvature, where they are most needed to resolve sharp changes in the solution, and bunch up in flat areas, where they are least necessary. In the flat areas, a stability constraint of the usual kind $\frac{\Delta t}{\Delta s} \leq$ constant then requires expensively small time steps. Another kind of spreading difficulty is shown in Figure 5, where a bump is growing upward. On each side of the bump, the normal points sideways. Hence any algorithm which moves points only along the normal can only move x a short distance. Since points are not allowed to slide along the curve, they must inevitably spread out along each side. Sethian also describes why "rezoning" to keep points equidistant along the curve doesn't work; the interpolation required smooths the curve unconscionably.

4.2. The ϕ Equation

This section contains a derivation of the evolution equation for the normal angle ϕ on which our curve movement algorithm is based, loosely following Duchon and Robert [27]. Choose an arclength parametrization [18] $\underline{x} = \underline{x}(t,s)$ of an infinite interface $\Gamma(t)$, with s increasing as x increases, and with the special property that

$$\underline{x}_t(t,s=0)\cdot\underline{x}_s(t,s=0)=0 \tag{1}$$

for each t. Thus we choose the point labelled by $s=0$ to move always along the normal to the curve. Given *any* arclength parametrization, we can shift the origin of arclength (by solving an ordinary differential equation) so that (1) is satisfied; hence this choice of parametrization involves no loss of generality. Recall that the normal velocity V is defined by [102]

$$V=\underline{x}_t\cdot\nu$$

where

$$\nu=(-y_s,x_s)$$

is the unit normal to $\Gamma(t)$. This fixes only one component of the vector $\underline{x}_t$. The other component, $\underline{x}_t\cdot\tau$ (where $\tau=(x_s,y_s)$ is the tangent to $\Gamma(t)$), depends on the choice of parametrization. The special property (1) is enough to determine $\underline{x}_t\cdot\tau$, and therefore the parametrization, as it turns out. Indeed, τ is a unit vector, so $\partial_s\underline{x}_t\cdot\tau=\partial_t(\frac{1}{2}\tau\cdot\tau)=0$, and thus

$$\partial_s(\underline{x}_t\cdot\tau)=\partial_s\underline{x}_t\cdot\tau+\underline{x}_t\cdot\partial_s\tau=-CV,$$

since [18] $\partial_s\tau=-C\nu$ and $\underline{x}_t\cdot\nu=V$. Hence integration and (1) imply

$$\underline{x}_t\cdot\tau=-\int_0^s CVds',$$

so $\underline{x}_t$ is given by

$$\underline{x}_t=V\cdot\nu-\int_0^s CVds'\cdot\tau. \tag{2}$$

The first term moves points along the normal with velocity V; the second slides points along the curve to conserve arclength. Take components to get the "X/Y equations"

$$x_t+Vy_s+x_s\int_0^s CVds'=0 \tag{3}$$

$$y_t-Vx_s+y_s\int_0^s CVds'=0. \tag{4}$$

Here $C=y_sx_{ss}-x_sy_{ss}$.

The X/Y equations have — for any V — a natural conserved quantity, the arclength deviation (or *eikonal*)

$$Q=1-(x_s)^2-(y_s)^2.$$

A short calculation shows that (3) and (4) imply a conservation law

$$\partial_tQ+\partial_s(Q\int_0^s CVds')=-CVQ. \tag{5}$$

This equation is linear in Q, so as long as CV is smooth, $Q=0$ is the unique solution with initial values 0. Thus a parametrization which starts out as an exact arclength parametrization and

evolves by the exact X/Y equations will remain an arclength parametrization. However, the nonzero right-hand side can cause exponential growth in a perturbation of Q. This is bad news for a numerical method based on the X/Y equations; it cannot preserve the property of being an arclength parametrization.

However, we can take advantage of the conservation of Q to reduce the number of degrees of freedom of our system from 3 (x, y and V) to 2, and conserve Q automatically at the same time. We eliminate the constrained variables x and y, in favor of unconstrained variables V and ϕ. To do this, introduce the normal angle ϕ by

$$x_s = \cos\phi\,, \quad y_s = -\sin\phi, \tag{6}$$

so that ϕ is the angle between the normal ν and the y-axis. Use (1),(3), and (4) to reconstruct x and y from ϕ and V by integration;

$$x(t,s) = x(0,0) + \int_0^t \sin\phi(t',0)V(t',0)dt' + \int_0^s \cos\phi(t,s')ds' \tag{7}$$

$$y(t,s) = y(0,0) + \int_0^t \cos\phi(t',0)V(t',0)dt' - \int_0^s \sin\phi(t,s')ds'. \tag{8}$$

The curvature C is the derivative of ϕ with respect to arclength:

$$C = -x_s y_{ss} + x_{ss} y_s = \partial_s \phi.$$

Finally, to construct an evolution equation for ϕ, differentiate (3) and (4) with respect to s, use (6) and take $\sin\phi$ times the first of the resulting equations plus $\cos\phi$ times the second. The result is the " ϕ equation"

$$\partial_t \phi + \partial_s V + \partial_s \phi \int_0^s V \partial_s \phi ds' = 0 \tag{9}$$

which will form the basis of our numerical method for moving curves.

Example: Suppose $V = 1$ is constant. Corresponding to the ill-posed Cauchy-Riemann initial value problem for the X/Y equations, the ϕ equation becomes Burgers' equation

$$\partial_t \phi + \partial_s (\frac{1}{2}\phi^2) = 0$$

if $\phi = 0$ at $s = 0$, for example if the curve is symmetric about $x = 0$. Thus even in the seemingly simple case when V is constant, we cannot expect global solutions.

4.3. Keeping track of arclength

A slight additional complication, present in the case when $\Gamma(t)$ is periodic, is the need to keep track of arclength. Both the ϕ equation (4.2.9) and the V equation (2.2.5) are to hold on the interval $-\infty < s < \infty$. As in Section 3.2, we want to reduce the problem to a finite interval by assuming that $\Gamma(t)$ is periodic. This means that

$$x(t,s+L(t)) = x(t,s) + 2\pi \tag{1}$$

$$y(t,s+L(t)) = y(t,s)$$

where $L(t)$ is the length of one branch of the interface, unfortunately not known *a priori*. Then we can sum under the integral as in Section 3.2 to get the periodic integral equation

$$\varepsilon_C C + \varepsilon_V V + U(x,y,t) + \tag{2}$$
$$+ \int_0^t \int_{-L/2}^{L/2} \Theta(x-x', t-t') K(y-y', t-t') V' ds' dt' = 0,$$

to hold for $-L/2 < s < L/2$. An easy calculation [46] shows that $L(t)$ satisfies the differential equation

$$\partial_t L = \int_{-L/2}^{L/2} CV ds; \tag{3}$$

thus the integral equation (2.2.5), the ϕ equation (4.2.9), and (3) comprise a *one*-space-dimensional moving boundary problem. Fortunately, in one space dimension, moving boundaries can easily be removed by a stretching transformation which puts them into the coefficients of equations on a fixed domain. Thus put

$$g(t) = \frac{2\pi}{L(t)}, \tag{4}$$

so that $-\pi \le \sigma = g(t)s \le \pi$, and let

$$\phi(t,s) = \tilde{\phi}(t,\sigma) \tag{5}$$
$$V(t,s) = g(t)\tilde{V}(t,\sigma).$$

It follows from (3) that g satisfies

$$\partial_t g + g^3 < \tilde{V} \partial_\sigma \tilde{\phi} > = 0 \tag{6}$$

where brackets denote the average

$$< f > = \frac{1}{2\pi} \int_{-\pi}^{\pi} f(\sigma) d\sigma. \tag{7}$$

Thus the ϕ equation becomes

$$\frac{1}{g^2} \partial_t \phi + \partial_\sigma V + \partial_\sigma \phi \int_0^\sigma (V \partial_\sigma \phi - < V \partial_\sigma \phi >) d\sigma' = 0 \tag{8}$$

upon dropping tildes. The integral equation becomes

$$g(\varepsilon_C \partial_\sigma \phi + \varepsilon_V V) + U(x,y,t) + \int_0^t \int_{-\pi}^{\pi} K(y-y', t-t') \Theta(x-x', t-t') V' d\sigma' dt' = 0. \tag{9}$$

Here x and y are constructed from V, ϕ, and g by

$$x(t,s) = x(0,0) + \int_0^t g(t') \sin\phi(t',0) V(t',0) dt' + \frac{1}{g(t)} \int_0^s \cos\phi(t,s') ds' \tag{10}$$

$$y(t,s) = y(0,0) + \int_0^t g(t') \cos\phi(t',0) V(t',0) dt' - \frac{1}{g(t)} \int_0^s \sin\phi(t,s') ds'. \tag{11}$$

These equations are to hold on the interval $[-\pi, \pi]$, with periodic boundary and given initial conditions for ϕ and V, and a given initial value for g.

4.4. The numerical method

First, we summarize the system of equations to be solved. The (rescaled) velocity satisfies a singular integral equation,

$$g\,(\varepsilon_C(\phi)\partial_s\phi + \varepsilon_V(\phi)V) + U(x,y,t) + \tag{1}$$
$$+\int_0^t\int_{-\pi}^{\pi}\Theta(x-x',t-t')K(y-y',t-t')V'ds'dt' = 0.$$

Here x and y are given by

$$x(t,s) = x(0,0) + \int_0^t g(t')\sin\phi(t',0)V(t',0)dt' + \frac{1}{g(t)}\int_0^s \cos\phi(t,s')ds' \tag{2}$$

$$y(t,s) = y(0,0) + \int_0^t g(t')\cos\phi(t',0)V(t',0)dt' - \frac{1}{g(t)}\int_0^s \sin\phi(t,s')ds'. \tag{3}$$

The curve is moved by calculating the normal angle ϕ and the arclength ratio g from

$$\frac{1}{g^2}\partial_t\phi + \partial_s V + \partial_s\phi\int_0^s (V\partial_s\phi - \langle V\partial_s\phi\rangle)ds' = 0, \tag{4}$$

and

$$\partial_t g + g^3\langle V\partial_s\phi\rangle = 0. \tag{5}$$

Brackets denote the average value:

$$\langle V\partial_s\phi\rangle = \frac{1}{2\pi}\int_{-\pi}^{\pi} V(t,s')\partial_s\phi(t,s')ds'.$$

Note that the actual normal velocity of the curve is gV, since we rescaled and dropped tildes.

Now we introduce continuous piecewise linear approximations in the time variable for the primary variables V, ϕ, and g, and require the equations (1), (4), and (5) to hold at the mesh points $t = n\Delta t$. We use the asymptotic value (2.2.6)

$$\int_{-\pi}^{\pi}\Theta(x-x',t-t')K(y-y',t-t')V'ds' \sim K(\|\underline{x}-\underline{x}'\|,t-t')V'g(t',s) \tag{6}$$

in the single layer potential at the top time level $t' > t-\Delta t$. The resulting semidiscrete equations are

$$g^n(\varepsilon_C(\phi^n)\partial_s\phi^n + \varepsilon_V(\phi^n)V^n) + U(x^n,y^n,n\Delta t) + \tag{7}$$
$$+\Delta t\sum_{m=0}^{n-2}\int_0^1\int_{-\pi}^{\pi}\Theta(x^n-x^{m+\alpha}(s'),(n-m-\alpha)\Delta t)K(y^n-y^{m+\alpha}(s'),(n-m-\alpha)\Delta t)V^{m+\alpha}(s')ds'd\alpha +$$
$$+\Delta t\int_0^1 K(\|\underline{x}^n-\underline{x}^{n-\alpha}\|,\alpha\Delta t)V^{n-\alpha}g^{n-\alpha}d\alpha = 0,$$

$$(\frac{1}{g^n})^2\frac{\phi^n-\phi^{n-1}}{\Delta t} + \partial_s V^n + \partial_s\phi^n\int_0^s (V^n(s')\partial_s\phi^n(s')-<V^n\partial_s\phi^n>)ds' = 0, \tag{8}$$

and

$$\frac{g^n-g^{n-1}}{\Delta t} + (g^n)^3 <V^n\partial_s\phi^n> = 0. \tag{9}$$

Here x and y are approximated by

$$x^n = x_0^0 + + \Delta t\sum_{m=0}^{n-1}{}' V_0{}^m g^m \sin\phi_0^m + \frac{1}{g^n}\int_0^s \cos\phi^n(s')ds' \tag{10}$$

and

$$y^n = y_0^0 + \Delta t\sum_{m=0}^{n-1}{}' V_0{}^m g^m \cos\phi_0^m - \frac{1}{g^n}\int_0^s \sin\phi^n(s')ds'. \tag{11}$$

The subscript 0 on V and ϕ indicates evaluation at $s = 0$, $\|\underline{x}\|$ is the Euclidean norm of the vector $\underline{x}$, and the prime on the sum over m means that the first and last terms are to be halved.

The top weight in the semidiscrete integral equation (7) can be evaluated exactly in terms of the error function, as in Chapter 3. A tedious calculation gives

$$\Delta t\int_0^1 K(\|\underline{x}^n-\underline{x}^{n-\alpha}\|,\alpha\Delta t)V^{n-\alpha}g^{n-\alpha}d\alpha = \frac{\sqrt{\Delta t}}{2}\Big[W_{20}(z)g^nV^n + \tag{12}$$

$$+ W_{11}(z)(g^{n-1}V^n + g^nV^{n-1}) + W_{02}(z)V^{n-1}g^{n-1}\Big]$$

where $z = \|\underline{x}^n - \underline{x}^{n-1}\|/\sqrt{4\Delta t}$ and

$$\begin{aligned} W_{20}(z) &= \text{erf}\,(z)(\frac{1}{z}-\frac{1}{z^3}+\frac{3}{4z^5}) + \frac{e^{-z^2}}{\sqrt{\pi}}(\frac{1}{z^2}-\frac{3}{2z^4}) \\ W_{11}(z) &= \text{erf}\,(z)(\frac{1}{2z^3}-\frac{3}{4z^5}) + \frac{e^{-z^2}}{\sqrt{\pi}}\frac{3}{2z^4} \\ W_{02}(z) &= \text{erf}\,(z)\frac{3}{4z^5} - \frac{e^{-z^2}}{\sqrt{\pi}}(\frac{1}{z^2}+\frac{3}{2z^4}). \end{aligned} \tag{13}$$

The other weights are computed by applying Gaussian quadrature in α and the trapezoidal rule in s, as in Chapter 3.

We could treat g differently: Introduce piecewise linear approximations only for V and ϕ, and solve the g equation exactly by transforming it into

$$\partial_t(\frac{1}{g^2}) - 2<V\partial_s\phi> = 0,$$

which is linear in $\frac{1}{g^2}$. The resulting equation for g,

$$(\frac{1}{g^{n-1+\alpha}})^2 = (\frac{1}{g^{n-1}})^2 + 2\Delta t\int_0^\alpha \beta^2 <V^n\partial_s\phi^n> +$$

$$\beta(1-\beta)(<V^n\partial_s\phi^{n-1}> + <V^{n-1}\partial_s\phi^n>) + (1-\beta)^2 <V^{n-1}\partial_s\phi^{n-1}> d\beta$$

can be used in the integral equation and the reconstruction of x and y. However, we can no longer evaluate the top weight in the integral equation exactly, and eliminating g eliminates only one of a large number of discrete degrees of freedom, so we defer this approach to future work.

Next we discretize the curve. Let ϕ_j approximate $\phi(j\Delta s)$ and V_j approximate $V(j\Delta s)$, with $\Delta s = \pi/J$ and a positive integer J. Replace ∂_s with the discrete derivative D constructed in Chapter 3;

$$D\phi_j = \sum_{-J}^{J}{}' D_{jk}\,\phi_k$$

where

$$D_{jk} = \frac{(-1)^{j-k}}{2}\cot\left[\frac{(j-k)\pi}{2J}\right] \qquad j \neq k$$

$$D_{jk} = 0 \qquad j = k.$$

As we saw in Chapter 3, this introduces a *consistency condition*

$$J^2\Delta t \to \infty \qquad \text{as} \quad J \to \infty, \Delta t \to 0. \tag{14}$$

We usually satisfy this condition by taking $J\Delta t = 1$.

The only new trick is in the construction of x and y from V and ϕ. The exact rescaled equations (1), (4), and (5) have the natural invariant

$$1 - g^2((x_s)^2 + (y_s)^2) = 0,$$

whose absolute constancy expresses conservation of arclength. We design our numerical method to conserve the analogous quantity

$$Q = 1 - (\frac{g}{\Delta s})^2((x_j - x_{j-1})^2 + (y_j - y_{j-1})^2)$$

by using the special numerical integration rule

$$x_j - x_0 = \frac{\Delta s}{g}\sum_1^j \cos\frac{1}{2}(\phi_i + \phi_{i-1}) \tag{15}$$

$$y_j - y_0 = \frac{-\Delta s}{g}\sum_1^j \sin\frac{1}{2}(\phi_i + \phi_{i-1})$$

to compute x and y. Standard integration rules do not conserve Q, because they express $x_j - x_{j-1}$ as a sum of cosines rather than as the cosine of a sum.

Thus we have the discrete equations of motion

$$\begin{aligned} & g\,\varepsilon_c(\phi_i)D\phi_i + g\,\varepsilon_v(\phi_i)V_i + U(x_i, y_i, n\Delta t) + \\ & + \Delta t \sum_{m=0}^{n-2} \Delta s \sum_{-J}^{J}{}' \int_0^1 \Theta(x_i - x_k^{m+\alpha}, (n-m-\alpha)\Delta t)K(y_i - y_k^{m+\alpha}, (n-m-\alpha)\Delta t)V_k^{m+\alpha} d\alpha + \\ & + \frac{\sqrt{\Delta t}}{2}\left[W_{20}(z_i)gV_i + W_{11}(z_i)(g^{n-1}V_i + gV_i^{\,n-1}) + W_{02}(z_i)g^{n-1}V_i^{\,n-1}\right] = 0 \end{aligned} \tag{16}$$

$$\frac{1}{g^2}\frac{\phi_i-\phi_i^{\,n-1}}{\Delta t} + DV_i + D\phi_i\,\Delta s\,\sum_0^i{}'(V_i D\phi_i - \langle VD\phi\rangle) = 0 \tag{17}$$

$$\frac{g-g^{n-1}}{\Delta t} + g^3\langle VD\phi\rangle = 0. \tag{18}$$

Here $z_i = \frac{\|\underline{x}-\underline{x}^{n-1}\|}{\sqrt{4\Delta t}}$ the integral over α is approximated by Gaussian quadrature, W_{ij} are given in (13),

$$x_i = x_0^{n-1} + \frac{\Delta t}{2}(V_0 g\sin\phi + V_0^{\,n-1}g^{n-1}\sin\phi^{n-1}) + \frac{\Delta s}{g}\sum_{k=1}^{i}\cos\frac{1}{2}(\phi_k+\phi_{k-1}), \tag{19}$$

$$y_i = y_0^{n-1} + \frac{\Delta t}{2}(V_0 g\cos\phi + V_0^{\,n-1}g^{n-1}\cos\phi^{n-1}) - \frac{\Delta s}{g}\sum_{k=1}^{i}\sin\frac{1}{2}(\phi_k+\phi_{k-1}), \tag{20}$$

unsuperscripted variables are evaluated at time level n, and

$$\langle VD\phi\rangle = \frac{\Delta s}{2\pi}\sum_{-J}^{J}{}' V_j D\phi_j.$$

We impose periodic boundary conditions $\phi_J = \phi_{-J}$, $V_J = V_{-J}$ and initial conditions for V, ϕ and g.

The computational details are very like those mentioned in Section 3.5, except that precomputation of the Θ-function values is now impossible. However, the special feature which made Newton's method attractive is still present; it costs almost nothing to evaluate the Jacobian, once we have evaluated the equations (16-18). Of course, the hand calculation involved in computing the matrix elements of the Jacobian is quite tedious and error-prone. But Newton's method performed well in the numerical experiments reported in the next section, requiring only 5-6 iterations to reduce the residual below 10^{-6} in Cray single precision (14 decimal digit) arithmetic. For $\varepsilon_V = 0$, Newton's method was occasionally (about one time in 1000) unable to reduce the residual below 10^{-6} even in 20 iterations; this is further evidence of the smoothing effect of velocity dependence.

4.5. Numerical results

First, we validate the method with a convergence study. We compute a theta-function bump on a flat interface, with initial data

$$y(0,s) = (g_0/\Theta(0,\delta))\Theta(s,\delta) \tag{1}$$

and a consistent exponential perturbation (2.3.16) of the initial temperature field. The physical parameters are

$$\varepsilon_C = \varepsilon_V = .02 \qquad A = .5 \qquad k_A = 4,$$

so there is a 50% variation in curvature dependence from the y-axis to the x-axis, with growth up along the y-axis favored by the smaller value of ε_C there. Starting with the almost invisible bump ($\delta = .05$, $g_0 = .05$) shown in Figure 6(a), the solution develops substantial gradients by time $t = 1.5$; see Figure 6(b). We used J points and N steps, with

$$J = 10,20,40,80, \qquad N = 15,30,60,120,$$

and $I = 4,6,8,10$ points for Gaussian integration of the weights. Table 5 exhibits the max-norm differences of the computed solution (x, y); on the finer meshes, a rough first order convergence is evident. Furthermore, the error (measured by differencing) grows more or less linearly in time, indicating stability of the method.

Richardson extrapolation to second order produced three approximate solutions, with maximum differences shown in the last two columns of Table 5. These decrease faster than the unextrapolated differences as the mesh becomes finer, but don't quite attain second order convergence. It is possible that the square-root singularity of K causes the convergence rate of the extrapolated solution to drop to $O(\Delta t^{3/2})$. At any rate, since the solution is of order unity, we have three good digits until $t = 1$.

Total computing time was 40 minutes on a Cray X-MP, over 90% of which was spent in evaluating the single layer potential. Thus the history-dependence of the velocity equation dominates the computational cost; this results in cost $O(N^2 J^2 I)$ to compute until time $T = N\Delta t$ with J points on the curve and I-point Gaussian quadrature.

A difficulty of the ϕ equation approach is that the periodicity of the curve cannot be maintained exactly. In the above computations, for example, x_J differed from π by several percent at $t = 1.5$. However, this difficulty is easily and naturally handled by rescaling; we simply divide x_j by x_J. To keep the pictures properly scaled, we then must divide y_j by x_J as well. We do not use this rescaling during the calculation, only when presenting graphical results.

We proceed next to the long-time computation of an anisotropic dendrite. The same initial interface, with physical parameters

$$\varepsilon_C = .04 \qquad \varepsilon_V = .02 \qquad A = .5 \qquad k_A = 4,$$

develops the structure shown in Figure 7. We used $J = 40$ points and $N = 280$ time steps, computing until time $t = 7$. In the last few pictures, we believe the beginning of a sidebranching instability to be appearing. It is cut off by impact on the neighboring dendrite before real sidebranch structure can develop, because of the periodicity of the calculation. Then the dendrites detach from their bases and the whole row of dendrites becomes a free-floating mass, separated from the ice below by a channel of water. (The last few pictures were rescaled to fit on the page.) The line connecting each dendrite to the mass of ice below is a numerical artifact, a piece of ice having zero thickness. In this region, the curve sometimes crossed itself and formed a loop; we then flattened the loop for graphical purposes, by replacing x_j by $\max(x_j, 0)$. When the sides of the curve left the channel available to them, they were also modified, by setting $x_j = \min(x_j, \pi)$.

We might see a true sidebranch structure develop, if we used a finer mesh and a narrower initial bump. The length scale of the dendrite should be determined by the initial conditions, so a narrower initial bump is equivalent to increasing the periodicity of the calculation. As the period (here equal to 2π) goes to infinity, we should recover an isolated dendrite.

An unexpected feature of the numerical calculation is the rapid growth of the condition number κ of the linear systems obtained by applying Newton's method to (16), (19), and (20). Write (16), (19), and (20) as a system

$$F = \begin{bmatrix} F_V \\ F_\phi \\ F_g \end{bmatrix} = 0,$$

where $F_V = 0$ is the velocity equation and so forth. Then

$$\kappa = \mathrm{cond}(DF)_\infty = \| DF \|_\infty \| DF^{-1} \|_\infty,$$

where DF is the Jacobian of F and $\| A \|_\infty$ denotes the maximum row sum of the matrix A. Table 6 exhibits κ as a function of t and J, in the computation of Figure 7. The growth with J is not surprising, because one term in DF is essentially the spatial derivative D, which approximates an unbounded operator as $\Delta s \to 0$. The growth with t, on the other hand, is probably due to the breakdown of the ϕ equation formulation itself. The dendrite is clearly approaching its neighbor, and when they touch the parametrization can no longer be continuous. Instead, it must separate into two separate parts, each a continuous function on a separate interval. The ϕ equation, on the other hand, can make sense only if ϕ is no worse that a measurable function, so that $\cos\phi$ and $\sin\phi$ can exist. But then x and y are Lipschitz and hence continuous. Thus the ϕ equation formulation breaks down when the curve crosses itself.

The final set of figures (Figure 8) show a dendrite with the same physical and numerical parameters as before, except that the Gibbs-Thomson relation has been made isotropic, with ε_C and ε_V equal to what were their minimum values in the previous calculation; $\varepsilon_C = .02$, $\varepsilon_V = .01$. Note the qualitatively different appearance. The dendrite now grows into an almost circular shape, and only then expands into a rectilinear shape filling the channel. A well-developed tip-splitting instability of the flat tip of the dendrite is then visible. Meiron [73] has exhibited similar tip-splitting instabilities in an approximate steady-state model. Nittmann & Stanley [85] also discuss connections between tip-splitting, sidebranching and anisotropy, in a more general context. This computation failed at about $t = 5.4$, due to exponent overflow. We believe this happened because 40 points is no longer sufficient to capture the structure at the center of the split, where a singularity seems to be forming. With only 40 points, smoothness cannot be maintained. Of course, it is also possible that the true solution itself blows up, in the sense that a real cusp develops at the split. Table 7 displays the condition number of the Jacobian as a function of t and J.

Each dendrite computation required about 2 hours of CPU time on a Cray X-MP. Gaussian elimination with partial pivoting and iterative improvement solved the linear systems well (in Cray single-precision 14-digit arithmetic) despite the large condition numbers, and Newton's method took less than 5 steps to reduce the residual below 10^{-6} at each time step.

Discussion and Conclusions

We have presented a numerical method for solving the supercooled Stefan problem with an anisotropic curvature- and velocity-dependent temperature boundary condition imposed on the moving boundary. We simplify the problem by eliminating the temperature field; thus only the moving boundary need be computed. We compute the normal velocity by solving a singular integral equation on the moving boundary, and move the curve by solving an evolution equation for the normal angle. An additional ordinary differential equation is solved for the arclength.

Our numerical method turns out to be stable, first-order accurate, and fairly expensive — though the high cost may be unavoidable given the intrinsic difficulty of the problem. The method costs

$$O\,(N^2J^2I) + O\,(NJ^3)$$

arithmetic operations to compute up to a fixed time $T = N\Delta t$, with time step Δt, J points on the curve, I Gaussian quadrature points per weight, and $J\Delta t = 1$. The first term, due to the history-dependence of the single layer potential, dominates in practice.

The method exhibits an $O\,(\Delta t)$ convergence rate, which compares favorably with the $O\,(\Delta t^{1/2})$ or worse of weak solution methods for *classical* Stefan problems (i. e. without curvature-dependence or supercooling). Furthermore, this method avoids "grid effects" which contaminate weak solution methods and prevent Richardson extrapolation to higher order. Grid effects are avoided by computing only the moving boundary and eliminating the temperature field.

Our velocity algorithm is constructed by studying the special case when the boundary is a graph. As far as the velocity is concerned, this situation already presents all the difficulties: The singularity of the kernel, the consistency condition for numerical integration over the curve, and the discretization of curvature can all be understood in this special case.

The general case, when the boundary is not the graph of a single-valued function, requires some study of the general problem of how to move a curve with a given curvature-dependent velocity. Methods which move points only along the normal fail: Points along the side of a bump spread apart, causing loss of accuracy, whereas points in other areas move too close together, requiring expensively small time steps to maintain numerical stability.

Thus we turn to a different formulation of curve movement, the "ϕ equation" introduced by Duchon & Robert [27]. This formulation takes V and ϕ as primary variables, reconstructing x and y only when needed. Thus arclength is automatically conserved in the exact equation. The numerical method then requires a special integration rule to evaluate x and y, in order to preserve the numerical equivalent of arclength. Taking V and ϕ as primary variables amounts to computing time and space derivatives of the parametrization, and therefore ensures smoothness of the resulting curve.

We worked with a spatially periodic curve, to simplify the boundary conditions, but this is not at all necessary. The general case would require some study of appropriate fictitious boundary conditions to truncate an infinite non-periodic curve (like a dendrite) without loss of accuracy or stability. Our curve movement algorithm is quite general: it applies without change to any periodic curve movement problem, and fictitious boundary conditions would permit its

extension to almost any curve.

The velocity calculation algorithm seems quite special to the Stefan problem; it depends on being able to reduce the equations determining the normal velocity to equations on the interface. Nevertheless, this approach naturally extends to solve a number of other problems, for example the supercooled Stefan problem with the heat equation $\partial_t u = \Delta u$ replaced by the Laplace equation $\Delta u = 0$ in each phase. Recent derivations [3, 83, 63] suggest that this may be a more reasonable model for the phenomenon of dendritic solidification. Numerically, the Laplace equation makes the problem much easier, because the single layer potential is no longer history dependent and no initial temperature field is necessary. Thus this simplification would eliminate the need to store previous locations of the interface and reduce the cost of the method to

$$O(NJ) + O(NJ^3);$$

the second term, the cost of Gaussian elimination, would presumably dominate in this case. Even so, we could expect a great decrease in computational cost.

Another interesting problem is to compute an infinite dendrite; much recent work [58, 72] has been devoted to this, because several important questions of pattern formation and velocity selection remain unanswered. The extension of our method to this case should be straightforward, requiring only fictitious boundary conditions to truncate the infinite curve.

Our numerical results lead to certain conclusions about the physical problem.

First, we confirm the smoothing effect of curvature and velocity dependence in the Gibbs-Thomson relation. Our computations indicate that sidebranching requires anisotropy; an isotropic Gibbs-Thomson relation produces tip-splitting rather than sidebranching.

Second, we see qualitatively similar final results, independent of the initial conditions — though of course smaller perturbations take longer to reach the same final state. This is evidence for a true shape selection mechanism.

Finally, our numerical method is accurate enough so that we can carry out a detailed comparison of numerical results with the predictions of both the linear stability theories we have discussed. The numerical results agree very closely with our new linear stability theory based on the integral equation, for time spans during which a small perturbation grows by an order or two of magnitude. The classical theory, however, predicts amplitudes which are in error by as much as 25%, though the exponents are correct in the long-time limit. Hence our results show decisively that the new integral-equation-based linear stability theory is correct and that the classical theory is quantitatively incorrect, though it produces the right exponents. We believe the reason for this error to be that the integral-equation-based theory includes subtle effects of the boundary conditions which the classical approach leaves out, in addition to transient effects due to the initial temperature field perturbation.

Acknowledgements

I would like to thank my thesis advisor, Alexandre Chorin, for his encouragement and advice. It has been instructive and enjoyable to work with him during my years in graduate school.

I would like to thank Ole Hald for his careful reading of the first draft, and Stanley Berger for serving as the outside reader. I have benefited from conversations with Matania Ben-Artzi, Ron DiPerna, John Neu, and James Sethian.

I thank Scott Baden and Paul Concus for assistance in using the computing facilities of the Lawrence Berkeley Laboratory of the University of California.

I am honored to have been a National Science Foundation Graduate Fellow and an IBM Predoctoral Fellow during my graduate years.

I am grateful to my wife Nancy, for her boundless confidence in me, her enthusiastic support, and most of all for telling me to study mathematics in the first place.

References

1. R. A. Adams, *Sobolev Spaces,* Academic Press, New York, 1975.
2. R. Alexander, P. Manselli, and K. Miller, "Moving finite element solution of the Stefan problem in two space dimensions," *Rend. Accad. Naz. Lincei (Rome)*, vol. serie VIII, vol. LXVII, fasc. 1-2, 1979.
3. N. D. Alikakos and P. W. Bates, "On the Singular Limit in a Phase Field Model of Phase Transitions," *Ann. Inst. Henri Poincare*, vol. 5, pp. 1-38, 1988.
4. A. Barbieri, D. C. Hong , and J. S. Langer, "Velocity Selection in the Symmetric Model of Dendritic Crystal Growth," *Phys. Rev. A*, vol. 35, pp. 1802-1808, 1987.
5. J. Bechhoefer and A. Libchaber, "Testing Shape Selection in Directional Solidification," *Phys. Rev. B.*, vol. 35, pp. 1393-1396, 1987.
6. E. Ben-Jacob, P. Garik, and D. Grier, "Interfacial Pattern Formation Far from Equilibrium," *Superlattices and Microstructures*, vol. 3, pp. 599-615, 1987.
7. M. Ben Amar and Y. Pomeau, "Theory of Dendritic Growth in a Weakly Undercooled Melt.," *Europhys. Lett.*, vol. 2, pp. 3307-3314, 1986.
8. E. di Benedetto and A. Friedman, "The ill-posed Hele-Shaw model and the Stefan problem for supercooled water," *Trans. Am. Math. Soc.*, vol. 282, pp. 183-201, 1984.
9. A. E. Berger, H. Brezis, and J. C. W. Rogers, "A Numerical Method for Solving the Problem $u_t - \Delta f(u) = 0$," *R.A.I.R.O. Anal. Num.*, vol. 13, pp. 297-312, 1979.
10. M. Berger, A. Ciment, and J. Rogers, "The Alternating Phase Truncation Method for Numerical Solution of Stefan Problems," *SIAM Jour. Num. Anal.*.
11. L. A. Caffarelli, "Compactness Methods in Free Boundary Problems," *Comm. P.D.E.*, vol. 5, pp. 427-448, 1980.
12. L. A. Caffarelli and L. C. Evans, "Continuity of the Temperature in the Two-Phase Stefan Problem," *Arch. Rat. Mech. Anal.*, vol. 81, pp. 199-220, 1983.
13. G. Caginalp and J. T. Lin, "A Numerical Analysis of an Anisotropic Phase Field Model," *To appear in IMA Jour.*.
14. G. Caginalp, "An Analysis of a Phase Field Model of a Free Boundary," *Arch. Rat. Mech. Anal.*, vol. 92, pp. 205-245, 1986.
15. G. Caginalp, "A Mathematical Approach to Crystal Growth," *Superlattices and Microstructures*, vol. 3, pp. 595-598, 1987.
16. J. W. Cahn and J. E. Hilliard, "Free Energy of a Nonuniform System. I. Interfacial Free Energy," *Jour. Chem. Phys.*, vol. 28, pp. 258-267, 1958.
17. A. P. Calderon and A. Zygmund, "Singular integral operators and differential equations," *Amer. J. Math.*, vol. 79, pp. 901-921, 1957.
18. M. P. do Carmo, *Differential Geometry of Curves and Surfaces,* Prentice-Hall, New Jersey, 1976.
19. J. Chadam and P. Ortoleva, "The Stabilizing Effect of Surface Tension on the Development of the Free Boundary in a Planar, One-dimensional Cauchy-Stefan Problem," *IMA*

Jour. Appl. Math., vol. 30, pp. 57-66, 1983.

20. S. Chandrasekhar, *Hydrodynamic and Hydromagetic Stability,* Dover, New York, 1981.
21. A.J. Chorin, "Curvature and Solidification," *Jour. Comp. Phys.*, vol. 57, pp. 472-490, 1985.
22. R. R. Coifman and Y. Meyer, "Au Dela des Operateurs Pseudo-Differentiels," *Asterisque*, vol. 57, pp. 1-183, 1978.
23. R. R. Coifman, A. McIntosh, and Y. Meyer, "L'integral de Cauchy Definit un Operateur Borne sur L^2 Pour les Courbes Lipschitziennes," *Ann. Math.*, vol. 116, pp. 361-387, 1982.
24. P. Collet and J.-P. Eckmann, "The Existence of Dendritic Fronts," *Commun. Math. Phys.*, vol. 107, pp. 39-92, 1986.
25. C. W. Cryer, "The Interrelation between Moving Boundary Problems and Free Boundary Problems," in *Moving Boundary Problems*, ed. D. G. Wilson A. D. Solomon, Academic Press, New York, 1978.
26. P. J. Davis and Philip Rabinowitz, *Methods of Numerical Integration,* Academic Press, New York, 1975.
27. J. Duchon and R. Robert, "Evolution d'une Interface par Capillarite et Diffusion de Volume I. Existence Locale en Temps," *Ann. Inst. Henri Poincare*, vol. 1, pp. 361-378, 1984.
28. J. Duchon and R. Robert, "Quelques Inegalites pour les Potentiels sur un Domaine Lipschitzien," *J. Math. Pures et Appl.*, vol. 64, pp. 457-468, 1985.
29. G. Duvaut, "Resolution d'un probleme de Stefan (Fusion d'un bloc de glace a zero degre)," *C. R. A. S. Paris Serie A*, vol. 276, pp. 1461-1463, 1973.
30. H. Dym and H. P. McKean, *Fourier Series and Integrals,* Academic Press, New York, 1972.
31. E. B. Fabes and N. M. Riviere, "Dirichlet and Neumann Problems for the Heat Equation in C^1-Cylinders," *Proc. AMS Conf. on Singular Integrals*, pp. 179-196.
32. E. B. Fabes and N. M. Riviere, "Potential Techniques for Boundary Value Problems on C^1-Domains," *Acta Math.*, vol. 141, pp. 165-186.
33. G. J. Fix, "Numerical methods for alloy solidification problems," in *Moving Boundary Problems*, ed. D. G. Wilson A. D. Solomon P. T. Boggs, Academic Press, New York, 1978.
34. G. J. Fix, "Numerical simulation of free boundary problems using phase field methods," in *The mathematics of finite elements and applications IV (Uxbridge, 1981)*, pp. 265-279, Academic Press, London-New York, 1982.
35. A. Friedman, *Partial Differential Equations of Parabolic Type,* Prentice-Hall, Englewood Cliffs, New Jersey, 1964.
36. A. Friedman, "The Stefan problem in several space variables," *Trans. Amer. Math. Soc.*, vol. 133, pp. 51-87, 1968.
37. O. Frostman, *Potentiel d'Equilibre et Capacite des Ensembles avec Quelques Applications a la Theorie des Fonctions,* Thesis, Lund 1935.

38. W. Gautschi, "A Computational Procedure for Incomplete Gamma Functions," *ACM Trans. Math. Soft.*, vol. 5, pp. 466-481, 1979.

39. C. W. Gear, *Numerical Initial Value Problems in Ordinary Differential Equations,* Prentice-Hall, Englewood Cliffs, New Jersey, 1971.

40. M. Gevrey, *Oeuvres,* Centre National de la Recherche Scientifique, Paris, 1970.

41. J. W. Gibbs, *Collected Works,* Yale University Press, New Haven, CT, 1948.

42. D. Gilbarg and N. S. Trudinger, *Elliptic Partial Differential Equations of Second Order,* Springer-Verlag, New York, 1983.

43. J. Glimm, O. McBryan, R. Menikoff, and D. H. Sharp, "Front Tracking Applied to Rayleigh-Taylor Instability," *SIAM J. Sci. Stat. Comput.*, vol. 7, pp. 230-251, 1986.

44. M. E. Gurtin, "On Phase Transitions with Bulk, Interfacial, and Boundary Energy," *Arch. Rat. Mech. Anal.*, vol. 94, pp. 101-123, 1985.

45. M. E. Gurtin, "On a Theory of Phase Transitions with Interfacial Energy," *Arch. Rat. Mech. Anal.*, vol. 87, pp. 187-212, 1985.

46. M. E. Gurtin, "On the Two-Phase Stefan Problem with Interfacial Energy and Entropy," *Arch. Rat. Mech. Anal.*, vol. 96, pp. 199-241, 1986.

47. M. E. Gurtin, "Toward a Nonequilibrium Thermodynamics of Two-Phase Materials," *Arch. Rat. Mech. Anal.*, vol. 100, pp. 275-312, 1988.

48. G. H. Hardy and J. E. Littlewood, "Some Properties of Fractional Integrals. I.," *Math. Zeitschr.*, vol. 27, pp. 565-606, 1928.

49. J. M. Hill, *One-dimensional Stefan Problems: an Introduction,* Wiley, New York, 1987.

50. P. C. Hohenberg and B. I. Halperin, "Theory of Dynamic Critical Phenomena," *Rev. Mod. Phys.*, vol. 49, pp. 435-479, 1977.

51. P. J. Van Der Houwen and H. J. te Riele, "Linear Multistep Methods for Volterra Integral and Integro-Differential Equations," *Math. Comp.*, vol. 45, pp. 439-461, 1985.

52. S. C. Huang and M. E. Glicksman, "Fundamentals of Dendritic Solidification-I. Steady-State Tip Growth," *Acta Met.*, vol. 29, pp. 701-715, 1981.

53. S. C. Huang and M. E. Glicksman, "Fundamentals of Dendritic Solidification-II. Development of Sidebranch Structure," *Acta Met.*, vol. 29, pp. 717-734, 1981.

54. J. M. Hyman, "Numerical Methods for Tracking Interfaces," *Physica*, vol. 12D, pp. 396-407, 1984.

55. E. Isaacson and H. B. Keller, *Analysis of Numerical Methods,* John Wiley and Sons, New York, 1966.

56. F. John, *Partial Differential Equations,* Springer-Verlag, New York, 1982.

57. O. Kellogg, *Foundations of Potential Theory,* Dover, New York, 1937.

58. D. A. Kessler and H. Levine, "Stability of Dendritic Crystals," *Phys. Rev. Lett.*, vol. 57, pp. 3069-3072, 1986.

59. D. A. Kessler, J. Koplik, and H. Levine, "Steady-State Dendritic Crystal Growth," *Phys. Rev. A*, vol. 33, pp. 3352-3357, 1986.

60. D. A. Kessler and H. Levine, "Velocity Selection in Dendritic Growth," *Phys. Rev. B*, vol. 33, pp. 7867-7870, 1986.

61. D. Kinderlehrer and L. Nirenberg, "The Smoothness of the Free Boundary in the One Phase Stefan Problem," *Comm. Pure Appl. Math.*, vol. 31, pp. 257-282, 1978.

62. D. Kinderlehrer and G. Stampacchia, *An Introduction to Variational Inequalities and Their Applications,* Academic Press, New York, 1982.

63. R. V. Kohn and P. Sternberg, "Local Minimizers and Singular Perturbations," *To appear.*

64. J. S. Langer, "Studies in the Theory of Interfacial Stability-II. Moving Symmetric Model," *Acta Met.*, vol. 25, pp. 1121-1137, 1977.

65. J. S. Langer and H. Muller-Krumbhaar, "Theory of Dendritic Growth-II. Instabilities in the Limit of Vanishing Surface Tension," *Acta Met.*, vol. 26, pp. 1689-1695, 1978.

66. J. S. Langer, "Instabilities and Pattern Formation in Crystal Growth," *Rev.Mod.Phys.*, vol. 52, pp. 1-28, 1980.

67. J. S. Langer, "Recent Developments in the Theory of Pattern Formation," *Physica A*, vol. 140, pp. 44-50, 1986.

68. J. L. Lavoie, T. J. Osler, and R. Tremblay, *SIAM Rev.*, vol. 18, pp. 240-265, 1976.

69. V. Laxmanan, "Dendritic Solidification-I. Analysis of Current Theories and Models," *Acta Met.*, vol. 33, pp. 1023-1035, 1985.

70. A. Majda, *Course Notes from Math 222,* Math Department, UC Berkeley, 1981.

71. E. A. McIntyre, Jr., "Boundary Integral Solutions of the Heat Equation," *Math. Comp.*, vol. 46, pp. 71-79, 1986.

72. D. I. Meiron, "Selection of Steady States in the Two-Dimensional Symmetric Model of Dendritic Growth," *Phys. Rev. A*, vol. 33, pp. 2704-2715, 1986.

73. D. I. Meiron, "Boundary Integral Formulation Of The Two-Dimensional Symmetric Model Of Dendritic Growth," *Physica D*, vol. 23, pp. 329-339, 1986.

74. G. H. Meyer, "Multidimensional Stefan problems," *SIAM J. Numer. Anal.*, vol. 10, pp. 552-538, 1973.

75. G. H. Meyer, "The Numerical Solution of Stefan Problems with Front-Tracking and Smoothing Methods," *Appl. Math. Comput.*, vol. 4, pp. 283-306, 1978.

76. G. H. Meyer, "The numerical solution of multidimensional Stefan problems — a survey," in *Moving Boundary Problems*, ed. D. G. Wilson, A. D. Solomon, and P. T. Boggs, Academic Press, New York, 1978.

77. G. H. Meyer, "The Method of Lines and Invariant Imbedding for Elliptic and Parabolic Free Boundary Problems," *SIAM J. Numer. Anal.*, vol. 18, pp. 151-164, 1981.

78. K. Miller, "Moving Finite Elements. II," *SIAM J. Numer. Anal.*, vol. 18, pp. 1033-1057, 1981.

79. G. Miranda, "Integral Equation Solution of the First Initial-Boundary Value Problem for the Heat Equation in Domains with Non-Smooth Boundary," *Comm. Pure Appl. Math.*, vol. 23, pp. 757-765, 1970.

80. R. C. Mjolsness and B. Swartz, "Some Plane Curvature Approximations," *Math. Comp.*, vol. 49, pp. 215-230, 1987.

81. L. Modica, "The Gradient Theory of Phase Transitions and the Minimal Interface Criterion," *Arch. Rat. Mech. Anal.*, vol. 98, pp. 123-142, 1987.

82. W. W. Mullins and R. F. Sekerka, "Stability of a Planar Interface During Solidification of a Dilute Binary Alloy," *Jour. Appl. Phys.*, vol. 35, pp. 444-451, 1964.

83. J. Neu, personal communication.

84. J. Neu, unpublished.

85. J. Nittmann and H. E. Stanley, "Tip Splitting without Interfacial Tension and Dendritic Growth Patterns Arising from Molecular Anisotropy," *Nature*, vol. 321, pp. 663-668, 1986.

86. S. Osher and J. A. Sethian, "Fronts Propagating with Curvature Dependent Speed : Algorithms Based on Hamilton-Jacobi Formulations," *To appear.*

87. V. K. Pinus and P. L. Taylor, "Stability and Instability in Crystal Growth: Symmetric Solutions of the Stefan Problem," *Phys. Rev. B*, vol. 32, pp. 5362-5367, 1985.

88. V. K. Pinus and P. L. Taylor, "Stability and Instability in Crystal Growth. II. Asymmetric Solutions of the Thermodiffusion Model," *Phys. Rev. B*, vol. 33, pp. 8697-8705, 1986.

89. L. I. Rubinstein, *The Stefan Problem,* A. M. S. Translations of Mathematical Monographs, Providence, Rhode Island, 1971.

90. L. I. Rubinstein, "Global Stability of the Neumann Solution of the Two-phase Stefan Problem," *IMA Jour. Appl. Math.*, vol. 28, pp. 287-299, 1982.

91. Y. Saito, G. Goldbeck-Wood, and H. Muller-Krumbhaar, "Dendritic Pattern Formation," *Physica Scripta*, vol. T19, pp. 327-329, 1987.

92. R. Seeley, "Singular integrals and boundary value problems," *Amer. J. Math.*, vol. 88, pp. 781-809, 1966.

93. J. A. Sethian, "Curvature and the Evolution of Fronts," *Comm. Math Phys.*, vol. 101, pp. 487-499, 1985.

94. J. B. Smith, "Shape Instabilities and Pattern Formation in Solidification : A New Method for Numerical Solution of the Moving Boundary Problem," *Jour. Comp. Phys.*, vol. 39, pp. 112-127, 1981.

95. I. Stakgold, *Boundary Value Problems of Mathematical Physics (2 vols.),* Macmillan, New York, 1970.

96. E. Stein, *Singular Integrals and Differentiability Properties of Functions of Several Variables,* Princeton University Press, Princeton, New Jersey, 1978.

97. G. Stein and E. Weiss, *Fourier Analysis on Euclidean Spaces,* Princeton University Press, Princeton, New Jersey, 1978.

98. J. Strain, "Linear Stability of Planar Solidification Fronts," *Physica D*, vol. 30, pp. 297-320, 1988.

99. J. M. Sullivan, D. R. Lynch, and K. O'Neill, "Finite Element Simulation of Planar Instabilities during Solidification of an Undercooled Melt," *Jour. Comp. Phys.*, vol. 69, pp. 81-

111, 1987.

100. F. Treves, *Basic Linear Partial Differential Equations,* Academic Press, New York, 1975.

101. F. Treves, *Introduction to Pseudodifferential and Fourier Integral Operators (2 vols.),* Plenum Press, New York, 1980.

102. C. Truesdell and R. A. Toupin, "The Classical Field Theories," in *Handbuch der Physik III/1 (ed. S. Flugge),* Springer-Verlag , Berlin Gottingen Heidelberg, 1960.

103. C. Verdi and A. Visintin, "Numerical Analysis of the Multidimensional Stefan Problem with Supercooling and Superheating," *Bollettino U. M. I.*, vol. (7) I-B, pp. 795-814, 1987.

104. C. Verdi and A. Visintin, "Error Estimates for a Semi-Explicit Numerical Scheme for Stefan-Type Problems," *Numer. Math.*, vol. 52, pp. 165-185, 1988.

105. A. Visintin, "Supercooling and Superheating Effects in Phase Transitions," *IMA Jour. Appl. Math.*, vol. 35, pp. 233-256, 1985.

106. G. B. Whitham, *Linear and Nonlinear Waves,* Wiley, New York, 1978.

107. E. T. Whittaker and G. N. Watson, *A Course of Modern Analysis,* Cambridge University Press, Cambridge, 4th ed. 1927, reprinted 1984.

108. D. J. Wollkind and R. D. Notestine, "A Non-linear Stability Analysis of the Solidification of a Pure Substance," *IMA Jour. Appl. Math.*, vol. 27, pp. 85-104, 1981.

Table 1			
Errors in planar Neumann solution			
N	I	$t=1, p=0.5$	$t=4, p=0.9$
20	4	.0114	.2429
40	6	.00439	.1567
80	8	.00162	.02315
160	10	.000581	.008696
320	12	.000205	.003123

Table 2

Max-norm differences for cosine graph

$V=1$, $\varepsilon_C=.01$, $\varepsilon_V=0$

$g_o=.02$, $k=4$, $q=q'=1$

t	32-16	64-32	128-64	(64/32)-(32/16)	(128/64)-(64-32)
0.125	0.00068	0.00040	0.00017	0.000115	0.000083
0.25	0.00230	0.00137	0.00062	0.000442	0.000180
0.375	0.00484	0.00298	0.00138	0.001114	0.000362
0.5	0.00869	0.00556	0.00264	0.002424	0.000708
0.625	0.01452	0.00971	0.00474	0.004896	0.001364
0.75	0.02330	0.01641	0.00827	0.009518	0.002624
0.875	0.03661	0.02742	0.01438	0.018235	0.005063
1.0	0.05704	0.04607	0.02538	0.035091	0.009816
1.125	0.08905	0.07900	0.04639	0.068942	0.021613
1.25	0.14039	0.14029	0.09015	0.140196	0.052824
1.375	0.22439	0.26210	0.19676	0.299807	0.131695
1.5	0.36218	0.52664	0.53837	0.691104	0.550101

Table 3

Comparison with linear stability theory

ε_C=.01, ε_V=0, V=1, A=0

g_o=.02

	$k=1$			$k=4$			$k=7$		
	$y_1=0.955337$			$y_1=2.43975$			$y_1=-0.360157$		
$16\times t$	$\tilde{g}$	g	$g/g_0e^{y_1t}$	$\tilde{g}$	g	$g/g_0e^{y_1t}$	$\tilde{g}$	g	$g/g_0e^{y_1t}$
0	.02000	.02000	1.00	.0200	.0200	1.00	.020	.0200	1.00
1	.02022	.02022	.95	.0219	.0219	.94	.019	.0194	.99
2	.02067	.02066	.92	.0253	.0252	.93	.019	.0189	.99
3	.02127	.02126	.89	.0294	.0293	.93	.019	.0185	.99
4	.02200	.02199	.87	.0343	.0341	.93	.018	.0181	.99
5	.02285	.02285	.85	.0400	.0397	.93	.018	.0177	.99
6	.02382	.02381	.83	.0467	.0462	.93	.018	.0173	.99
7	.02490	.02490	.82	.0546	.0539	.93	.017	.0169	.99
8	.02610	.02609	.81	.0638	.0627	.93	.017	.0165	.99
10	.0288	.02881	.79	.087	.0851	.93	.016	.0158	.99
12	.0320	.03200	.78	.12	.1154	.93	.016	.0151	.99
14	.0357	.03569	.77	.17	.1566	.93	.015	.0144	.99
16	.0399	.03992	.77	.23	.2124	.93	.015	.0138	.99
18	.0448	.04474	.76	.3	.288	.93	.014	.0131	.98
20	.0503	.05023	.76	.5	.391	.93	.014	.0126	.98
22	.0565	.05644	.76	*	.530	.93	.013	.0120	.98
24	.0635	.06348	.76	*	.719	.93	.012	.0115	.98

* The extrapolated values for $k=4$ and $t\geq 1.25$ are not converging swiftly enough to guarantee one good digit. (g and $\tilde{g}$ are accurate within 2 units in the last digit shown).

Table 4

Max-norm differences for periodic bump graph

$\varepsilon_C = .01$, $\varepsilon_V = 0$, $A = 0$

$\delta = .05$, $g_o = .02$, $q = q' = V = 1$

t	32-16	64-32	128-64	64/32-32/16	128/64-64/32
0.125	.00017	.00010	.00005	.000040	.000009
0.25	.00061	.00037	.00017	.000126	.00028
0.375	.00138	.00084	.00040	.000305	.000056
0.5	.00252	.00157	.00076	.000622	.000099
0.625	.00418	.00267	.00132	.001166	.000163
0.75	.00659	.00434	.00217	.002085	.000255
0.875	.01008	.00686	.00350	.003635	.000480
1.0	.01515	.01071	.00559	.006263	.000963
1.125	.02256	.01667	.00895	.010789	.001920
1.25	.03350	.02615	.01452	.018793	.003820
1.375	.04996	.04174	.02425	.033514	.007642
1.5	.07532	.06867	.04238	.062018	.016094

Table 5

Max-norm differences for periodic dendrite

ε_C=.02, ε_V=.01, A=.5, k_A=4

δ=.05, g_o=.05, q=q'=V=1

t	20-10	40-20	80-40	10/20-20/40	20/40-40/80
0.2	.0093	.0030	.0018	.0040	.0014
0.4	.0127	.0067	.0041	.0056	.0023
0.6	.0184	.0133	.0078	.0099	.0035
0.8	.0303	.0234	.0133	.0166	.0051
1.0	.0506	.0384	.0211	.0262	.0074

Table 6

Growth in condition number for an anisotropic dendrite

$\varepsilon_C = .04$, $\varepsilon_V = .02$, $A = .5$, $k_A = 4$

$\delta = .05$, $g_o = .05$, $q = q' = V = 1$

t	$J=10$	$J=20$	$J=40$
1.0	$1 \cdot 10^2$	$2 \cdot 10^2$	$3 \cdot 10^2$
2.0	$1 \cdot 10^2$	$2 \cdot 10^2$	$4 \cdot 10^2$
3.0	$3 \cdot 10^2$	$7 \cdot 10^2$	$3 \cdot 10^3$
4.0	$4 \cdot 10^3$	$2 \cdot 10^4$	$6 \cdot 10^4$
5.0	$3 \cdot 10^4$	$7 \cdot 10^4$	$3 \cdot 10^5$
6.0	$6 \cdot 10^4$	$2 \cdot 10^5$	$6 \cdot 10^5$
7.0	$1 \cdot 10^5$	$2 \cdot 10^5$	$1 \cdot 10^6$

Table 7

Growth in condition number for an isotropic dendrite

$\varepsilon_C = .04$, $\varepsilon_V = .02$, $A = 0$

$\delta = .05$, $g_o = .05$, $q = q' = V = 1$

t	$J=10$	$J=20$	$J=40$
1.0	$8 \cdot 10^1$	$2 \cdot 10^2$	$3 \cdot 10^2$
2.0	$1 \cdot 10^2$	$2 \cdot 10^2$	$5 \cdot 10^2$
3.0	$4 \cdot 10^2$	$2 \cdot 10^3$	$8 \cdot 10^3$
4.0	$5 \cdot 10^3$	$2 \cdot 10^4$	$6 \cdot 10^4$
5.0	$2 \cdot 10^4$	$8 \cdot 10^4$	$3 \cdot 10^5$
6.0	$2 \cdot 10^4$	*	*
7.0	$3 \cdot 10^4$	*	*

* The calculation blew up at $t = 5.4$ for $J = 20$ and $t = 5.3$ for $J = 40$; the condition number at blow-up was in each case $9 \cdot 10^5$.

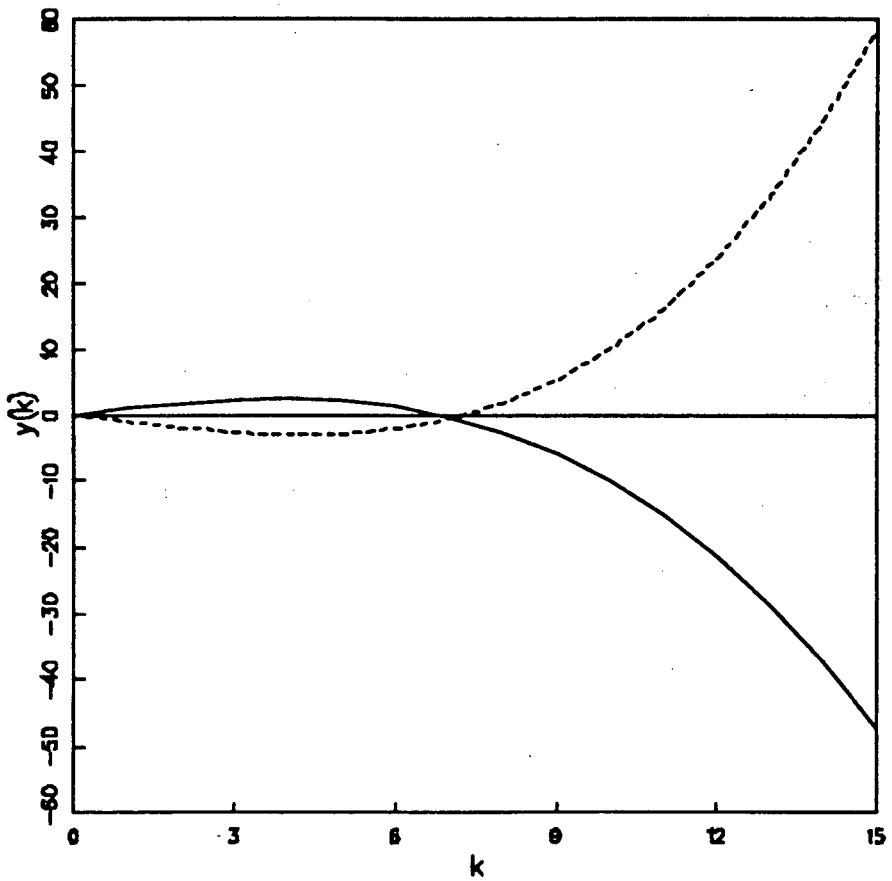

Figure 1(a). Linear growth exponents $y_i(k)$.

A perturbation to a planar constant-speed interface behaves asymptotically like $e^{y_1 t}$; the coefficient of $e^{y_2 t}$ vanishes. In this picture, y_2 is dashed. Here $\varepsilon_c = .01$, $V = 1$; there are only a few unstable modes.

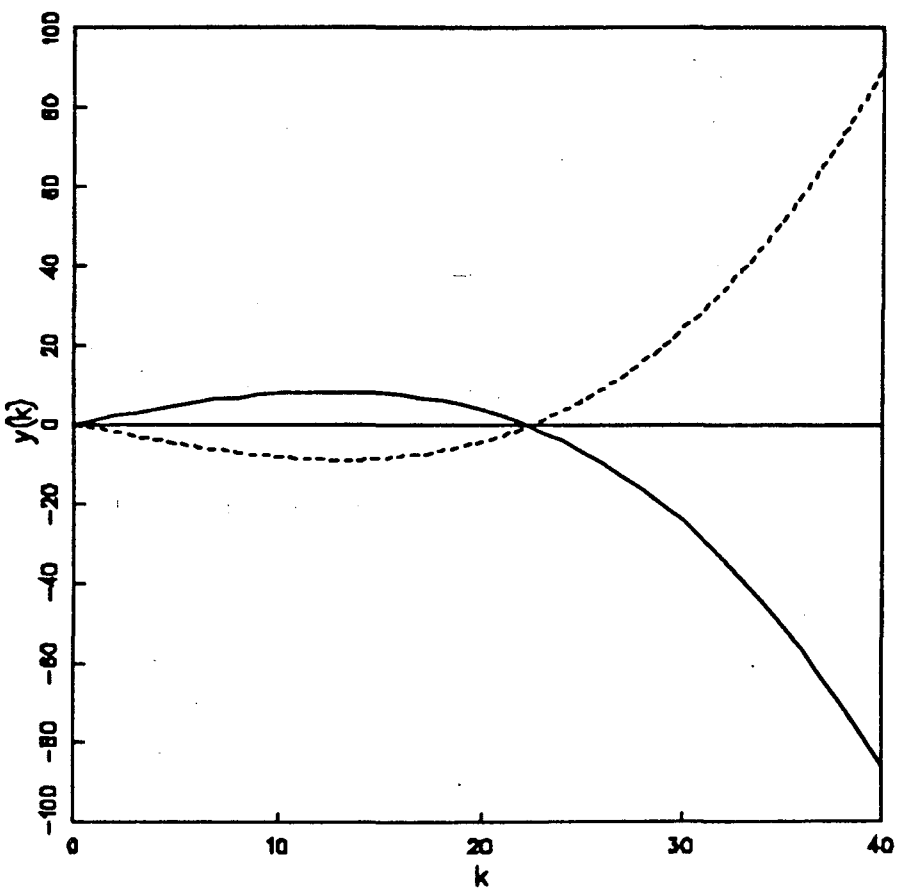

Figure 1(b). Linear growth exponents $y_i(k)$.

Here V is still 1, but $\varepsilon_c = .001$; the band of unstable modes is wider.

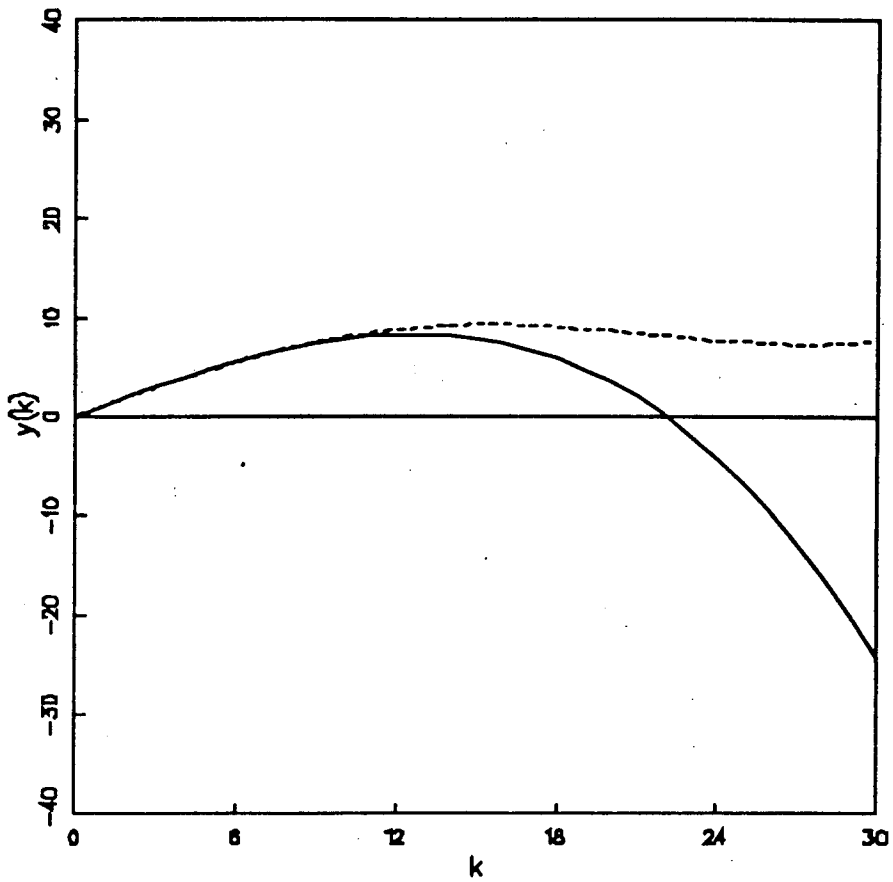

Figure 2(a). Exact and discrete linear growth exponents $y_1(k)$ **and** $\tilde{y_1}(k)$. Here $\varepsilon_C = .001, J = 30$, and the numerical approximation introduces a small-scale instability.

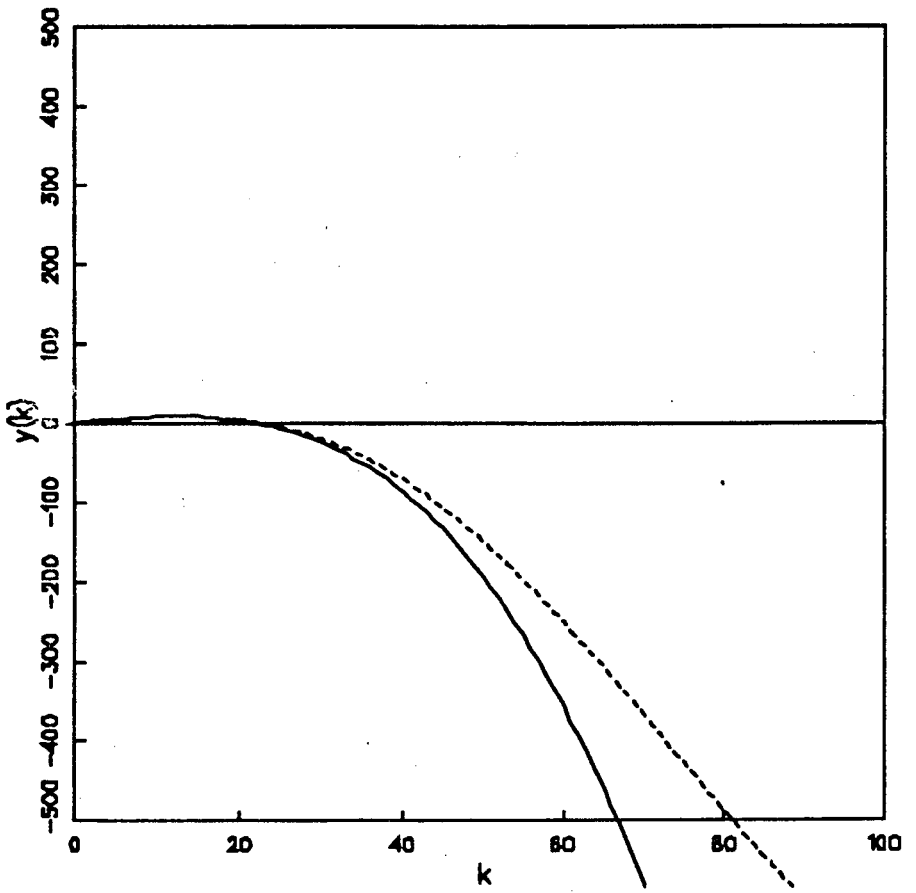

Figure 2(b). Exact and discrete linear growth exponents $y_1(k)$ **and** $\tilde{y}_1(k)$. Here $\varepsilon_c = .001$, but $J = 100$; this is enough points to damp the instability.

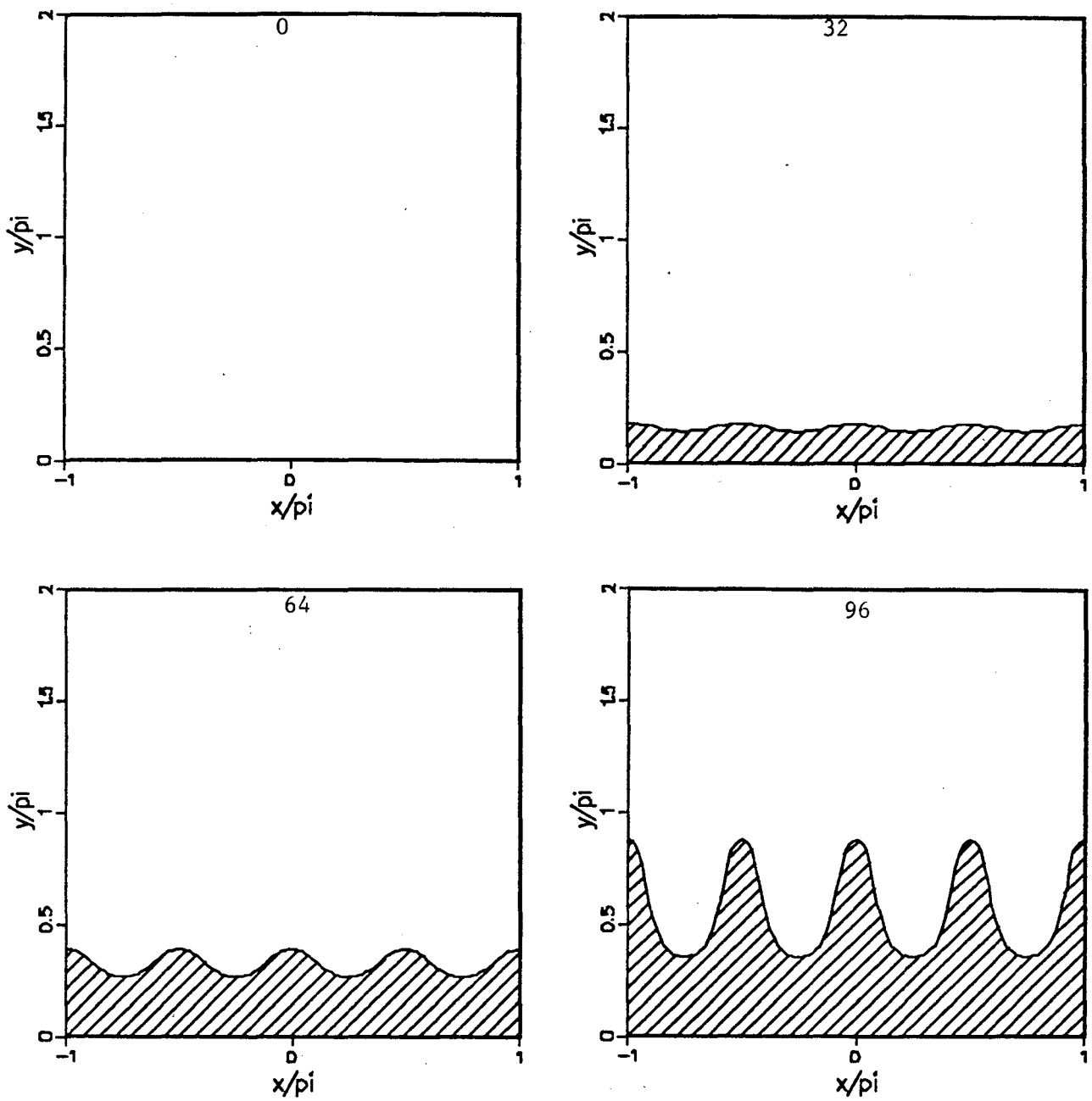

Figure 3. Evolution of cosine graph

The physical parameters are $\varepsilon_C = .01$, $V = q = q' = 1$. The initial state has $g_0 = .02$, $k = 4$. The final state (computed with $J = 64$ and $N = 96$) has $T = 1.5$. The shaded region is ice, the white region is water.

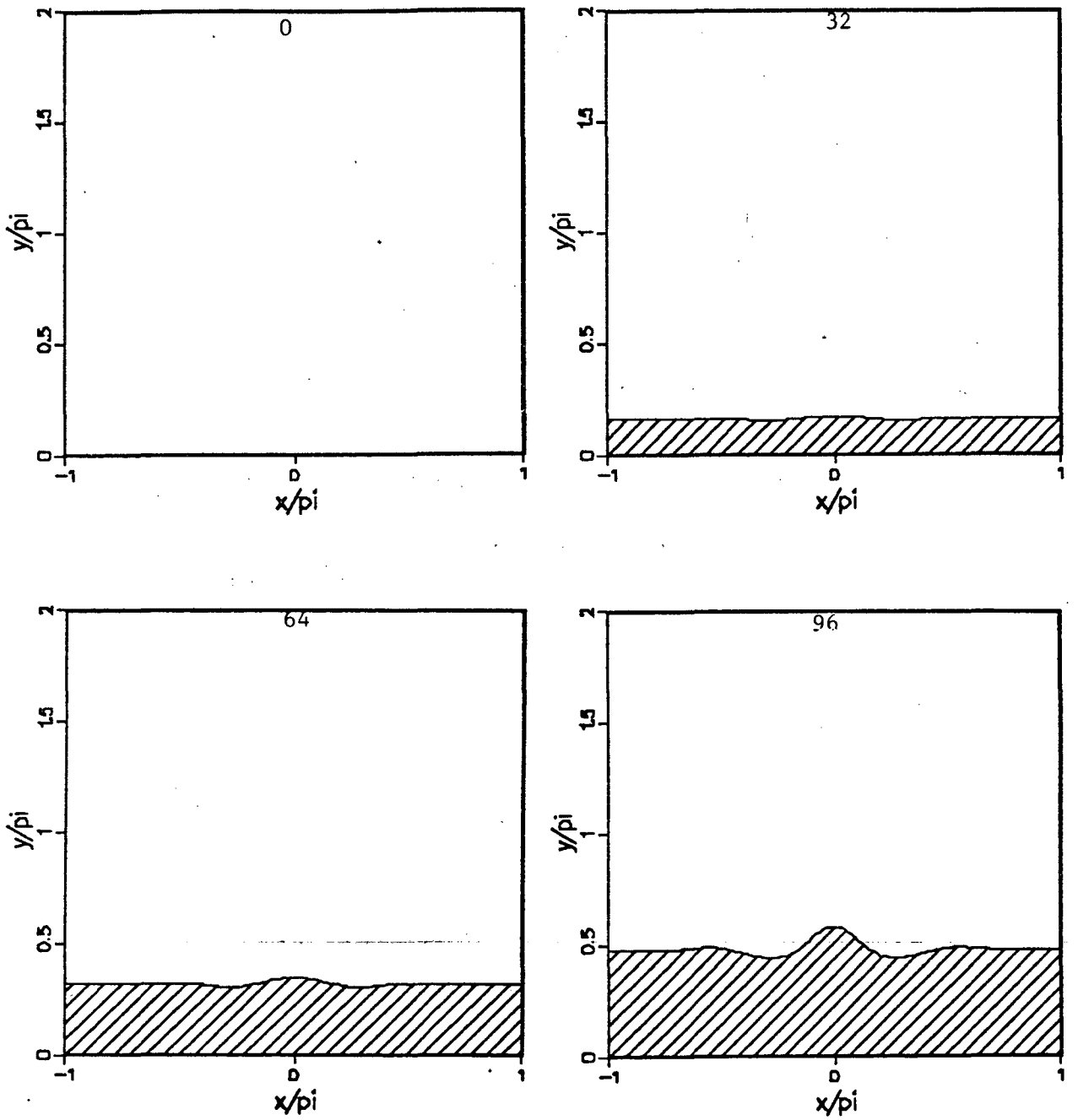

Figure 4. Evolution of bump graph

The physical parameters are $\varepsilon_c = .01$, $\delta = .05$, $g_0 = .02$: The initial state is an almost invisible bump on a flat interface. We computed with $J = 64$ points and $N = 96$ time steps up to time $T = 1.5$.

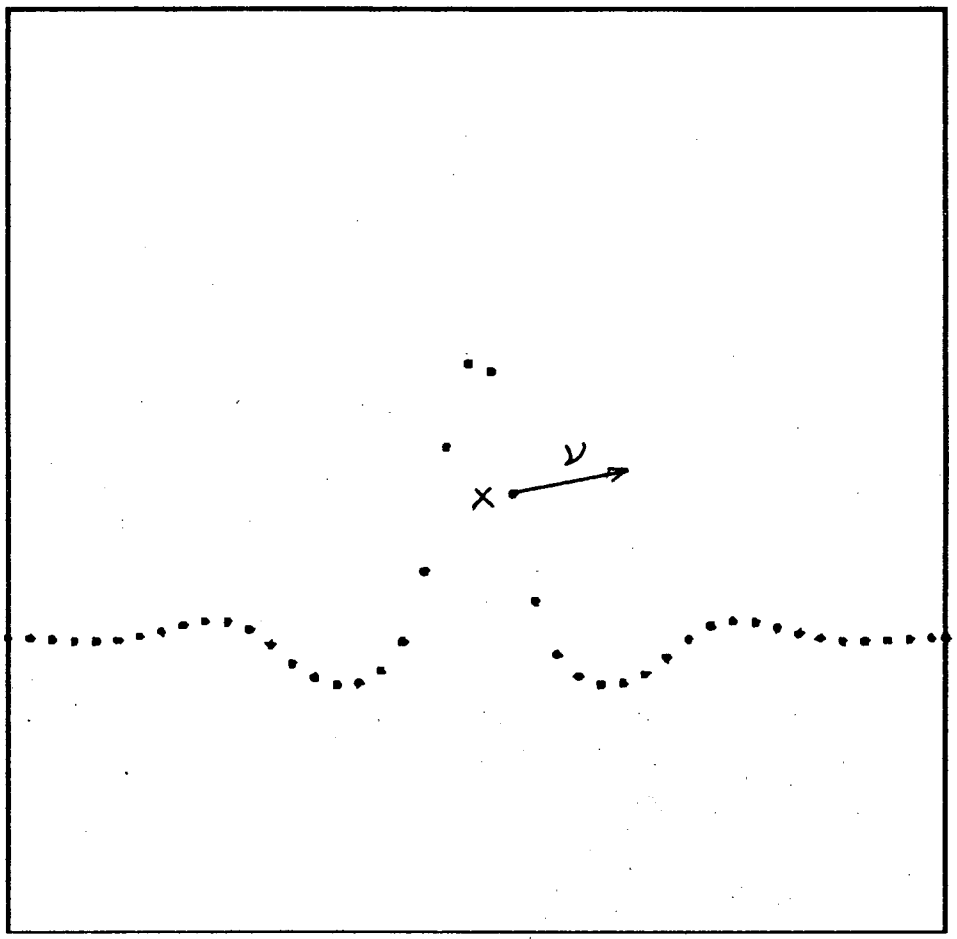

Figure 5. Difficulties of moving points only along the normal

Since the normal points almost exactly sideways on the sides of the bump and the bump is moving upwards, x cannot move along the curve; stretching is inevitable.

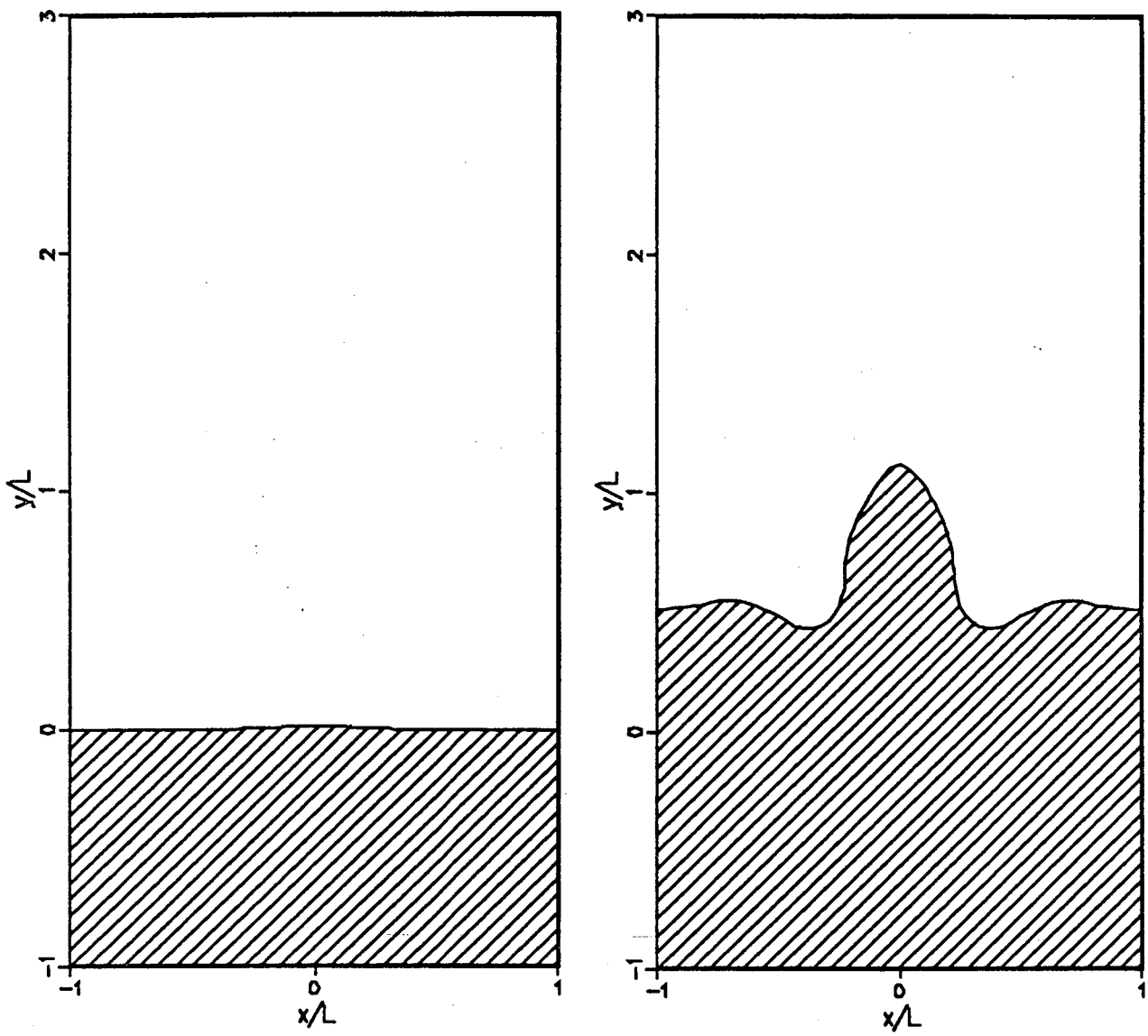

Figure 6. Initial and final states for dendrite convergence study

Physical parameters: $\varepsilon_C = \varepsilon_V = .02$, $A = .5$, $k_A = 4$. Numerical parameters: $J = 40$, $N = 60$, $t = 0$ and $t = 1.5$. The initial state is an almost invisible bump on a flat interface, while the final state has developed substantial gradients. L is half the distance between x_J and x_{-J} before rescaling.

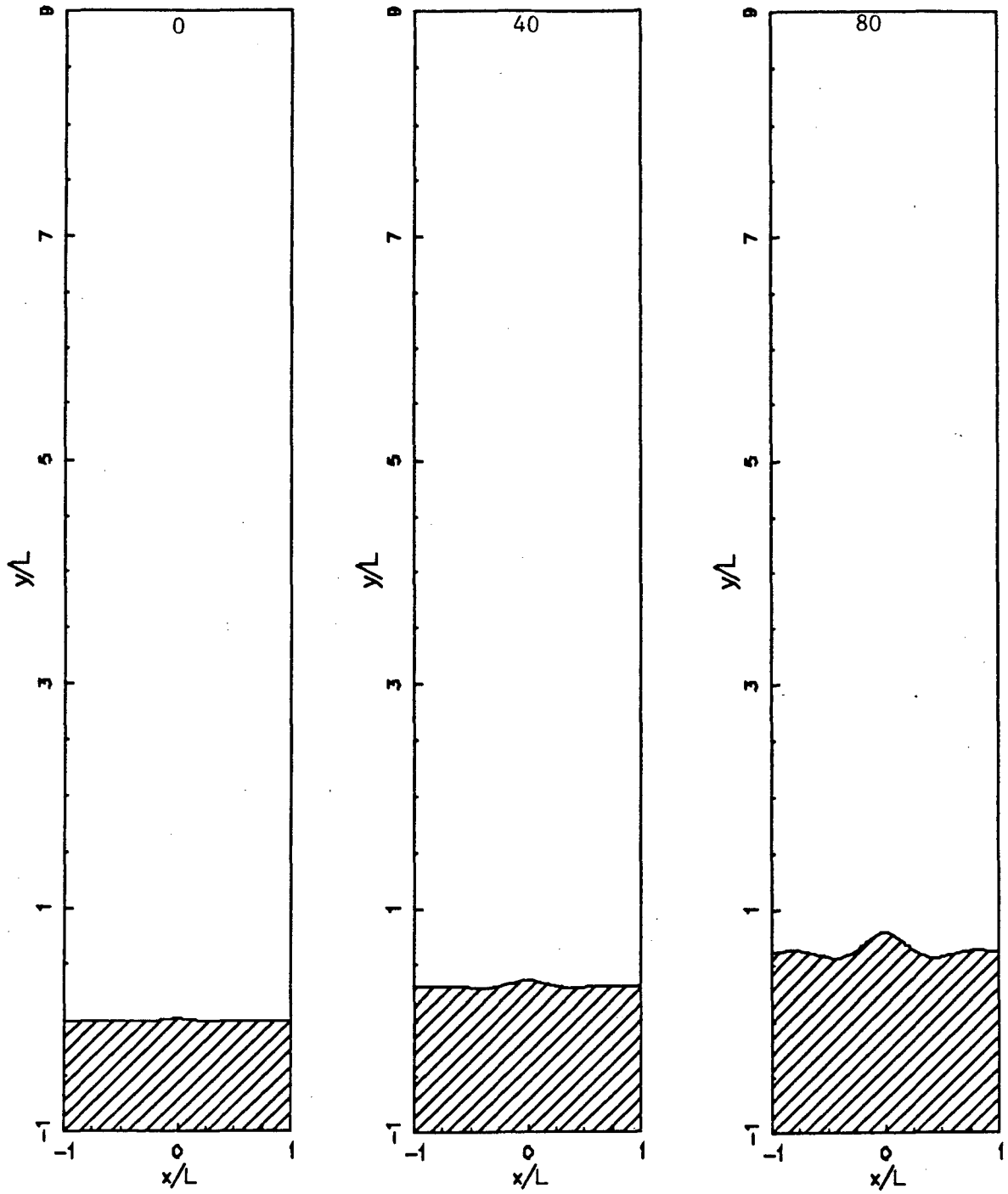

Figure 7(a). Evolution of an anisotropic dendrite.

Physical parameters: $\varepsilon_C = .04$, $\varepsilon_V = .02$, $A = .5$, $k_A = 4$, $q = q' = V = 1$. Initial conditions: $\delta = .05$, $g_0 = .05$: The initial state is an almost invisible bump on a flat interface. The numerical parameters are $J = 40$, $N = 280$, $I = 10$, and we compute up to time $T = 7$. On this page, pictures are spaced 40 time steps apart, because the dendrite moves very slowly at first. Each figure is numbered on the top with the time step.

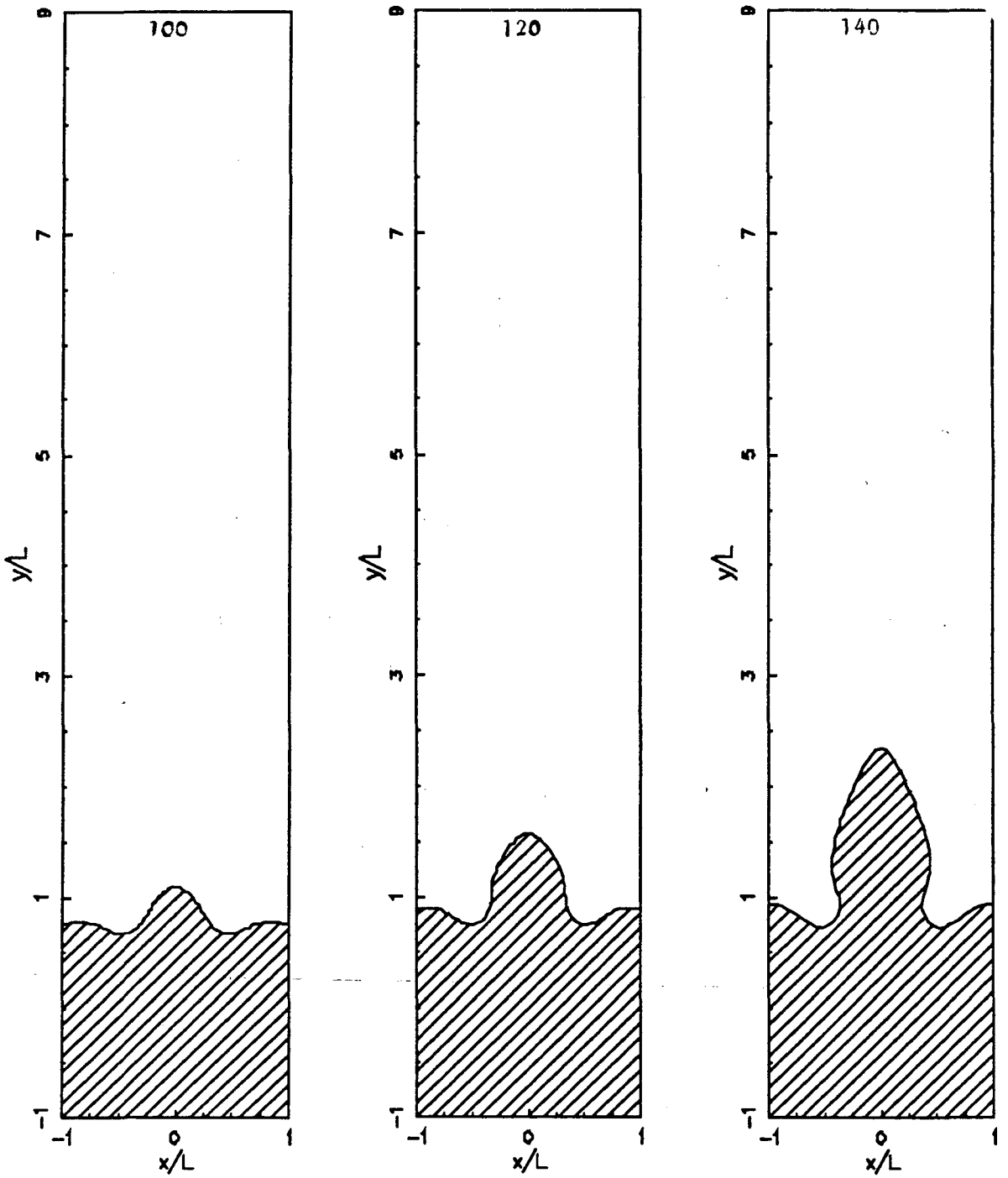

Figure 7(b). Evolution of an anisotropic dendrite (continued).

Now the development picks up speed, and pictures are taken 20 time steps apart.

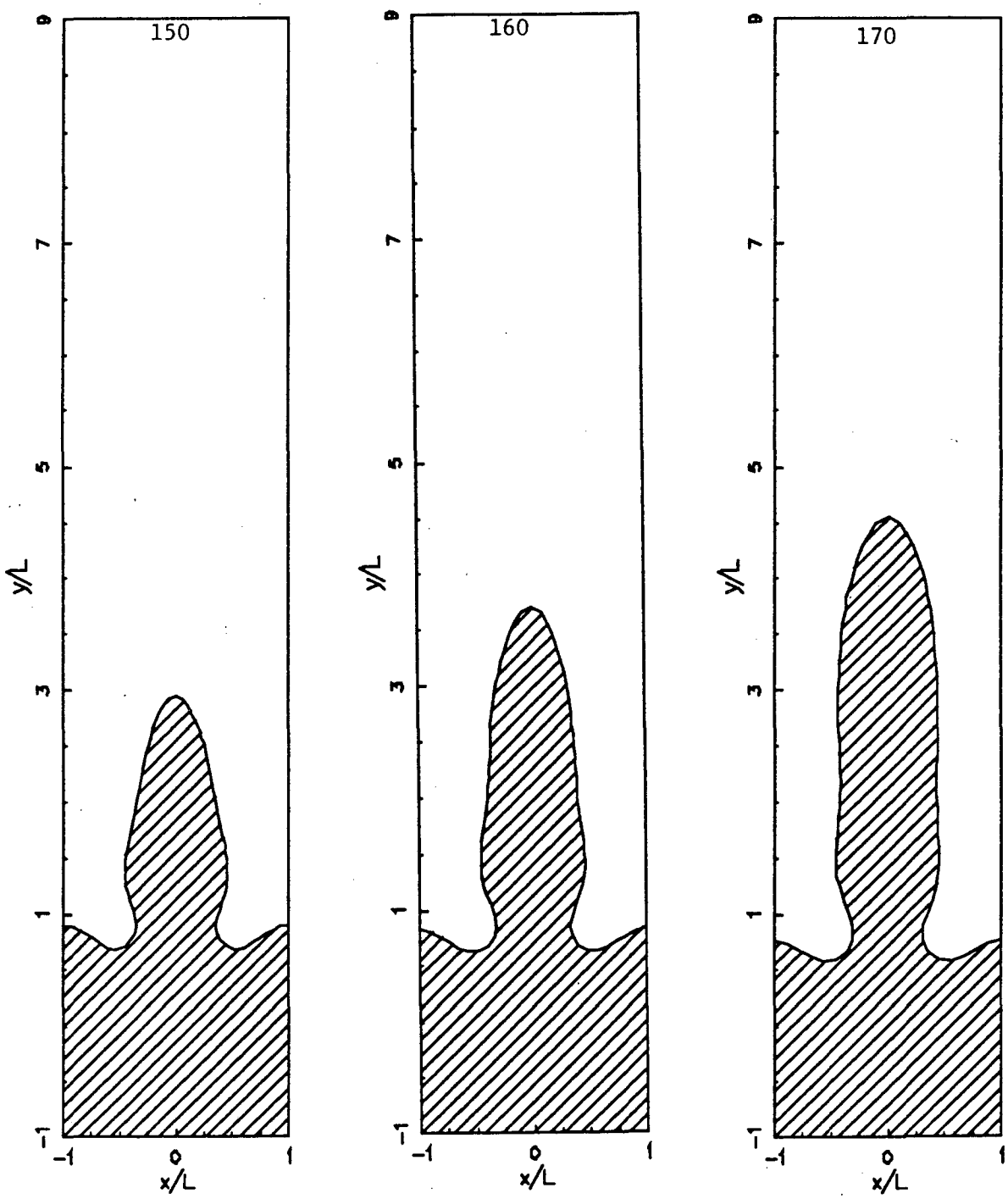

Figure 7(c). Evolution of an anisotropic dendrite (continued).
These pictures are taken 10 time steps apart.

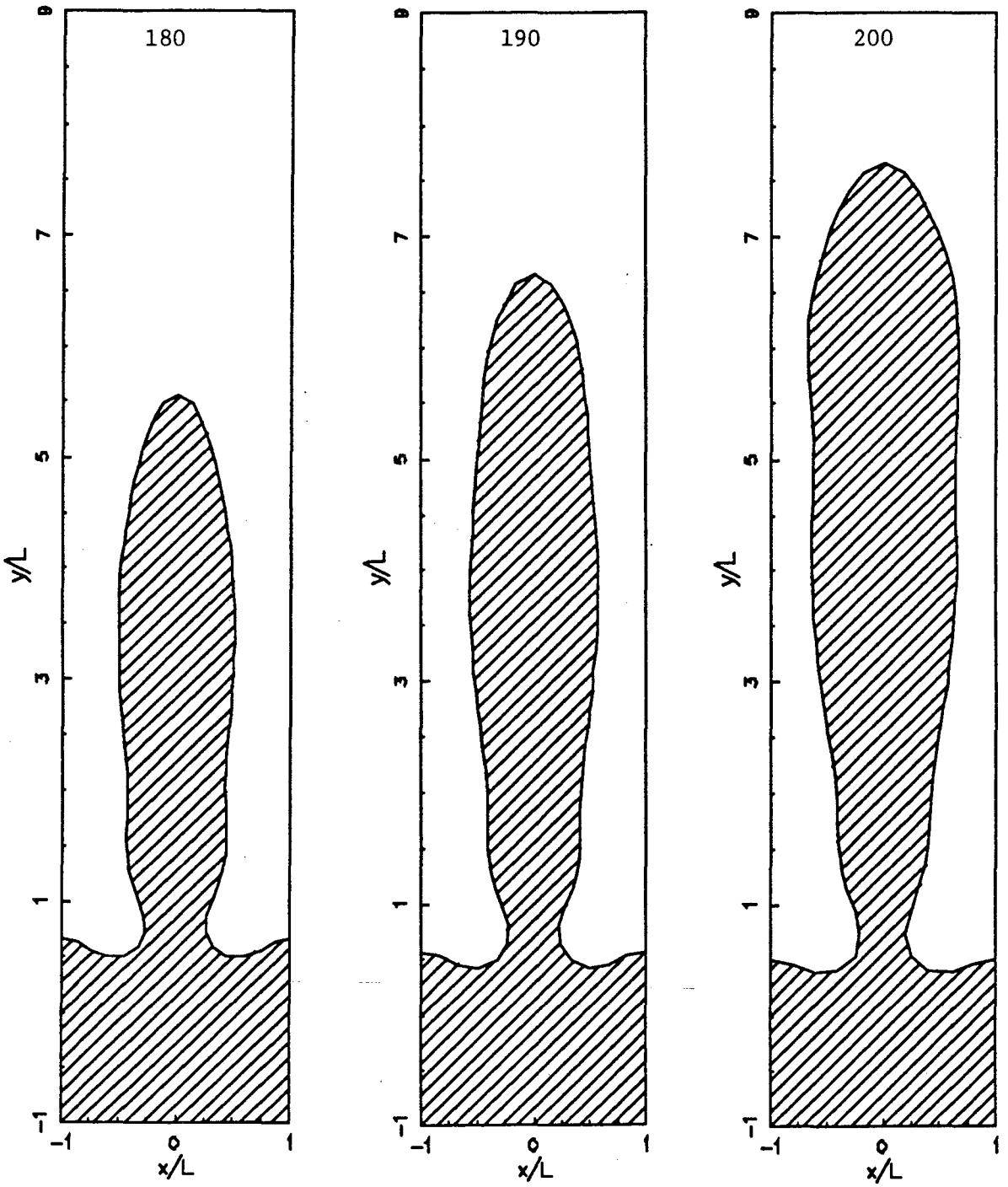

Figure 7(d). Evolution of an anisotropic dendrite (continued).

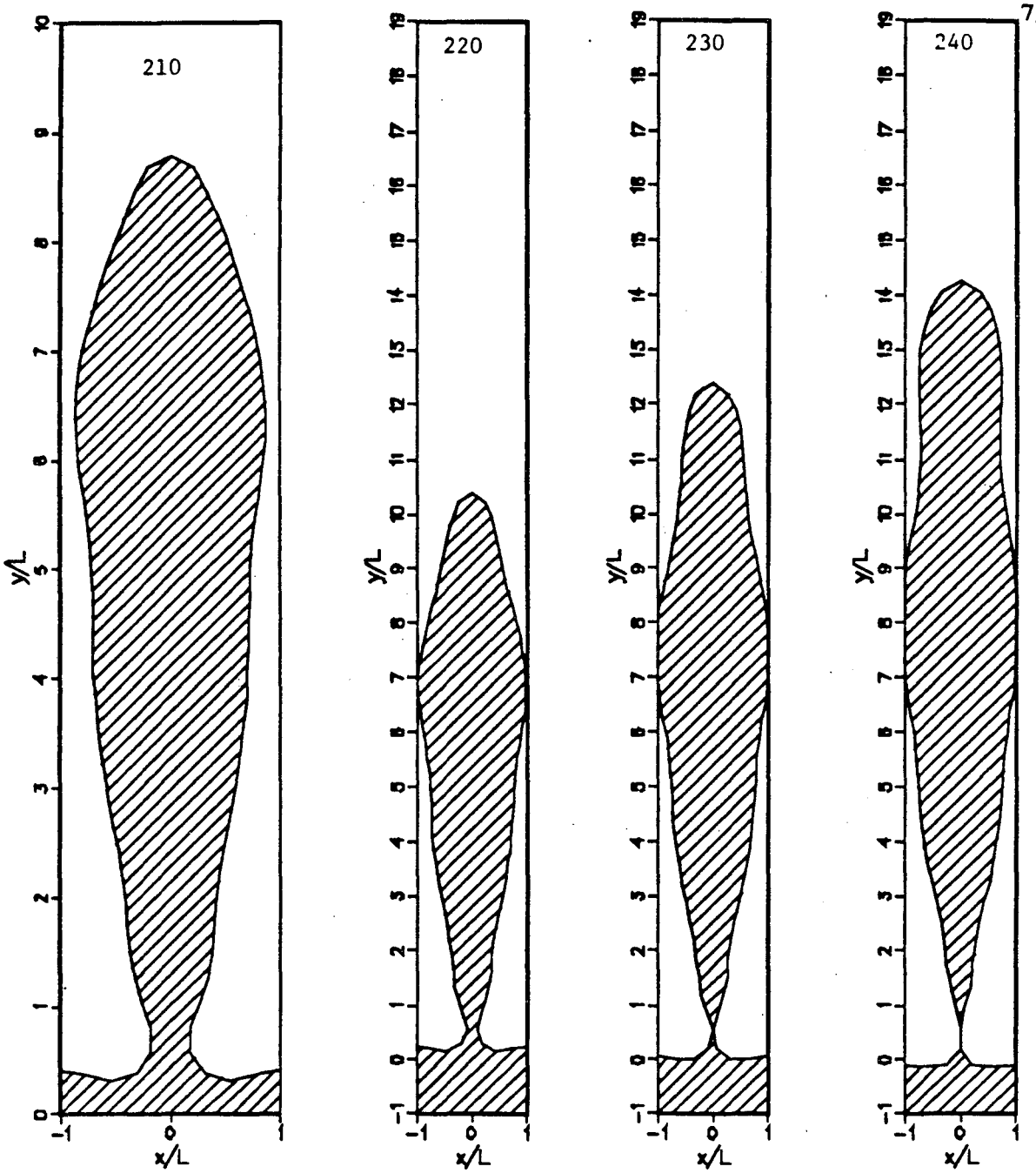

Figure 7(e). Evolution of an anisotropic dendrite (continued).

Rescaling was necessary at time step 220, because the dendrite became too long and thin to fit on the page. At step 210, a definite sidebranching instability appears; however, it doesn't have time to develop before it makes contact with the neighboring dendrite.

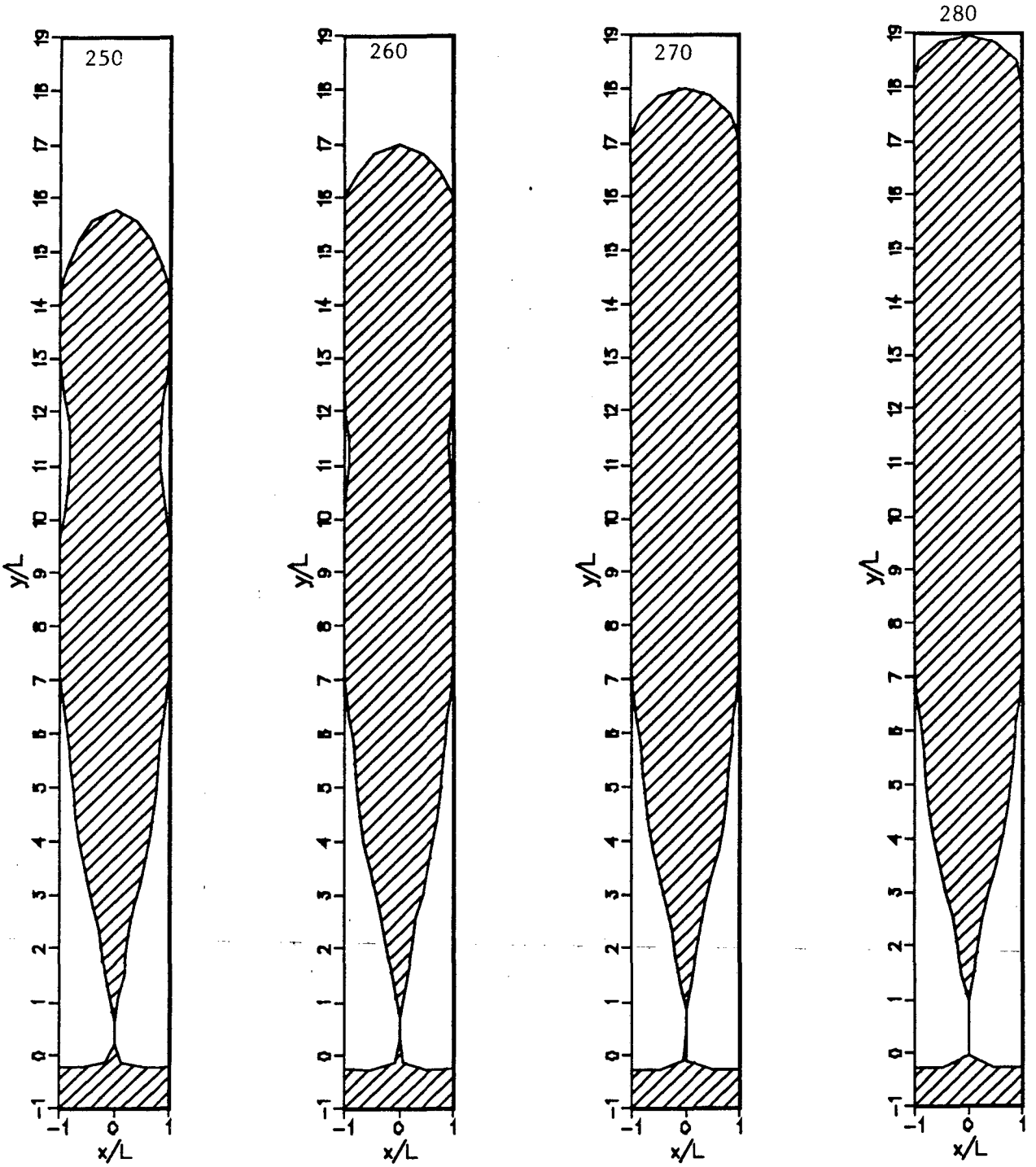

Figure 7(f). Evolution of an anisotropic dendrite (continued).

The dendrite has completely filled the channel available to it, and a mass of ice separates from its parent and makes its way forward. A trapped body of water is left behind. The front of the advancing mass is strongly reminiscent of the periodic solidification fronts described in Langer's paper [66].

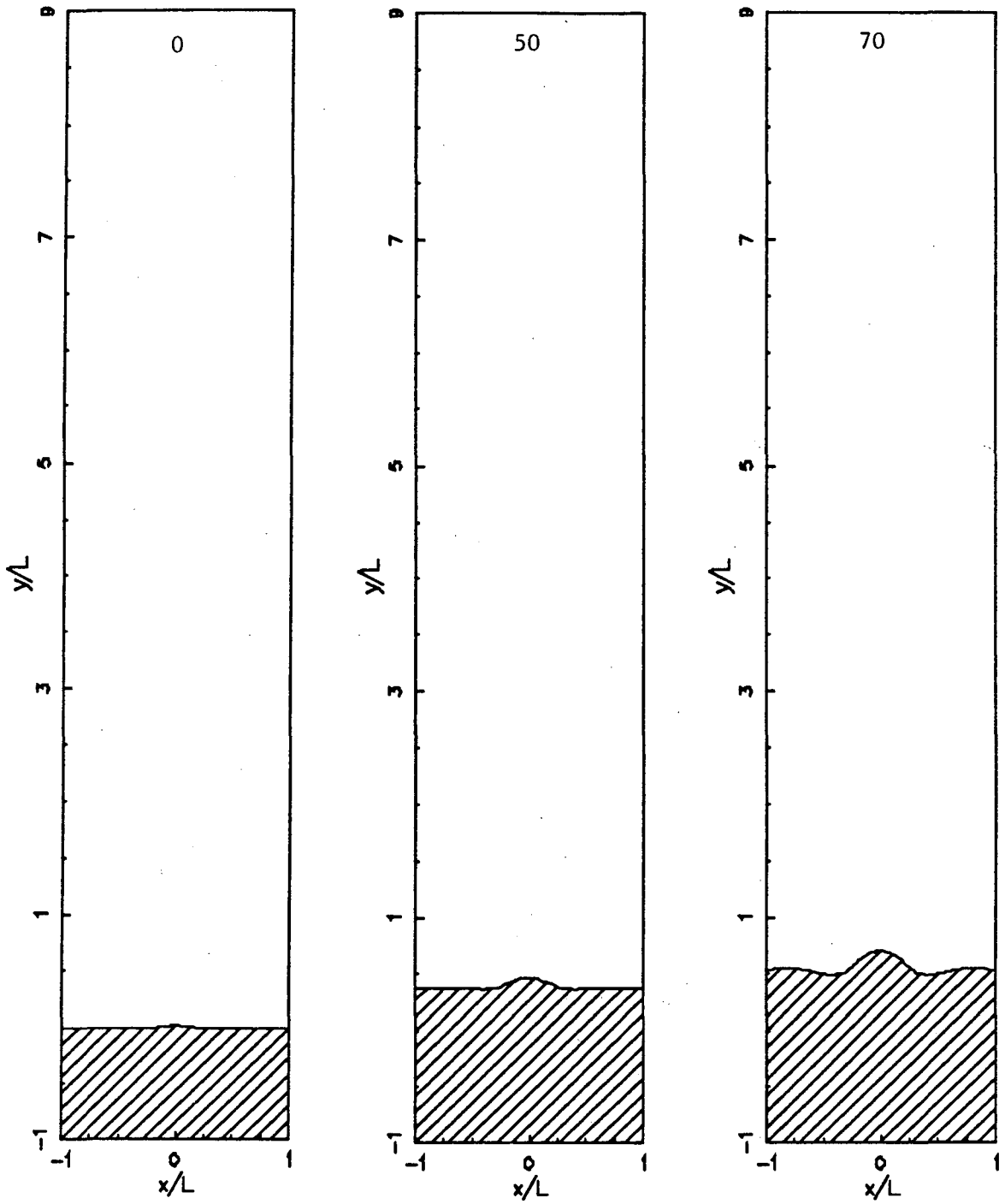

Figure 8(a). Evolution of an isotropic dendrite.

Physical parameters: $\varepsilon_C = .02$, $\varepsilon_V = .01$, $A = 0$, $q = q' = V = 1$. Initial conditions: $\delta = .05$, $g_0 = .05$. The numerical parameters are $J = 40$, $N = 210$, $I = 10$, and we compute up to time $T = 5.25$. The initial state is an almost invisible bump on a flat interface.

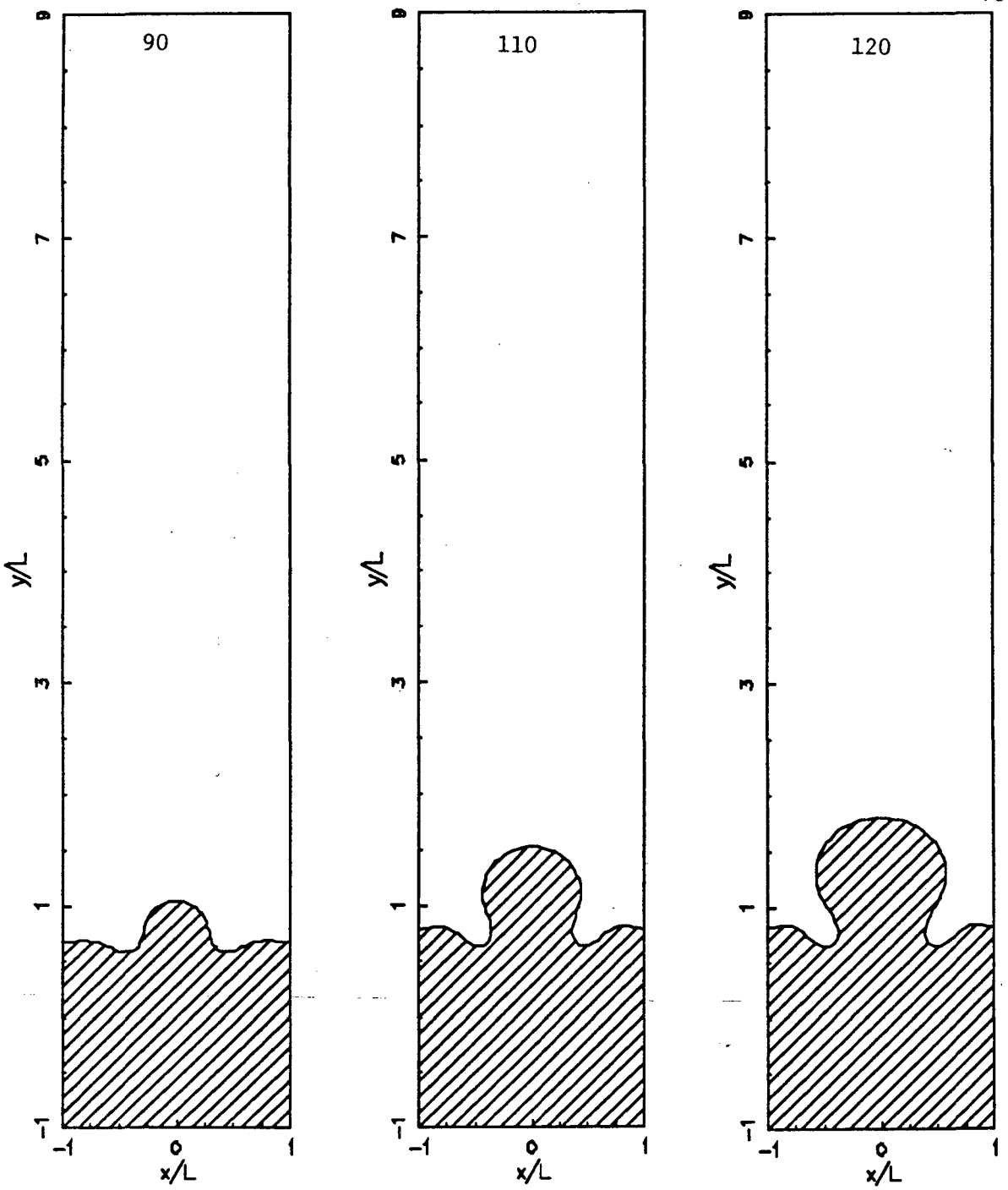

Figure 8(b). Evolution of an isotropic dendrite (continued).

The dendrite grows into a nearly circular shape at first, because the influence of its neighbor is negligible.

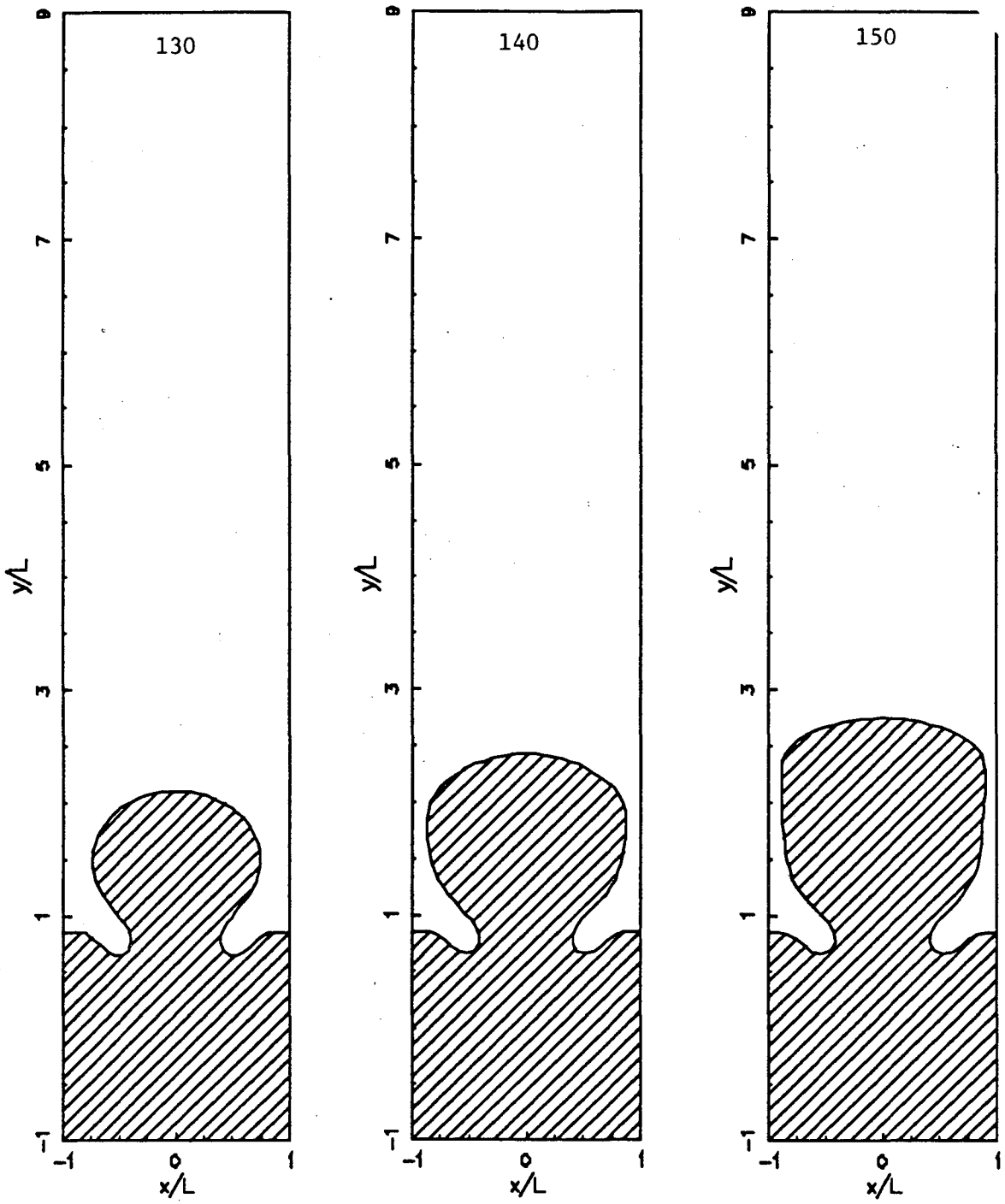

Figure 8(c). Evolution of an isotropic dendrite (continued).

Circular growth continues till the dendrite almost fills its channel; then it must square off somewhat.

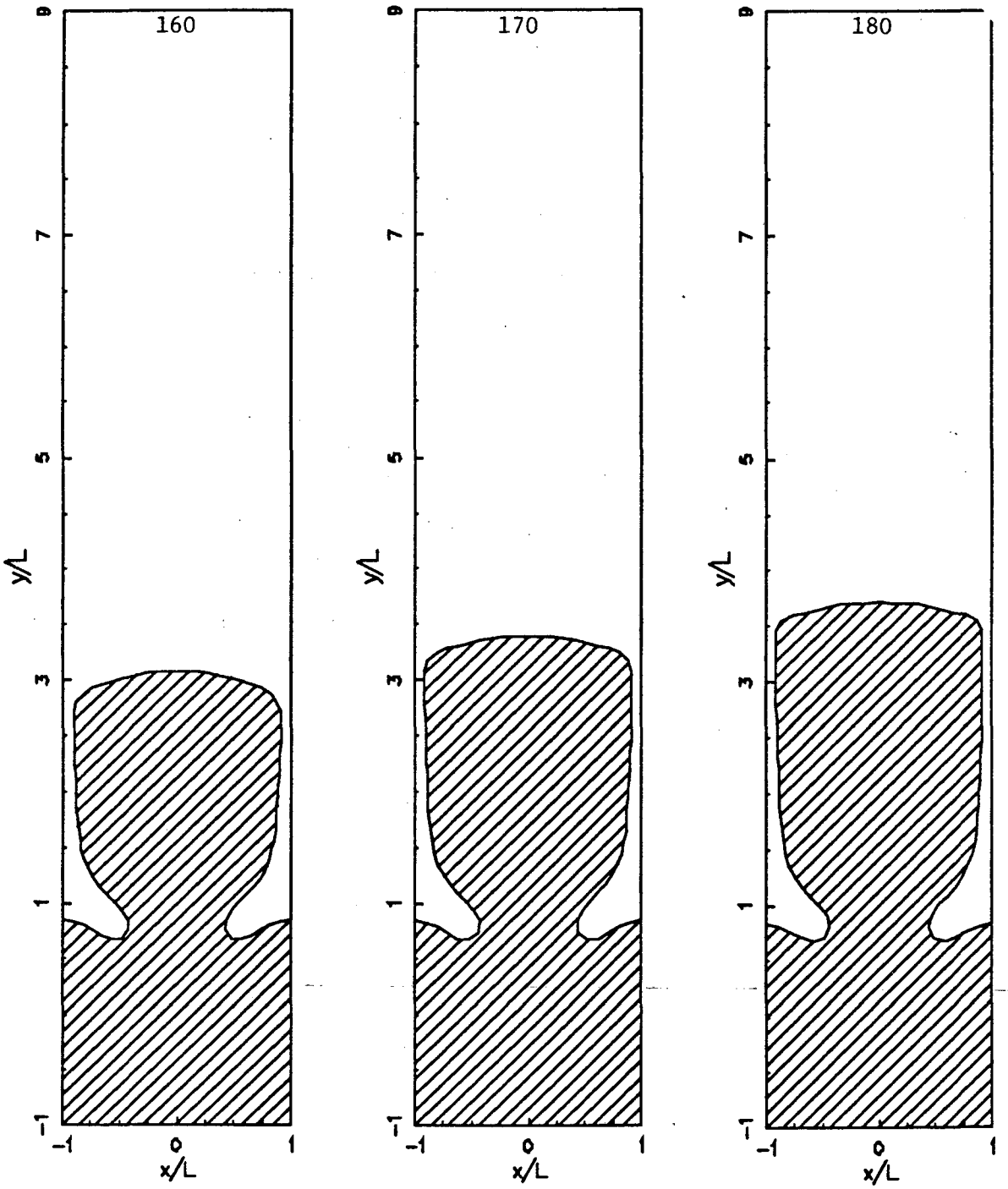

Figure 8(d). Evolution of an isotropic dendrite (continued).

Now an almost flat front moves steadily forward: Clearly this is an unstable situation, by linear stability theory.

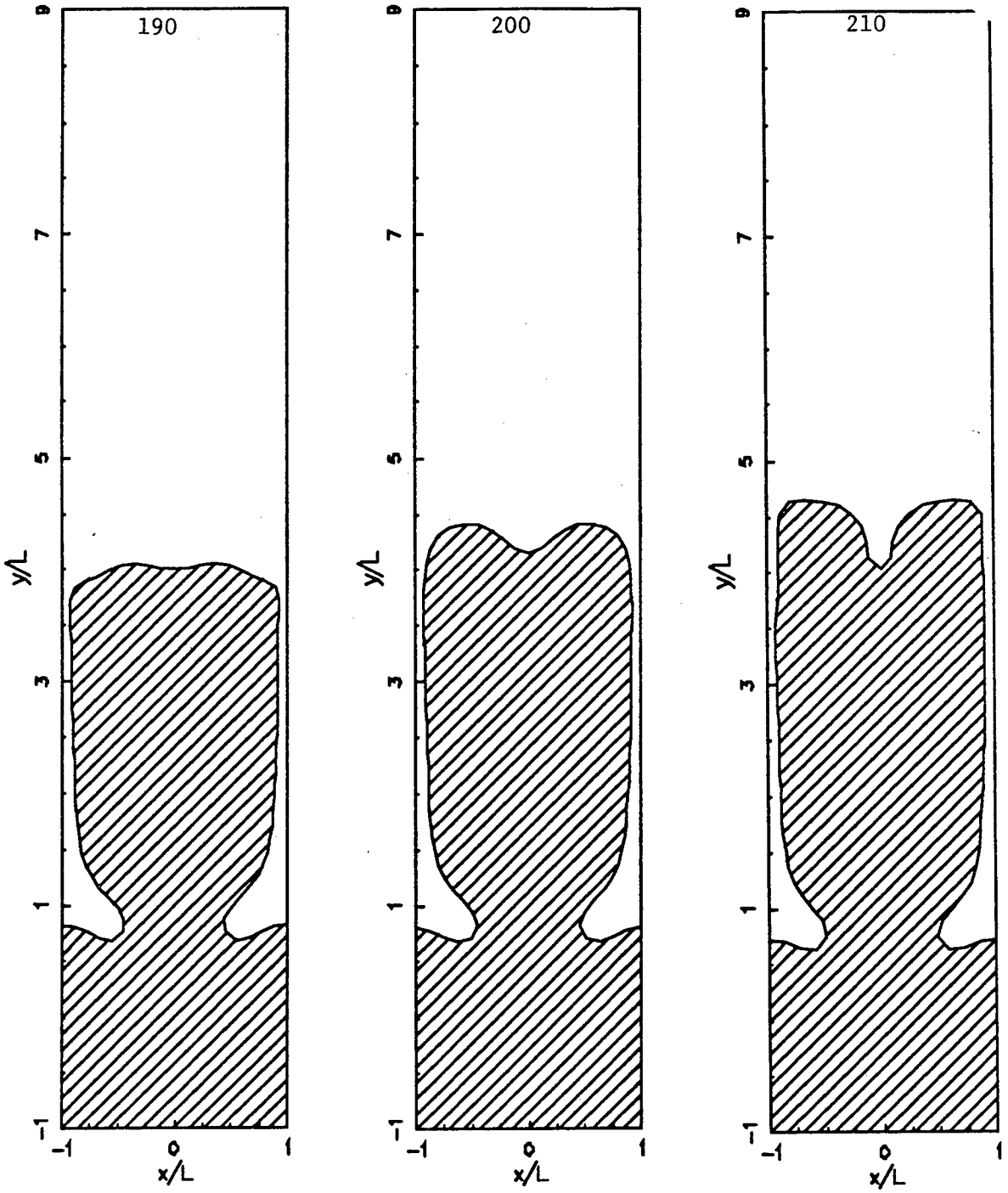

Figure 8(e). Evolution of an isotropic dendrite (continued).

A clearly delineated tip-splitting instability now becomes evident. Shortly after time step 210, $J = 40$ points were no longer sufficient to resolve the steep bend in the center, and the computation failed.

LAWRENCE BERKELEY LABORATORY
TECHNICAL INFORMATION DEPARTMENT
UNIVERSITY OF CALIFORNIA
BERKELEY, CALIFORNIA 94720